Terms and Conditions of Use of Digitised Theses from Trinity College Library Dublin

Copyright statement

All material supplied by Trinity College Library is protected by copyright (under the Copyright and Related Rights Act, 2000 as amended) and other relevant Intellectual Property Rights. By accessing and using a Digitised Thesis from Trinity College Library you acknowledge that all Intellectual Property Rights in any Works supplied are the sole and exclusive property of the copyright and/or other IPR holder. Specific copyright holders may not be explicitly identified. Use of materials from other sources within a thesis should not be construed as a claim over them.

A non-exclusive, non-transferable licence is hereby granted to those using or reproducing, in whole or in part, the material for valid purposes, providing the copyright owners are acknowledged using the normal conventions. Where specific permission to use material is required, this is identified and such permission must be sought from the copyright holder or agency cited.

Liability statement

By using a Digitised Thesis, I accept that Trinity College Dublin bears no legal responsibility for the accuracy, legality or comprehensiveness of materials contained within the thesis, and that Trinity College Dublin accepts no liability for indirect, consequential, or incidental, damages or losses arising from use of the thesis for whatever reason. Information located in a thesis may be subject to specific use constraints, details of which may not be explicitly described. It is the responsibility of potential and actual users to be aware of such constraints and to abide by them. By making use of material from a digitised thesis, you accept these copyright and disclaimer provisions. Where it is brought to the attention of Trinity College Library that there may be a breach of copyright or other restraint, it is the policy to withdraw or take down access to a thesis while the issue is being resolved.

Access Agreement

By using a Digitised Thesis from Trinity College Library you are bound by the following Terms & Conditions. Please read them carefully.

I have read and I understand the following statement: All material supplied via a Digitised Thesis from Trinity College Library is protected by copyright and other intellectual property rights, and duplication or sale of all or part of any of a thesis is not permitted, except that material may be duplicated by you for your research use or for educational purposes in electronic or print form providing the copyright owners are acknowledged using the normal conventions. You must obtain permission for any other use. Electronic or print copies may not be offered, whether for sale or otherwise to anyone. This copy has been supplied on the understanding that it is copyright material and that no quotation from the thesis may be published without proper acknowledgement.

Relationship between the molecular interaction and the structure of the bent core liquid crystals in the nematic phase

by

Yun Jang

A thesis submitted for the
degree of Doctor of Philosophy

in the

Advanced Electronic Materials Lab.
Department of Electronic and Electrical Engineering

TRINITY COLLEGE
THE UNIVERSITY OF DUBLIN

June 2012

Declaration of Authorship

I, Yun Jang, declare that this thesis titled, 'Relationship between the molecular interactions and the structure of the bent core liquid crystals in the nematic phase' and the work presented in it are entirely my own. I confirm that:

- It has not been submitted as an exercise for a degree at this or any other University.
- It is entirely my own work, except where otherwise stated.
- I have quoted from the work of others, the source is always given. With the exception of such quotations, this thesis is entirely my own work.
- I agree to deposit this thesis in the Universitys open access institutional repository or allow the library to do so on my behalf, subject to Irish Copyright Legislation and Trinity College Library conditions of use and acknowl-
e

Signed:

Date:

" All nematics are cybotactic. Some exhibit additional structure with varying degrees of evanescent density fluctuations. When mesogens with a propensity to form transient strata cooperatively tilt in those strata, the clusters become inherently biaxial.". (E.T. Samulski)

It was a great pleasure to deal with a magical substance, liquid crystals.

Acknowledgements

When I look back, my decision to study abroad for a PhD was a challenge to me as I had been away from College life for a long time and I was not alone anymore. I am able to make this achievement because of the encouragement, support and guidance of people around me. Firt of all, I would like to appreciate the supervision of **Prof. Jagdish K. Vij,**. He is an excellent supervisor as well as a teacher. He provided plentiful opporunities to study in this field and encouraged me in all respects. I also thank the college for providing me with the studentship and the facilities. I sincerely thank **Pro. J-K. Song,** for having led me to Vij's lab. He is a former colleage, a senior and a mentor. His encouragement made it possible for me to study in Trinity College Dublin. I would like to thank **Dr V. P. Panov,** for his valuable discussions, instructions, advices and hospitality during my study in TCD. He is one of the best experts in the field of electro-optic experiments. Many experiments mentioned in this thesis were carried out with him. Actually, we enjoyed talking about not only topics regarding the research but also matters of personal interest and concern. I was pleased to discuss results with **Dr. Uttam Manna**. He was always kind of sharing their know-how in the laboratory. I thank **Prof. A. Kocot** for their helpful advice, the experimental data in Fig. 5.10 and 5.12 were drawn by him.

Samsung Electronic company granted me a chance to study here. In particular, I sincerely thank President **Dr. Kyung-Hyun Kim,** and Vice President **Dr. H-S Kim,** for endless concerns. **Dr. S. S. Seomun** originally introduced me this lab and helped me to prepare for the study. He also gave me many tips and information about Ireland. I would like to express my sincere gratitude to all my colleagues in Samsung Electronics for their supports and assistance.

I and my family owe a lot to many Koreans in Ireland. We might have endured many difficulties wothout them. Specially, my soulmate and sworn brother **Mr. Sichul Seong** and his lovely wife, Wendy and two princes are unforgettable people in Ireland. Uncountable helps and hostalities have been given from them. Another sworn brother, **Mr. Sunchil Choi** should be mentioned. Sometimes, our family remind the night we arrived at Dublin Airport and warm welcome by his wife, Claire. That was the beginning of our long journey in Ireland. **Mr. Eunlyong Lee** and his family, **Mr Hyunchul Kim** and his family cannot be missed. All the members of the Korean Golf Association of Ireland including **Dr. kungha Sur**,

Mr. Dongkook Kim, are in the center of my memory in Ireland. All of them have made my family's living in Dublin homelike and fruitful. I could concentrate on my study by virtue of their help. I sincerely thank all of them for all respects.

I also won affections of Koreans in TCD. **Pr. Youngwan Choi** from Joongang University in Korea, **Pr. Hun Mok**, **Dr, Soonjung Jung, Jiwon Yoon,** and many graduate and undergraduate students are good friends and mentors. They have helped me in all respects.

Lastly I come to my parents and families, parents-in-law and families-in-law in Korea. They always have thoughts and affection for me, my wife and Seoyoung and Seojin. Their endless love always make me happy and feel like living togehter despite the long distance between the two countries. This has been an endless strength for me and my family in Ireland.

Finally, I thank my wife Hyunyoung Jung and two daughters for being always there with me. I could do everything thanks to them.

I dedicate this thesis to all the above people.

To my Hyunyoung ,

Seoyoung,
& Seojin. . .

Summary

The relationship between the molecular interaction and the molecular structure of the bent core mesogens in the nematic phase is investigated in detail. Various physical phenomena are observed and interpreted.

1. Cybotactic clusters in the nematic phase of 4-cyanosubstituted bent-core mesogens are reviewed. These were investigated by an X-ray technique by the Halle group. The formation of the clusters in the nematic phase is governed by the molecular structure of the bent core mesogens.

2. The dielectric response of the materials is investigated. The materials show different types of nematic phases ranging from the usual one that is consistent with the Maier and Meier model to the nematic phase with cybotactic clusters. The dielectric behavior dependent on the molecular structure is interpreted in terms of the short-range correlations expressed in terms of the Kirkwood correlation factors included in the Maier-Meier equation. The nematic phase of C4 with the short terminal chains is well explained by the M-M model based on the molecular field theory. The materials with longer chains (C7, C9) show different behavior from C4. The results from the dielectric experiments agree with those from the X-ray experiments.

3. In order to investigate the origin of the cybotactic clusters, IR spectroscopy is used. For C4, the results from IR experiments show that the averaged tilt angle of the molecules from the normal to the substrates is zero in the nematic phase, whereas molecules in the cluster are tilted with respect to the averaged layer normal. The latter is parallel to the laboratory Z axis for C9.

4. Birefingence, IR and optical contrast spectroscopic techniques are used to find whether or not any conformational change occurs with temperature. Results of the three different techniques indicate that no significant conformational change takes place with change of temperatures.

5. The chirality and the phase behavior of C5 is investigated and interpreted in terms of a pair of two bent-core molecules. The phase behavior of C5 in the nematic phase is intermediate between the usual nematic phase and the nematic phase with cybotactic clusters. Interestingly, only C5 among

the investigated materials shows chirality in the nematic phase. Basically, a V-shaped molecule has C_{2v} symmetry which is achiral. A simpler system that comprises a pair of two bent-core molecules can have several other symmetries one of which gives rise to chirality.

6. The optical biaxiality of PAL1 in the nematic phase prior to its transition to a smectic phase is investigated by a system using PEM under various surface anchoring conditions. Results of the experiment give the following new information: i) the minor director is switchable by the electric field. ii) the minor director can be aligned by the application of simple rubbing process to a glass plate coated with homeotropic alignment layer on which the major director has homeotropic configuration with a small tilt angle. iii) the switching speed is too slow to be applied for LCD displays. This is due to the reorientation of the biaxial clusters rather than the molecules in the nematic phase under the applied in-plane electric field.

7. The conventional LC modes used in LCDs for mass production are reviewed. Basically, the switching is an act of converting the state of polarized light that passes through the LC layer to achieve a certain transmission for a gray level. Therefore, the design of a LCD mode begins from an understanding of the polarization conversion by the LC layer. Each mode is analyzed in terms of the *Stokes parameters* on the *Poincare sphere*. Such an analysis is used in understanding the principle of the compensation for the retardation at oblique angles. The biaxial nematic phase is more favorable than the uniaxial nematic phase in achieving wider viewing angle without the use of a compensation film. The inherent optical biaxiality can be used for realizing a gray scale by switching of the minor director by electric field as well as to minimizing the transmttance for the black state at oblique angles.

Many of the new findings in this thesis are related to the analysis of the results from the experiments and the application of the proper models to understand the physical phenomena.

Contents

List of Figures

The captions listed here are not full captions but concise ones.

List of Tables

Abbreviations

LC	**L**iquid **C**rystal
LCD	**L**iquid **C**rystal **D**isplay
N	**N**ematic type phase (achiral)
$\mathbf{N}_u$	Uniaixial **N**ematic type phase (achiral)
$\mathbf{N}_{u'}$	Uniaixial **N**ematic type phase with clusters (achiral)
$\mathbf{N}_b$	Biaxial **N**ematic type phase (achiral)
$\mathbf{N}_b^p$	Polar Biaxial **N**ematic type phase (achiral)
$\mathbf{N}_{cybC}$	**N**ematic type phase with smetic C type cluster
CybC	**C**ybotactic phase with smetic C type cluster
Sm*A*	**Sm**ectic **A** type phase (achiral)
Sm*C*	**Sm**ectic **C** type phase (achiral)
DFNs	**D**ual **F**requency **N**ematics
BCMs	**B**ent **C**ore **M**esogens
Cr	**Cr**ystal phase
I	**I**sotropic phase
I'	Cybotactic **I**sotropic phase
$^{\circ}C$	Degree Centigrade
ITO	**I**ndium **T**in **O**xide
dc, DC	**D**irect **C**urrent
ac, AC	**a**lternating **c**urrent
E	**E**lectric field
T	**T**emperature
T_{N-I}	transition **T**emperature from the **N**ematic phase to the **I**sotropic phase
n	refractive index

S	S order parameter
D	D order parameter
P	P order parameter
C	C order parameter
PEM	**P**hoto **E**lastic **M**odulater
IR	**I**nfra **R**ed
POM	**P**olarized **O**ptical **M**icroscopy
C_n, C_2	n (2)-fold rotational symmetry group
C_{nh}	C_{nh} symmetry group
D_n, D_2	n (2)-fold rotational symmetry and flipping symmetry group
D_{nh}	D_{nh} symmetry group
p	**p**itch
q	wave vector
α	polarizability
λ	wavelength of light
β	angle between molecular dipole moment and long axis
β'	angle between transition dipole moment and long axis
β''	angle between transition dipole moment with respect to the cluster normal
ϵ, ϵ', ϵ''	dielectric susceptibility, real part, imaginary part of
θ_V	bending angle between two arms of a bent-core mesogen
θ'	tilt angle of molecules in the cluster
Γ	retardation
Φ	azimuthal angle
μ	dipole moment
S_0, S_1, S_2, S_3	the *Stoke parameters*
Q	scattering vector
g	the Kirkwood correlation factor
MFA	**M**olecular **F**ield **A**pproximation
T	*T*esla, the unit of magnetic field strength

List of Publications

1. Yun Jang, Vitaly P. Panov, Antoni Kocot, J. K. Vij, A. Lehmann, C. Tschierske, *"Optical confirmation of biaxial nematic (N_b) phase in a bent-core mesogen"*, **Applied Physics Letters**, **95**, 183304, (2009).

2. Yun Jang, Vitaly P. Panov, C. Keith, C. Tschierske, J. K. Vij, *"Sign reversal in the dielectric anisotropy as functions of temperature and frequency in the nematic phase of a bent-core mesogen"*, **Applied Physics Letters**, **97**, 152903, (2010).

3. Yun Jang, Vitaly P. Panov, A. Kocot, A. Lehmann, and C. Tschierske, and J. K. Vij, *"Short-range correlations seen in the nematic phase of bent-core liquid crystals by dielectric and electro-optic studies"*, **Phys. Rev. E**, **84**, 060701, (2011).

4. Yun Jang, Vitaly P. Panov, C. Tschierske and J. K. Vij, *"Dielectric and optical studies of cybotactic nematic phase: in terms of the cluster model."*, (in preparation)

5. Yun Jang, C. Tschierske and J. K. Vij, *"Chirality observed in the nematic phase of an achiral bent-core mesogen"*, (in preparation)

List of Presentations

1. Yun Jang, Vitaly P. Panov, Antoni Kocot, J. K. Vij, A. Lehmann, C. Tschierske, *"Optical confirmation of biaxial nematic (N_b) phase in a bent-core mesogen"* **accepted in the 23nd International Liquid Crystal Conference, ILCC 10, Krakow, Poland**, P-1/ 99/528 (2012).

2. Yun Jang, J. K. Vij and C. Tschierske, *"In- Plane Switching of a Bent-Core LC(PAL1) with Negative Dielectric Anisotropy in the Homeotropic Cell"*, **The 17th International Display Workshops, IDW 10, Fukuoka, Japan**,LCT3 - 4L (2010).

Part. I

Introduction and Experimental techniques

Chapter 1

Introduction

"In this chapter, *the fundamentals of liquid crystals, and theoretical and mathematical tools required to realize the subject matter of this work are described.* "

1.1 Preface

We cannot live a day without watching displays. Displays are prevailent in our everyday life as a part of window to the world connecting people to people. Presently, LC (Liquid Crystal) technologies are leading the current display industry by replacing CRT (Cathode Ray Tube) technology which had dominated almost half a century before the emergence of LCD (Liquid Crystal Display). As in all other areas of science, such a great success of LCD is due to understanding and academic achievement in the liquid crystal field which have been advanced originally by inspiration from several pioneering scientists and subsequently by the contributions, small or large, by many other scientists inspired by the previous discoveries. At this moment, many scientists and engineers in the industrial as well as the academic field are researching for new types of LC technologies able

to overcome the limitations of conventional LCDs. For a better LCD, it is essential to accumulate understandings of new types of liquid crystals and to improve performance of the devices using the LCs. This thesis also, building on the basis of the efforts of many other scientists, focuses on a small part of the liquid crystal field; the cybotactic nematic phase. The term, cybotactic, is originally used in solution chemistry to describe the region around a solute molecule (the cosphere) in which the solvent molecules are more ordered. This term was introduced by de Vries in the liquid crystal field [1, 2], where it means an assembly of molecules in a nematic mesophase that is arranged in a short-range smectic-like array. This relatively elusive phase is observed predominantly in a number of bent-core mesogens in the entire nematic phase [3]. This thesis reports the relationship between molecular structure and the emergence of the phase, along with the physical observations, through various experimental methods and a theoretical model for this phase. The thesis consists of ten chapters, and for convenience, the chapters are grouped into 5 parts.

Part. I (Chap. 1 and 2) provides an Introduction and describes the experimental methods used.

Chapter 1 is the introduction, which briefly outlines the basic concepts of liquid crystals with various molecular shapes and their various phases, the physical properties, and describes some mathematical expressions necessary to understand the subject matter of this work. Further detailed discussion and additional theoretical background will be introduced in each part for better understanding. However, this may not suffice either to give a full introduction to the field of bent-core liquid crystals or to provide the requisite mathematical and theoretical background for the subject matter described in this work. Those describing a broad overview of bent-core LCs or a deeper and more detailed theoretical overview of the areas covered by this thesis are referred to [4, 5] for a summarized review of general topics in bent-core liquid crystals, and to references [6] and [7] for a profound understanding of general topics of liquid crystals.

Chapter 2 briefly introduces experimental methods used for the studies.

Specifically, this chapter deals with a PEM (Photo elastic modulator) which is used to investigate birefringence as well as reorientation of the minor director in the biaxial nematic phase (Chap.8). This PEM system was mainly set up by Dr Panov who is an expert in the optical experiments.

Part. II (Chap. 3 and 4) deals with the relationship between molecular structure and the cybotactic clusters in terms of X-ray analysis done by the Halle group and the cybotactic model by Photinos *et al.* .

In **Chapter 3**, the materials under study and the results of X-ray experiments done by the Halle group will be introduced and interpreted as the presence of the cluster in the nematic phase. Another interpretation regarding similar phenomena was reported by Kumar and coworkers. This controversy stimulated us to study these works, because most of quantitative analyses regarding the cybotactic cluster are based on the interpretation of X-ray results. We investigate the same materials by dielectric and optical methods. These materials were previously investigated by X-ray. In **Chapter 4**, the cluster model will be introduced. This model was proposed by Photinos and coworkers [8–10] and is a key to explain a macroscopic biaxiality of nematic mesogens under an external stimulus such as the anisotropic anchoring condition, an electric or a magnetic field.

In Part. III (Chap. 5 and 6), the dielectric and optical behavior of the materials is studied in terms of the cluster model.

In **Chapter 5**, theoretical background of dielectric properties of LCs is introduced. Dielectric properties of nematic LCs are one of the most important features for application to electro-optic switching. Here, we address the behavior in terms of Meier Maier and Maier-Saupe models. The Maier-Saupe model is based on the molecular mean field theory. Experimental results and the interpretation of the materials are presented. We shall compare the results from the X-ray experiment to those of dielectric experiments and these will be discussed. As a result, the conclusion is made that the presence of the clusters in the nematic phase of bent-core mesogens is evidenced by dielectric studies. The unusual physical behavior of

cybotactic LCs in the nematic phase needs to be investigated through other techniques. In **Chapter 6**, optical contrast spectroscopy using *Fredriks transition* is used for investigating crossover frequency and in turn the result will be compared with a relaxation frequency measured by dielectric spectroscopy. Temperature dependence of birefringence for the materials is measured which is converted to macroscopic order parameter and used for investigating the possiblity of the conformational change. The order parameter obtained by the optical technique is combined with the results from IR (Infra Red) experiments, which give information about molecular parameters such as the tilt of molecules in the cluster. The results are interpreted in terms of the cluster model.

In Part. IV (Chap. 7), Chirality and Biaxiality of nematic phase are investigated .

In **Chapter 7**, the chirality of one of the materials is presented. So far, the chirality of an achiral bent-core mesogen has been observed as a type of self assembly of achiral bent-core mesogen. We observe another mechanism which gives rise to chirality. This also can be interpreted in terms of a simplest cluster composed of two bent-core mesogens. In **Chapter 8**, the electro optical behavior of biaxial nematic phase is investigated under the various anchoring conditions and electrode structures.

In Part. V (Chap. 9 and 10 Appendix), Application to the device and Possibilty.

In **Chapter 9**, the application of the the phases is reviewed and the possiblity will be discusssed. **Chapter 10** contains a summary of the results and the conclusions of this thesis.

1.2 What is a Liquid Crystal?

The liquid crystalline phase is a state of matter. The mechanical properties and the symmetry properties of liquid crystals are intermediate between those of an isotropic liquid and of a crystalline solid. The fluidity of a liquid crystal resembles that of a liquid while other anisotropic properties such as the birefringence and order are more similiar to those of a solid. For this reason, other words 'mesophase' or 'mesomorphic phases' (mesomorphic: of intermediate form) [6] is used to call it. In order to understand the nature of liquid crystals, it is useful to recall the difference between a crystal and a liquid. In crystals, the centers of mass of the molecules are located on a three-dimensional periodic lattice. However, such centers of mass are not ordered in liquids but are distributed isotropically to be fluid. This fluidity is at the expense of long range positional order and results in different X-ray diffraction patterns; while X-ray diffraction patterns in crystals show sharp Bragg reflections characteristic of the lattice, those in liquids exhibit only diffuse peaks. In liquid crystals, some degree of anisotropy is present, which gives rise to some sort of additional X-ray diffraction patterns. The anisotropy in a liquid crystal, that is, the degree of ordering of the molecules, may vary depending on several factors. The first possibility is that there exists only orientational order, but no positional order. This corresponds to a nematic liquid crystal phase. The second possibility is one-dimensional positional order, which means a two-dimensional freedom. The phase consists of a set of two-dimensional liquid layers stacked on each other. This corresponds to the case of smectic liquid crystals. The third possibility is two-dimensional ordering, which corresponds to the columnar phases. Thus the most important feature of liquid crystals is the degree of ordering (as quantified by order parameters). Besides the above definition of liquid crystals, there is another important classification of liquid crystals; thermotropic and lyotropic mesophases. The latter mesophase is formed by dissolving an amphiphilic mesogen in suitable solvents, under appropriate conditions of concentration and temperature in which the order parameters depend on the concentration of the solution. The former is a mesophase formed by heating a solid

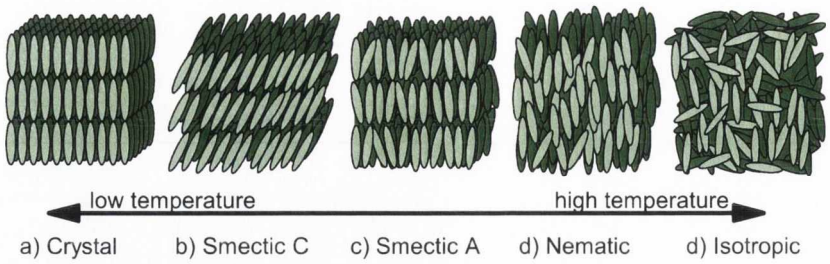

Figure 1.1: Schematic of phases.

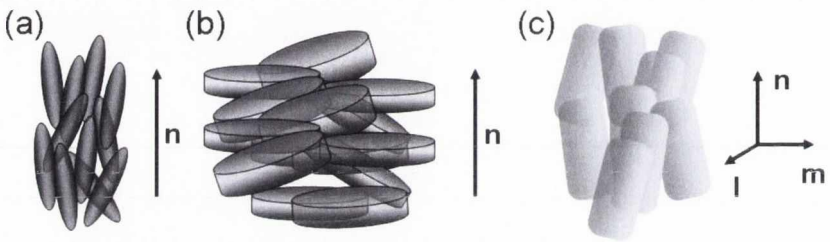

Figure 1.2: The representative schematics of three different nematic phases composed of different shaped molecules; the uniaxial nematic phases with positive birefringence (N_u^+) and negative birefringence(N_u^-) are composed of rod like molecules and disc like molecules respectively. A biaxial nematic phase((N_b) is composed of board like molecules with orthorghmbic(D_{2h} symmetry.)

or cooling an isotropic liquid, or by heating or cooling a thermodynamically stable mesophase. The order parameters of thermotropic mesophases depend strongly on temperature. Therefore, in the thermotropic liquid crystals, the sequence of liquid crystalline phases is controlled by the temperature. A typically simplified phase sequence from high to low temperatures of thermotropic liquid crystals having rod-like molecular shape is isotropic - nematic - smectic A - smectic C - crystal as shown in Fig. 1.1. The word 'smectic' derives from the Greek 'smegma' meaning soap-like, or layered structures. Actually, soap itself has a thin layered structure and is a smectic liquid crystal. The word 'nematic' comes from the Greek word 'nema' meaning thread - referring to the typical type of defects visually observed in the nematic phase, which usually constitute a uniaxial medium with non-polar symmetry. The nematic phase may be uniaxial (calamitic and discotic) and biaxial, as shown in Fig. 1.2.

1.3 Molecular structure and the phase behavior.

The molecular structure of a liquid crystal is found to have a significant influence on its properties and on its phase behavior. The typical structure of a calamitic mesogen consists of a rigid core containing several substituents and one or two flexible terminal groups. The core moiety plays the key role in creating the anisotropy for the formation of the liquid crystalline phase while the phase is stabilized by the terminal chain/chains which in turn reduce the stability of the crystalline phase. In calamitic phases which include nematic and smectic phases, and their chiral analogues, the rod shaped molecules are predominantly aligned along a single direction called a director defined by a unit vector, **n**. Such a concept has been extended to disc-shaped and V-shaped mesogens (bent-core mesogens, BCMs) which have taken their place in the hierarchy of structures. Discotic phases (nematic and columnar) and banana phases (B1 to B7) have been interpreted in terms of the molecular shape of the mesogens. Along with the typical calamitic LCs, most of liquid crystal-forming molecules (mesogens) contain flexible groups and can have an infinite number of different conformations. These exist in fast equilibrium under experimental conditions. Such internal degrees of freedom can also be allowed in mesogens with a flexible core part by reorientation about single bonds, rotational isomerisation about carbon-carbon bonds, inversion at a nitrogen atom, and so on. It is worth pointing out that if the stability of a mesophase is affected by anisotropic molecular shape, intramolecular structural changes allowed in the mesophase can also be influenced by either the type or orientational order of mesogens in the phase. Such a complicated behavior has been observed in dimers in which the two mesogenic groups are linked by a flexible chain [11, 12]. It is notable that the extent of the flexibility of a dimer is crucial for creating an anisotropic shape of the molecule by conformational change. As mentioned above, in a usual calamitic mesogen, the terminal flexible chain/chains are attached to an end of a core moiety of the mesogen. The usual reason for attaching such flexible chains is to enhance the thermodynamic stability of fluid phases at the expense of solid phases, so that liquid crystalline mesophases may be observed. The properties of the

mesogens in terms of optical or dielectric response are only influenced to a limited extent by the presence of attached flexible chains, though the phase behavior is often altered in a progressive manner with increasing chain length as the tendency for micro-phase separation of flexible and nonflexible molecular moieties develops. However, in the case of a dimer, the flexible part is confined by two mesogenic groups and this flexible part alters the relative orientation of the mesogenic groups within the molecule. Such a flexibility of the molecule in the mesophase gives rise to unusual phase behavior [11, 13]. The type of the core part such as V-shape also plays an important role in creating the elusive phase behavior of the mesogen [4, 5]. From the viewpoint of the molecular structure, one of most representative features of BCM (bent-core Mesogen)s is a bending angle (θ_V) defined as the angle between two arms of a BCM. Luckhurst [14] predicted a relationship between θ_V and the stability of nematic phases. For the linear shape, the system only forms a uniaxial nematic (N_u) phase as do the usual calamitic mesogens. With θ_V decreasing, the region of N_u in the phase diagram decreases and that of the biaxial nematic phase (N_b) increase up to an angle of 109.5 ° and decreases below an angle of 109.5 °. This means that this class of molecular structures determined by θ_V is between rod-like (calamitic) and disc-like mesogens as shown in Fig. 1.3. As θ_V changes, then their resulting structures embrace those of both rod-like and disc-like mesogens. Consequently, it is no surprise then to find that the liquid crystal phases of bent-core molecules include calamitic nematic and smectic phases as well as columnar phases. Besides, the BCMs have received special attention, not only due to unique phase behaviors, but also due to the unusual properties, such as amplification of chirality [4, 5], and a formation of tetrahedratic nematic phase [16, 17]. Recently, Keith *et al* [18] reported interesting results and interpretations regarding relationship between molecular structure and the presence of SmC like nanostructure, termed by de Vries as cybotactic clusters. According to the X-ray studies done by the authors [18], the phase behavior and X-ray patterns of homologous series of bent-core mesogens show strong dependency on the length of terminal groups. Thus the materials are classified into two categories in terms of the presence of cybotactic cluster. Such cybotactic clusters are commonly observed

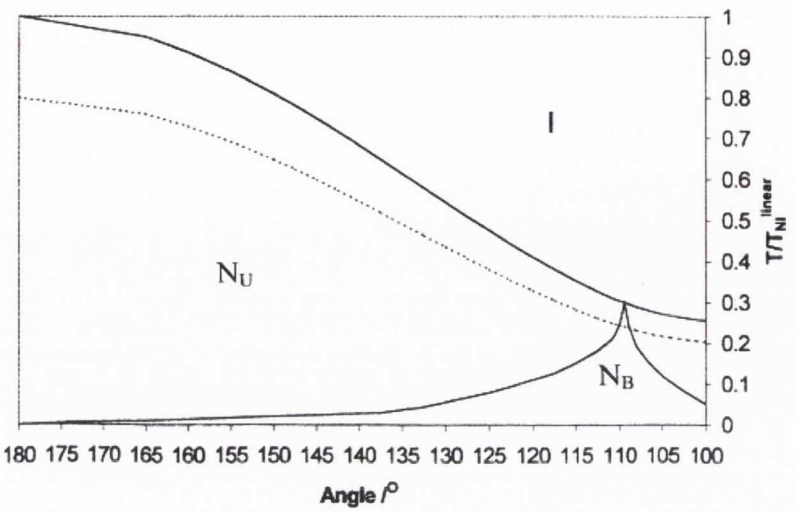

Figure 1.3: Phase diagram of a bent-core mesogen as a fuction of the bending angle(Θ_V). This phase diagram was predicted by Luckhurst *et al.* [14, 15] on the basis of molecular field theory. The N_b phase of a bent-core mesogen without transverse dipole takes place around around 109.5° of Θ_V. The dashed line indicates the freezing point which is taken to occur at a reduced temperature of 0.8. Redrawn from Ref. [14].

not only as pretransitional effects [19] of a lower temperature smectic phase in calamitic nematic liquid crystals, but also as stable structural features over wide temperatures [20–24]. The formation of clusters is considered as a key model for an interpretation of a non spontaneous biaxial nematic phase [25]. According to the cluster model [8], a nematic phase consists of biaxial and possibly polar micro-domains, each of which is occupied by a cluster of intimately correlated molecules whose relative ordering defines a set of local directors. In the absence of either external aligning fields or anisotropic surface anchoring, the primary directors of these clusters can be spontaneously ordered along a common direction **n**, whereas their transverse directors are randomly distributed, thus forming a macroscopically uniaxial state. Under the external stimulus, this state can acquire macroscopic biaxial ordering [26]. Consequently, the macroscopic phase behavior arises from the collective alignment of the directors of the clusters. The term, cybotactic nematic is used herein for the uniaxial nematic phase with the clusters. Fundamentally, cybotactic nematic phases of SmA-type (N_{cybA}), where the clusters have a SmA-like structure, and the skewed cybotactic nematic phase, composed

of SmC-like clusters (N_{cybC}), can be distinguished. SmA-type cybotactic clusters are locally uniaxial. However, more complex is the situation for N_{cybC} phases as the SmC type clusters are intrinsically biaxial due to the tilt of molecules within the cluster layer. Therefore an identification of the cluster species is also important in understanding phase behavior of the cybotactic nematic phases. The work described in this thesis is mainly focused on the cybotactic nematic phase composed of bent-core molecules which have a V-shaped mesogenic group, in other words have a bent-core.

1.4 Order parameters

The axis of the preferred orientation of the molecules is usually characterized by a unit vector $\mathbf{n}$ known as the director. $\mathbf{n}$ has the usual vector properties except that it satisfies the physically reasonable condition $\mathbf{n} \equiv -\mathbf{n}$. The director determines only the axis of the preferred orientation of the molecules and has nothing to do with the degree of orientation. The degree of orientation is described by the order parameter. The simplest form of order parameter is written as

$$S = \frac{1}{2}\left\langle 3\cos^2\theta - 1 \right\rangle, \tag{1.1}$$

where θ is the angle between the long axis of an individual molecule and the director. S represents the degree of orientation of the molecular long axis in nematic ordering, and is suitable for representing the ordering of nematic liquid crystals. The ordering of a biaxial phase or the ordering of impurity molecules in nematics cannot be represented by Eqn. (1.1), and requires a tensor order parameter. The simplest second rank tensor order parameter in diagonalized form can be written as [27]

$$S_{ij} = \left\langle \frac{1}{2}(3l_i l_j - \delta_{ij}) \right\rangle, \tag{1.2}$$

where l_i is the direction cosine of the director with respect to a molecular axis i. Equation (1.2) is referred to the Saupe ordering matrix. The non-zero components of this tensor in polar coordinates are

$$\begin{aligned} S_{xx}^{X} &= \left\langle \frac{1}{2}(3\sin^2\theta\cos^2\phi - 1) \right\rangle, \\ S_{yy}^{Y} &= \left\langle \frac{1}{2}(3\sin^2\theta\sin^2\phi - 1) \right\rangle, \\ S_{zz}^{Z} &= \left\langle \frac{1}{2}(3\cos^2\theta - 1) \right\rangle, \end{aligned} \tag{1.3}$$

where θ and ϕ are the Euler angles for the director in the x, y, z system described in Fig. 1.4. Eqns. (1.2) and (1.3) are sometimes useful to express the molecular distribution function, but it also expresses only uniaxial orderings of each molecular axis. For example, S_{xx} represents the extent to which x axes of molecules are aligned along a direction. However, with these order parameters, we cannot describe whether the fluctuation of the x axis of a molecule is isotropic or hindered. Therefore, we need a better expression of the order parameter for the biaxial phases. The tensor representation can be extended to describe the orientational ordering of biaxial molecules in a biaxial phase by introducing a fourth rank ordering tensor [7, 28]. Following the notation used in reference [7],

$$S_{\alpha\beta,ij} = \left\langle \frac{1}{2}(3l_{i,\alpha}l_{j,\beta} - \delta_{ij}\delta_{\alpha,\beta}) \right\rangle, \tag{1.4}$$

where $l_{i,\alpha}$ is the cosine of the angle between the molecule axis α and the laboratory or phase axis i. By a suitable choice of coordinates without loss of generality, the 81 components of $S_{\alpha\beta,ij}$ can be reduced to nine such that $i = j$ and $\alpha = \beta$. This is equivalent to defining three diagonal Saupe ordering matrices, one for each of the three axes, $i = X, Y, Z$.

$$S_{\alpha\alpha}^{(i)} = \left\langle \frac{1}{2}(3l_{i,\alpha}^2 - 1) \right\rangle, \tag{1.5}$$

Taking the diagonal component of these three matrices allows the construction of a 3×3 matrix.

$$S_{\alpha\alpha}^{(i)} = \begin{pmatrix} S_{xx}^{X} & S_{yy}^{X} & S_{zz}^{X} \\ S_{xx}^{Y} & S_{yy}^{Y} & S_{zz}^{Y} \\ S_{xx}^{Z} & S_{yy}^{Z} & S_{zz}^{Z} \end{pmatrix}, \tag{1.6}$$

Note that x, y and z are the molecular axes, and X, Y and Z are the laboratory or the phase axes. Hence, for example, S_{yy}^{X} represents the extent to which the y axis of molecules aligns along the X axis in the laboratory coordinate system. The generalized biaxial order parameters can be defined as follows. The long axis ordering is described by $S = S_{zz}^{Z}$, which is the same as Eqn. (1.1) and S_{zz} in Eqn. (1.3). The phase biaxiality for a uniaxial molecule is given by $P = S_{zz}^{X} - S_{zz}^{Y}$, which represents the anisotropic fluctuation of the molecular long axis in the laboratory coordinate, hence it is connected to the macroscopic phase biaxiality. For biaxial molecules in a uniaxial phase the biaxial order parameter is $D = S_{xx}^{Z} - S_{yy}^{Z}$, which represents the anisotropic fluctuation of molecular short axes x and y along the laboratory Z axis. D does not represent the phase biaxiality. It is also possible to define a biaxial order parameter with respect to the X and Y axes, such that $D' = S_{xx}^{X} - S_{yy}^{X}$, and $D'' = S_{xx}^{Y} - S_{yy}^{Y}$. Another biaxial order parameter $C = D' - D''$ represents a phase biaxiality induced by the hindered rotation around the molecular long axis. Thus, S, P, D and C describe the full set of the order parameters for a biaxial molecule. These order parameters are also defined using Euler angles (see Fig. 1.4) as

$$\begin{aligned} S &= S_{zz}^{Z} = \left\langle \frac{1}{2}(3\cos^2\theta - 1) \right\rangle, \\ D &= S_{xx}^{Z} - S_{yy}^{Z} = \left\langle \frac{3}{2}(3\sin^2\theta\cos 2\psi) \right\rangle, \\ P &= S_{zz}^{X} - S_{zz}^{Y} = \left\langle \frac{3}{2}(3\sin^2\theta\cos 2\phi) \right\rangle, \\ C &= (S_{xx}^{X} - S_{yy}^{X}) - (S_{xx}^{Y} - S_{yy}^{Y}) \\ &= \left\langle \frac{3}{2}\left[(1+\cos^2\theta)\cos 2\phi\cos 2\psi - 2\cos\theta\sin 2\phi\sin 2\psi\right] \right\rangle, \end{aligned} \tag{1.7}$$

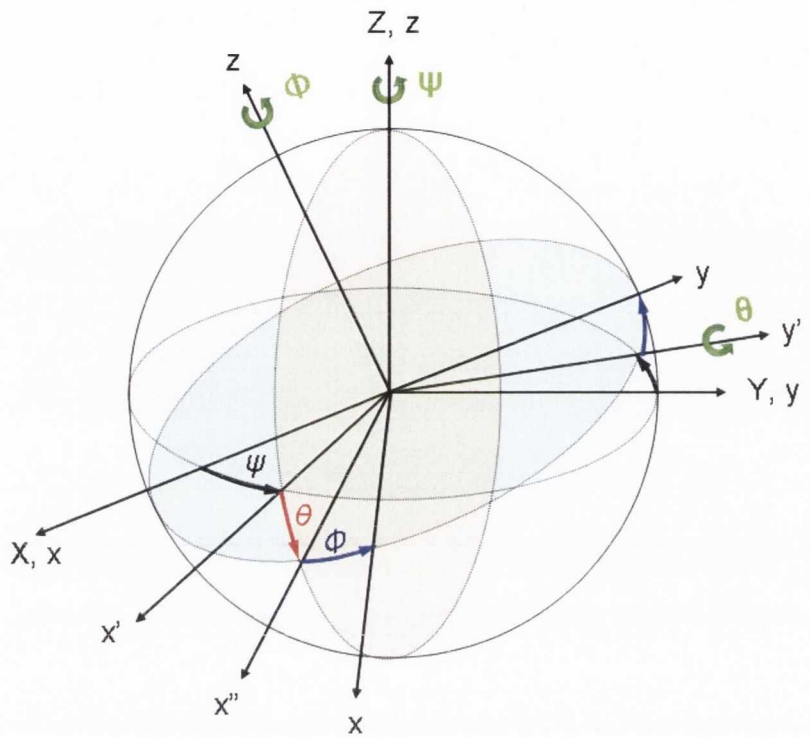

Figure 1.4: Euler angles

These order parameters are useful for connecting the microscopic molecular properties to the macroscopic phase properties.

1.5 Group symmetry and chirality

Point group symmetry is an important property of molecules and is widely used in some branches of physical science: spectroscopy, quantum chemistry and crystallography. It describes the geometric, conformational and configurational properties of the material. This symmetric feature is associated with physical properties of the molecules and the phase composed of them. There are many mathematical groups in the rotational and the reflectional symmetry [29]. Schönflies notation commonly used in liquid crystals is introduced. Rotational symmetry of order n, also called n-fold rotational symmetry means that rotation by an angle of

$360°/n$ (180°, 120°, 90°, 72°, 60° *etc.*) does not change the object. Reflection symmetry, or mirror symmetry is a symmetry with respect to reflection. The notation C_n corresponds to n-fold rotational symmetry along a fixed axis. D_n consists of the n-fold rotational symmetry operations in C_n together with the flipping symmetry operations along the axis perpendicular to the rotational symmetry axis, that is, the object having D_n symmetry operation is invariant under the up-side down flipping. In addition to this, one may add a mirror plane perpendicular to the axis of rotational symmetry, which produces the additional groups C_{nh} and D_{nh} respectively. If the n-fold rotational symmetry axis also has n-mirror planes containing the axis, it produces C_{nv}. The D_{nd} or D_{nv} group has vertical mirror planes containing the main rotation axis, but instead of having a horizontal mirror plane it has an isometry which is the combination of a reflection in the horizontal plane and a rotation by an angle $180°/n$. The geometric schematics of each groups is shown in Fig. 1.5.

Chirality is a property of asymmetry important in several branches of science. The word chirality is derived from the Greek, $\chi\epsilon\iota\rho$, "hand", a familiar chiral object. An object or a system is chiral if it is not identical to its mirror image, that is, it cannot be superposed onto it. A chiral object and its mirror image are called enantiomorphs (Greek opposite forms) or, when referring to molecules, enantiomers. A non-chiral object is called achiral (sometimes also amphichiral) and can be superposed on its mirror image. Therefore, a chiral object does not have a mirror plane or a center of inversion. The Neumann principle (named after Franz Neumann) states that any physical property of a medium must be invariant under the symmetry operations of the point group of the medium [29]. Fundamentally, chirality can occur on three levels in the liquid crystal phases [5]. The first level is the chirality of the molecule, which is configurational and conformational in nature. Configurational chirality is based on the connectivity of atoms and groups via covalent bonds and in most cases is stable at the temperature and time scale of usual experiments. Conformational chirality is due to a rotation around covalent bonds. Whether these conformers are stable or not also depends on temperature and time scale. Standard organic molecules have an infinite number of different

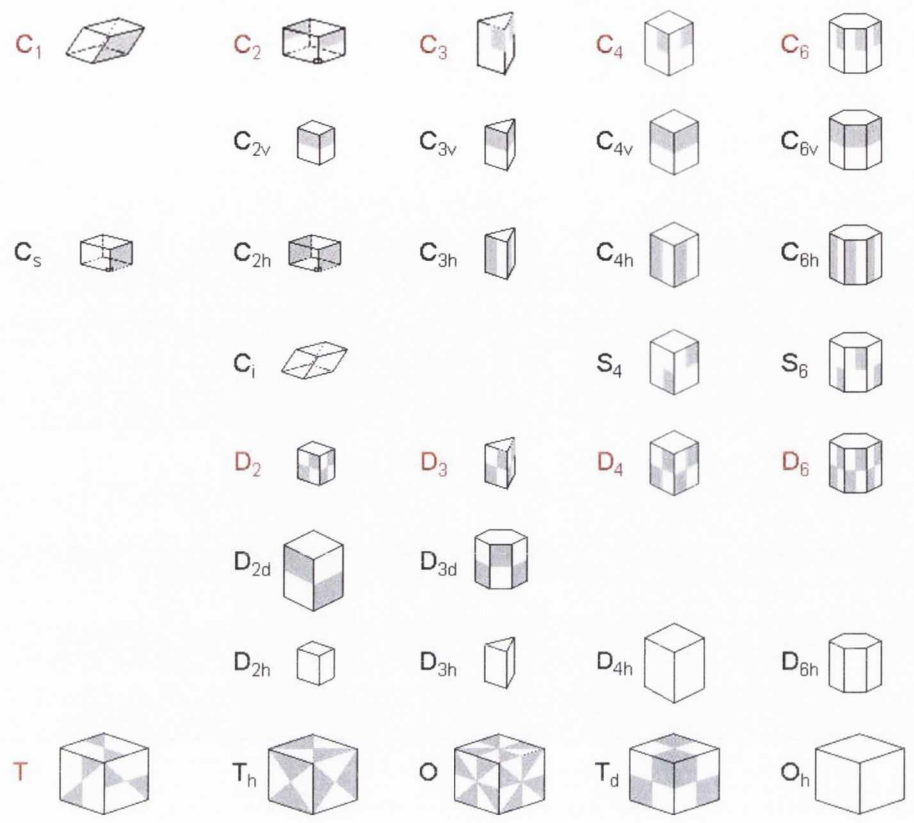

Figure 1.5: Schematics of Symmetry in solid unit cells. Ref [30]

chiral conformations, which exist in a fast equilibrium under normal experimental conditions. The second level of chirality arises from the organization of molecules with formation of chiral structures via non-covalent interaction. In liquid crystals, for example, chiral molecules organize into a helical superstructure in nematic or smectic phase. This chirality is due to the specific shape of macroscopic objects. It should be pointed out that a lower level of chirality may influence the higher level chirality due to diastereomeric relations which makes one combination energetically more favorable than the other, but it is not required for chirality occurring at a higher level. For example, even though a bent-core mesogen is configurationally achiral, whereas the banana phase can be chiral. In this case the helix sense can be either right or left with a probability of 1 : 1. In terms of chirality, the point groups can be classified into chiral and achiral groups. The symmetry groups possessing chirality of 32 groups in Fig. 1.5, are C_n, D_n and T groups without a mirror plane or a center of inversion, while the symmetry groups with polarity

are groups without center of inversion. We find that nematic and SmA is $D_{\infty h}$ group since these have a symmetry axis parallel to the director and infinite C_2 axes perpendicular to the director.

Chapter 2

Experimental Methods

"In this chapter, *various experimental techniques are used for the investigation of the phase. Along with brief introduction made to the techniques, the principle of PEM system is introduced in more details. In this thesis, a single PEM system is used to meausre the optical parameters of samples. "*

2.1 Introduction

In order to investigate the possible mechanisms for the phase behavior under study, complementary techniques are used in this thesis. In chapter 3, X-ray experiments and their interpretation will be introduced, which were carried out by the Halle group. In Chap. 5, dielectric experiments are carried out to investigate the relationship between the structure and the correlation factors associated with the short range interaction between the molecules. The dielectric spectra are recorded for both homeotropic and planar cells using Novocontrol Gmbh, Germany, dielectric analyzer. Cells for dielectric experiments were prepared by using two low resistance-ITO (Indium Tin Oxide) glass plates (20 $\Omega/\square$), coated with

polymer alignment layers corresponding to planar and homeotropic anchoring surface conditions. These cells are also used for the optical investigation using a POM. The results of dielectric experiments using brass electrodes are consistent with the result of cells made of low resistance ITO glass in the window of frequency range. Therefore, we can use the low resistance ITO glasses as substrates for the dielectric and optical experiments. In Chap. 6, three optical techniques are used. Firstly, in order to confirm the phenomenon of sign reversal in $\Delta\epsilon'$, measurements using optical contrast spectroscopy are carried out [31]. While the planar cell used in dielectric experiments is cooled from the isotropic to the nematic phase, the transmittance of cells between cross polarizers is measured and recorded as a function of frequency and temperature. This method is very effective in determining threshold voltage (V_{th}) and the sign of dielectric anisotropy ($\Delta\epsilon'$) [31]. Secondly, the measurements of birefringence are carried out. The temperature dependent birefringence gives information related to anisotropic shape of the molecules as well as the orientational order parameter. Finally, a technique of IR spectroscopy is also used for examining the molecular conformational behavior [32], and used for investigating the macroscopic properties and the microscopic tensor order parameters [32, 33]. IR spectroscopy is used to characterizing vibrational bands. The infrared spectra of the materials under homeotropic anchoring conditions are measured as a function of the polarizer rotation angle and recorded using a Bio-Rad FTS-6000 spectrometer with a resolution of 1 cm^{-1}. These spectra are averaged over 64 scans. An IR-KRS5 grid polarizer is used to polarize the IR beam. The sample for the IR experiment was aligned in between two KBr windows that are coated with a homeotropic polymer alignment layer. Thickness of the cells can be assumed approximately to be the thickness of the film type spacers (10 μm) which were also used in the dielectric and the optical cells. The texture of the sample was monitored using a polarized optical microscope (POM) that was used for identifying the phase prior to its investigation by polarized IR spectroscopy. In Chap. 8, a Photo-Elastic Modulator (PEM) based system is used for the optical investigations of a liquid crystal in its biaxial nematic phase. It provides simultaneous measurements of both the retardation (Γ) and the azimuthal angle (Φ)

(defined as the angle between the optic axis of the cell and the polarizer). Red light LED is used as the source with a corresponding 632.8 nm narrow-band optical filter. Commercially available ITO coated planar glass cells (E.H.C., Japan) with a 2.5, μm cell gap were used for the experiments. Most of the techniques used in this thesis are commercially available. The detailed information of the apparatus used is listed as below:

i) Microscopy and electro-optic measurement

• **Optical Microscope:** Olympus BX-52 (Olympus Company), including the objective lens (Olympus, LM PlanFI, 50X / 0.5NA), the condenser (Instech, 0.65 NA), and Leica DFC480 (Leica, Digital camera for microscope)

- http://www.olympusfluoview.com/brochures/pdfs/bx52.pdf

- http://www.leica-microsystems.com/

ii) IR and Visual Spectroscopy for investigating macroscopic order parameter and molecular orientation [34, 35].

iii) PEM (photo-elastic modulator) system for measuring birefringence and azimuthal angle [36, 37],

• **Photo-Elastic Modulator (PEM) system:** PEM modulator (HINDS Instruments)

- http://www.hindsinstruments.com/PEM_Components/products/default.aspx

- see also references [36, 37] for applications.

iv) Dielectric response measurement using a broadband high resolution dielectric spectrometer (Novocontrol GmbH, Germany) [38, 39].

• **Broadband dielectric spectrometer:** This system includes Alpha-A High Performance Modular Measurement System (Novocontrol GmbH, Impedance analyzer, $3\times10^{-5} - 2 \times 10^{7}$ Hz), Agilent 4291B RF Impedance/Material Analyzer (Agilent, $1 \times 10^{6} - 1.8 \times 10^{9}$ Hz) and Quatro Cryosystem (Novocontrol GmbH, temperature controller, $-160 - +400$°C). Analysis software, WINFIT (Novocontrol GmbH, software) is required.

- http://www.novocontrol.de/

- http://www.home.agilent.com/agilent/home.jspx

• **Optical Spectrometer:** Lambda 900 UV/VIS/NIR spectrometer (PerkinElmer,

broadband high resolution spectrometer), and Avaspec-2048 (Avantes, fast fiber optic spectrometer).

- http://www.perkinelmer.com/default.htm

- http://www.avantes.com/ The experimental techniques mentioned above are very useful to investigating the properties of liquid crystals, but details of commercial methods are briefly summarised.

In this chapter, a PEM system is introduced in more detail, as it is helpful in understanding the general concepts of LC optics. The PEM [40] is a device that exploits the photoelastic effect to produce a phase retardation with a highly precise sinusoidal time variation. This can be used to modulate the polarization state of a light beam. A PEM system used in this thesis adopt a single PEM, used for the investigating the major directors as well as the minor directors of a biaxial nematic phase. The PEM components produced by HINS instruments are used in the PEM system designed by Dr V. P. Panov,.

2.2 Polarization of optical waves

Many birefringent optical systems including liquid crystal cells are made of anisotropic layered media that consist of a train of polarizers and crystal plates. The effect of each individual element on the polarization state of the light beam can be easily pictured without the aid of any matrix algebra. However, when an optical system consists of complex structures of optical components such as a twisted or deformed liquid crystal cell, the calculation of the transmission becomes complicated and it is greatly facilitated by a systematic approach. Mainly, the transmittance of a cell is determined by the polarization state of the light passing through the optical system, on the assumption that scattering and the absorption of light in the medium can be neglected. For mathematical simplicity, the monochromatic plane wave is often written as

$$E = A\exp[i(\omega t - \mathbf{k}\cdot\mathbf{r})] \tag{2.1}$$

Here $f\mathbf{k}= n\omega/c$ is the constant of propagation, n is the refractive index of the media and c is the velocity of light. $\boldsymbol{r}$ represents the coordinate vector of the given point of space and t designates the time. The time evolution of the electric field vector is exactly sinusoidal: that is, the electric field must oscillate at a definite frequency ω. The polarization state of a beam of monochromatic light is specified by its electro field vector $E(\boldsymbol{r},t)$. For the purpose of describing various representations of the polarization states, we consider a propagation of a light beam along the Z axis. Because it is a transverse wave, the components of the electric field vector can be given [41] as:

$$E_x = A_x \cos(\omega t - kz + \delta_x) \tag{2.2}$$

$$E_y = A_y \cos(\omega t - kz + \delta_y), \tag{2.3}$$

where we have used two independent and positive amplitudes A_x, A_y and added two independent phases δ_x, δ_y to reflect the mutual independence of the two components. A beam of light is said to be elliptically polarized if the curve traced by the endpoint of the electric field vector is an ellipse (in the xy plane) (see Fig. 2.3). This is the most general case of a polarized beam of light. At a given point in the space ($z = 0$), the equation of ellipse can be given by:

$$\left(\frac{E_x}{A_x}\right)^2 + \left(\frac{E_y}{A_y}\right)^2 - 2\frac{\cos\delta}{A_x A_y} E_x E_y = \sin^2\delta. \tag{2.4}$$

Here we can define relative phases as $\delta = \delta_y - \delta_x$, which is also called the retardation. If δ is nπ, here n is an interger, Eqn. (2.4) becomes linear. If δ is (2n + 1)$\pi/2$, Eqn. (2.4) becomes circle. Therefore the ellipticity of the polarization ellipse is affected by δ. The ellipticity angle θ and the inclination angle ϕ defined as $\tan^{-1}$ $= \pm\frac{b}{a}$ are also determined by δ and ψ defined as the azimuthal angle of osillation direction with respect to the x axis. a and b are semi-major and semi-minor axes of the ellipse, respectively (see Fig. 2.3(b)).

$$\tan 2\phi = \tan 2\psi \cos\delta \tag{2.5}$$

$$\sin 2\theta = -\sin 2\psi \sin\delta \tag{2.6}$$

This relatively complicated expression of a polarization state can be simplified by the Jones vector which is introduced in 1941 by R.C Jones [42]. In this representation, Eqn. (2.1) is expressed in terms of its complex amplitudes as a column vector:

$$J = \begin{pmatrix} A_x e^{i\delta_x} \\ A_y e^{i\delta_y} \end{pmatrix}. \tag{2.7}$$

The Jones vector contains complete information about the amplitudes and the phases of the electric field vector components. It thus specifies the polarization state of the wave uniquely. If we are interested only in the polarization state of the wave, it is convenient to work with the normalized Jones vectors.

$$J(\psi, \delta) = \begin{pmatrix} \cos\psi \\ e^{i\delta} \sin\psi \end{pmatrix} \tag{2.8}$$

The most important application of Jones vectors is to use the Jones calculus. Jones matrix algebra is a powerful 2×2 matrix method in which the electric field vector (or the state of polarization) is represented by a two-element column vector, while each crystal plate or polarizer is represented by a 2×2 matrix. The entire optical system is represented by a 2×2 matrix obtained by the multiplication of all the matrices in sequence. The transmission of light is thus described by the multiplication of the input vector with the matrix. The Jones matrix method is suitable for carrying out the optical calculation only in the case of normal incidence of light. In 1982, Pochi Yeh [43] developed an Extended Jones matrix method to calculate the transmission characteristics of a birefringent network for off-axis light. This new 2×2 matrix is still easy to manipulate algebraically and accounts for the effects of the Fresnel refraction and single refraction at the interface. However, this method neglects multiple reflections, so it is not suitable for dealing with reflections. For example, Bragg reflection and selective reflection cannot be modeled using the Extended Jones matrix method.

Another widely used representation for polarization states is the *Stokes parameters* of a quasimonochromatic plane wave. The quasimonochromatic wave has frequency spectrum confined to a narrow bandwidth $\Delta\omega$ (i.e., $\Delta\omega << \omega$) Now ω denotes the center frequency and the amplitude is a function of time. Time averaged quantities of the *Stokes parameters* are given as belows:

$$S_0 = \langle\langle A_x^2 + A_y^2 \rangle\rangle \tag{2.9}$$

$$S_1 = \langle\langle A_x^2 - A_y^2 \rangle\rangle \tag{2.10}$$

$$S_2 = 2\langle\langle A_x A_y \cos\delta \rangle\rangle \tag{2.11}$$

$$S_3 = 2\langle\langle A_x A_y \sin\delta \rangle\rangle \tag{2.12}$$

$$S_0^2 \geq S_1^2 + S_2^2 + S_3^2 \tag{2.13}$$

where the amplitudes A_x, A_y and the relative phase δ are assumed to be time dependent, the the double brackets denote averages performed over a time interval. The four parameters have the same dimension as the intensity and these also satisfy Eqn. (2.13). If the beam is entirely unpolarized, $S_1 = S_2 = S_3 = 0$. If it is completely polarized, $S_1^2 + S_2^2 + S_3^2 = 1$. Therefore the degree of polarization is defined as

$$\gamma = \frac{(S_1^2 + S_2^2 + S_3^2)^{1/2}}{S_0} \tag{2.14}$$

The parameter S_0 describes the total intensity of the beam. The parameter S_1 describes the linear polarization along the x or y axis; the probability that the light is linearly polarized along the x axis is $\frac{1}{2}(1 + S_1)$ and along the y axis, $\frac{1}{2}(1 - S_1)$. Thus the values S_1 = 1,-1 correspond to complete polarization in x and y directions, respectively. The parameter S_2 describes the linear polarization along the angles $\phi = \pm 45°$ to the x axis; the probability that the light is linearly polarized along these directions respectively, $\frac{1}{2}(1 + S_2)$ and $\frac{1}{2}(1 - S_2)$. Thus the values S_2=1,-1 correspond to complete polarization along directions. Finally, the parameter S_3 represents the degree of circular polarization; the probability that the lightwave had right-hand circular polarization is $\frac{1}{2}(1 - S_3)$, and left-hand circular polarization, $\frac{1}{2}(1 + S_3)$. The *Stokes parameters* can be expressed in terms of the

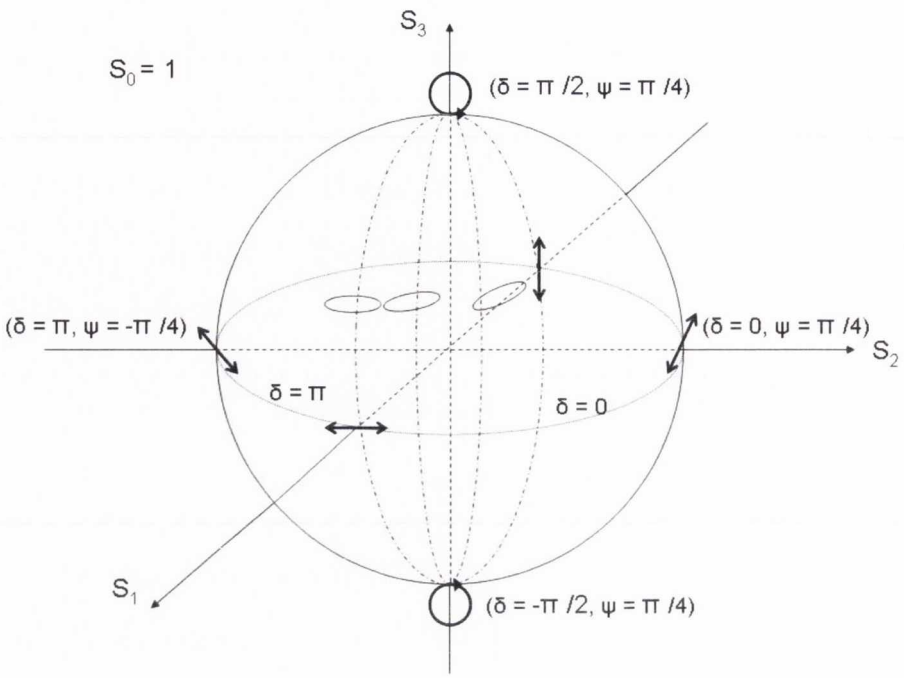

Figure 2.1: showing polarization states at various points).

parameters in the Jones vector which are given by

$$S_0 = 1,\ S_1 = \cos 2\psi,\ S_2 = \sin\psi\cos\delta,\ S_3 = \sin\psi\sin\delta, \tag{2.15}$$

Although the *Stokes parameters* are introduced for describing partially polarized light, they are also used to describe the polarization state of polarized light. In the case of completely polarized light ($S_1^2 + S_2^2 + S_3^2 = 1$), all points with coordinate of the *Stokes parameters* are confined on the surface of a unit sphere, called the *Poincare sphere* (see Fig. 2.1) The method using the *Poincare sphere* provides qualitative and semiquantitative solutions to complex problems which arise when polarised light propagates through birefringent and optically active media. A few examples using the method will be introduced in Chap. 9, which deals with the application of biaxial nematic phase. The Jones algebra is adequate for coherent and monochromatic light, whereas the *Stokes* algebra is better for natural light, which mostly is incoherent, polychromatic and unpolarised. Most widely used algebra is the Müller matrix, to characterize the transmission (or reflection) of a device for light at some wavelength and with arbitrary polarization. The Müller matrix

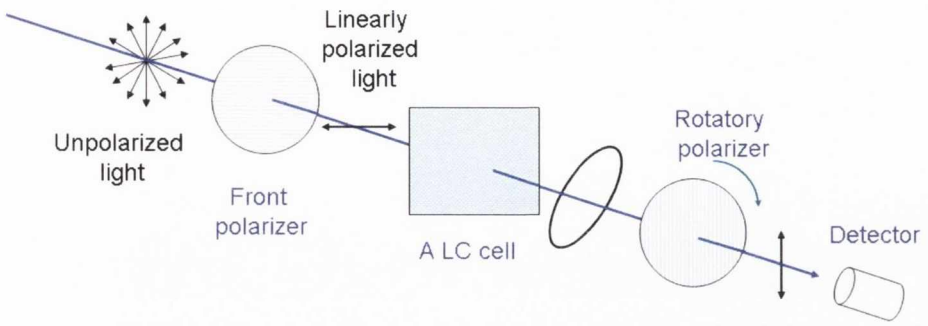

Figure 2.2: Schematic of a optical system.

can separate those properties that depend on the orientation of the device from those that are independent of the orientation. An arbitrary optical-polarization component could be described by a 4×4 matrix, connecting the *Stokes* vector for the entering light with the *Stokes* vector for the transmitted light:

$$\begin{pmatrix} S_0' \\ S_1' \\ S_2' \\ S_3' \end{pmatrix} = M \begin{pmatrix} S_0 \\ S_1 \\ S_2 \\ S_3 \end{pmatrix} \tag{2.16}$$

The output beam is characterized by the *Stokes parameters* of which is determined by the Müller matrix of the media. Usually, this method is very useful to characterize the LC cell as well as to design the optical property of a certain cell.

2.3 Measurement of the state of polarization of light.

Figure 2.2 shows an optical system composed of a pair of polarizers and a LC cell and arbitrary polarization states after passing through each optical component. The most simple method to measure the polarization state of light is measuring its intensity with the rear polarizer rotating. The intensity dependent on the direction of the rear polarizer is determined by the polarization state of

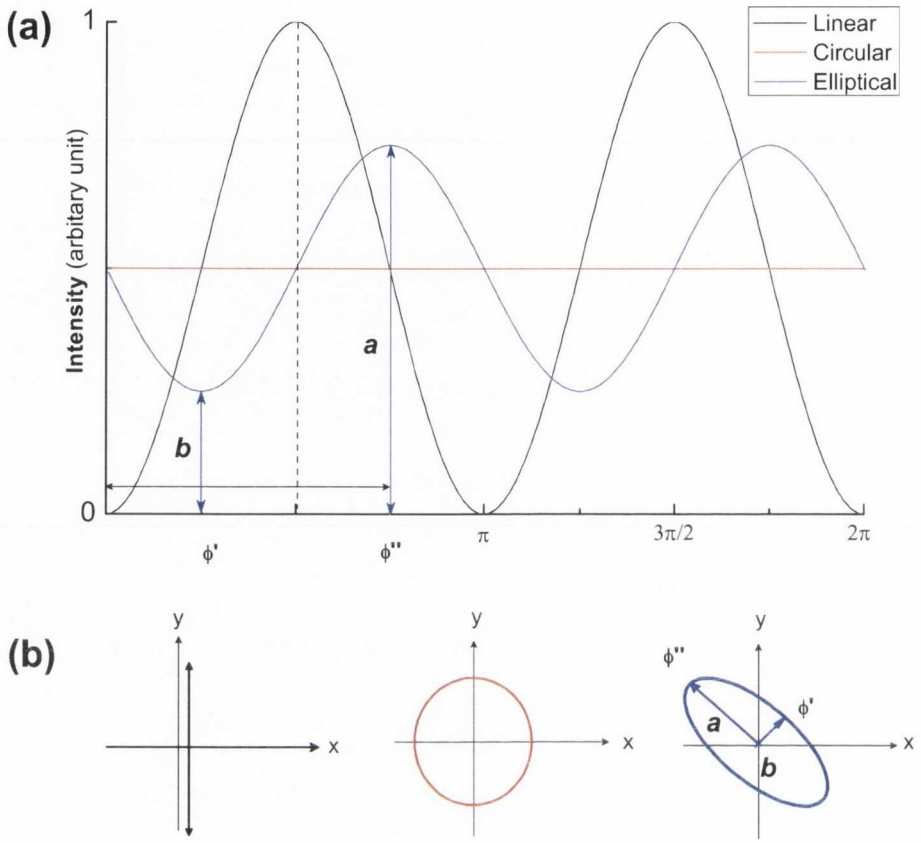

Figure 2.3: Schematic representation of intensity of various polarized light as the rear polarizer rotates. (a) shows the intensity curves of three representive polarized lights (linear, circular, ellipsical) dependent on the angle between the front and the rear polarizers. (b) shows the polarization of the three lights.

the beam, as shown in Fig. 2.3. Here the rotation angle is denoted as ϕ. This is the angle between the x-axis and the transmittance axis of the rear polarizer (see Fig.2.2). However, this method does not give complete information of the state of polarization. In terms of the *Stokes parameters*, by rotation of the rear polarizer, we can only obtain S_1 and S_2 (see Eqns. (2.11) and (2.12)). This means that the handedness of the polarization state is undetectable. In order to solve this problem, several methods using additional optical components have been developed. In this thesis, a single PEM system is used to measure the optical parameters such as the birefringence and the optical rotation.

2.4 PEM

A mechanically stressed sample exhibits birefringence which is proportional to the resulting strain. This is termed as *photo elastic effect*. The PEM produces oscillating birefringence at a fixed frequency in the low frequency ultrasound range (20 kHz to 100 kHz). In its simplest form, the PEM consists of a rectangular bar of a suitable transparent material, for example fused silica, attached to a piezoelectric transducer. The bar vibrates along its long dimension at a frequency determined by the length of the bar and the speed of longitudinal sound wave in the optical element material. The transducer is tuned to the same frequency and is driven by an electronic circuit which controls the amplitude of vibration. The oscillating birefringence effect is at its maximum at the center of the fused silica bar (see Fig. 2.4). The off state has no birefringence. When the optical element is compressed by piezoelectric transducer, the polarization component parallel to the modulator axis travels slightly faster than the vertical component, in other words, the slow axis of the optical element is vertical to the modulator axis. Meanwhile, when the optical element is extended, the horizontal component leads the vertical component after light passes through the modulator.

Due to its high sensitivity, wide spectral range, and high precision phase modulation, the PEM has been used in a wide range of physical measurements. Basically, the PEM can be applied to any system for which a specified polarization state must be generated or, conversely, for the analysis of the polarization states of any given light beam. In order to measure a complete polarization state represented by the *Stokes parameters* a commercially available dual PEM system is used in this case. This system can measure the four *Stokes parameters* simultaneously. However, a single PEM is still widely used. An excellent theoretical and experimental work concerning the determination of polarization states using a single PEM has been reported [44]. We now present the theory for the general case of a monochromatic light beam of arbitrary polarization whose state is to be determined transmitted at normal incidence firstly through a PEM and then through an analyzer before striking a photodetector. The Müller matrix for the PEM and for the analyzer

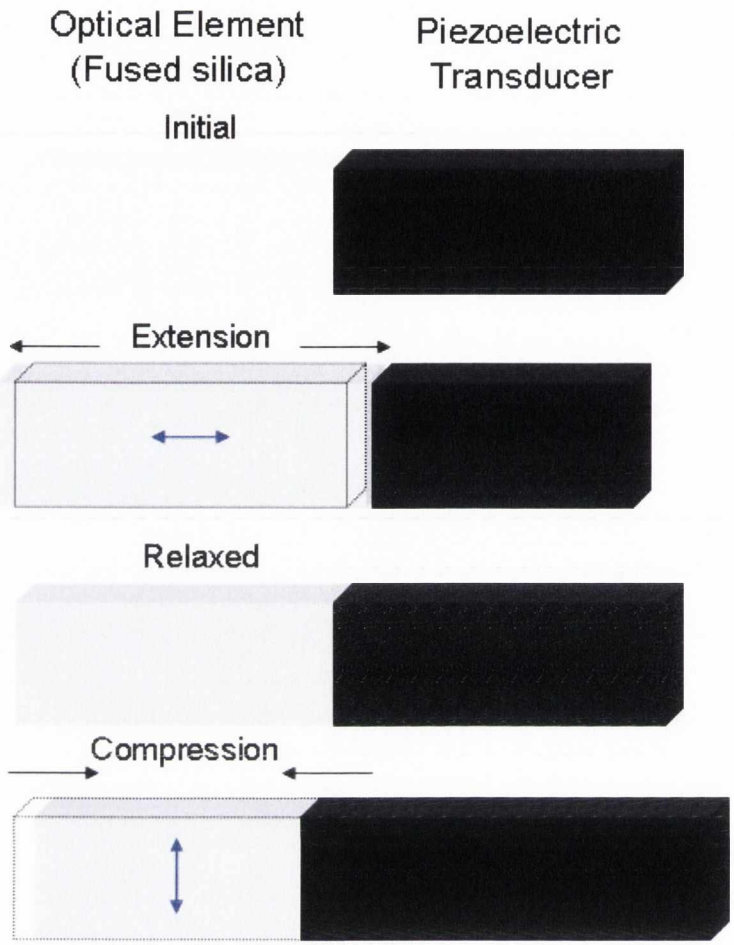

Figure 2.4: Optical assembly of PEM and vibrational motion. Blue arrows indicate slow axis of the retarder.

can be written as follows:

$$M_{PEM} = \begin{pmatrix} 1 & 0 & 0 & 0 \\ 0 & \cos(4\eta)\sin^2(\delta/2) + \cos^2(\delta/2) & \sin(4\eta)\sin^2(\delta/2) & -\sin(2\eta)\sin\delta \\ 0 & \sin(4\eta)\sin^2(\delta/2) & -\cos(4\eta)\sin^2(\delta/2) + \cos^2(\delta/2) & \cos(2\eta)\sin\delta \\ 0 & \sin(2\eta)sin\delta & -\cos(2\eta)\sin\delta & \cos\delta \end{pmatrix} \tag{2.17}$$

$$M_A = \tfrac{1}{2}\begin{pmatrix} 1 & \cos(2\varphi) & \sin(2\varphi) & 0 \\ \cos(2\varphi) & \cos^2(2\varphi) & \cos(2\varphi)\sin(2\varphi) & 0 \\ \sin(2\varphi) & \cos(2\varphi)\sin(2\varphi) & \sin^2(2\varphi) & 0 \\ 0 & 0 & 0 & 0 \end{pmatrix} \tag{2.18}$$

. Here, η and φ denote the angle which x axis makes with the modulator axis and transmittance axis of the analyzer, respectively. $\delta = \delta_0 \sin(\Omega t)$ is the retardation produced by the PEM, δ_0 is the amplitude of the retardation, and Ω is the modulating frequency of the PEM. We can apply these matrices to Eqn. (2.15) as follows.

$$\begin{pmatrix} S_0' \\ S_1' \\ S_2' \\ S_3' \end{pmatrix} = M_A \cdot M_{PEM} \begin{pmatrix} S_0 \\ S_1 \\ S_2 \\ S_3 \end{pmatrix} \tag{2.19}$$

The photodetector measures only output intensity, a fact that greatly simplifies the algebra. Multiplying out Eqn. (2.19), the output intensity is given by:

$$\begin{aligned} S_0' = \frac{1}{2}S_0 + \frac{1}{2}S_1 \cos(2\varphi - 2\eta)\cos(2\eta) \\ + \frac{1}{2}S_2 \cos(2\varphi - 2\eta)\sin(2\eta) - \frac{1}{2}S_1 \sin(2\varphi - 2\eta)\sin(2\eta)\cos\delta \\ + \frac{1}{2}S_2 \sin(2\varphi - 2\eta)\cos(2\eta)\cos\delta + \frac{1}{2}S_3 \sin(2\varphi - 2\eta)\sin\delta \end{aligned} \tag{2.20}$$

In view of the lock-in technique employed, we further expand the retardation in terms of Bessel functions to get the Fourier components. The standard expansions are

$$\begin{aligned} \sin\delta &= \sin[\delta_0 \sin(\Omega t)] \\ &= 2J_1\delta_0 \sin(\Omega t) + 2J_3\delta_0 \sin(3\Omega t) + ..., \end{aligned} \tag{2.21}$$

$$\begin{aligned} \cos\delta &= \cos[\delta_0 \cos(\Omega t)] \\ &= J_0\delta_0 2J_2\delta_0 \cos(2\Omega t) + 2J_4\delta_0 \cos(4\Omega t) + ..., \end{aligned} \tag{2.22}$$

Using Eqns. (2.21), (2.22) and Eqn. (2.20) are rewritten as:

$$
\begin{aligned}
S_0' = \frac{1}{2}S_0 + \frac{1}{2}S_1\cos(2\varphi - 2\eta)\cos(2\eta) + \frac{1}{2}S_2\cos(2\varphi - 2\eta)\sin(2\eta) \\
-\frac{1}{2}S_1 J_0\delta_0\sin(2\varphi - 2\eta)\sin(2\eta) + \frac{1}{2}S_2 J_0\delta_0\sin(2\varphi - 2\eta)\cos(2\eta) \\
+S_3 J_1\delta_0\sin(\Omega t)\sin(2\varphi - 2\eta) \\
-S_1 J_2\delta_0\cos(2\Omega t)\sin(2\varphi - 2\eta)\sin(2\eta) \\
+S_2 J_2\delta_0\cos(2\Omega t)\sin(2\varphi - 2\eta)\cos(2\eta) \\
\ldots\ldots\ldots\ldots\ldots
\end{aligned} \tag{2.23}
$$

The terms of Eqn. (2.23) reflect the magnitudes of output signals of the detector. The terms without Ωt are associated with the DC signal denoted as I_{DC} and the terms containing $1\Omega t$ and $2\Omega t$ mean the first and second harmonic signals (I_{1F} and I_{2F}), respectively. From Eqn. (2.23), it is seen that all these low Fourier components are strongly dependent on the orientations (the values of η and φ) of the two optical components as well as the amplitude of the retardation . Thus the extraction of the four *Stokes parameters* can be made by appropriate choice of setting for η and φ. Basically, various optical configurations can be set for the investigation of the *Stokes parameters* and optical parameters of an optical cell. From Eqn. (2.23), the *Stokes parameters* are given as the signals at specific η and φ.

$$
\begin{aligned}
S_0 &= I_{DC}(0°, 45°) + I_{DC}(0°, -45°) \\
&= I_{DC}(45°, 0°) + I_{DC}(45°, 90°)
\end{aligned} \tag{2.24}
$$

$$
\begin{aligned}
S_1 &= k_2 I_{2F}(45°, 0°) \\
&= k_2 I_{2F}(45°, 90°)
\end{aligned} \tag{2.25}
$$

$$
\begin{aligned}
S_2 &= k_2 I_{2F}(0°, 45°) \\
&= k_2 I_{2F}(0°, -45°)
\end{aligned} \tag{2.26}
$$

$$
\begin{aligned}
S_3 &= k_1 I_{1F}(0°, 45°) \\
&= k_1 I_{1F}(0°, -45°) \\
&= k_1 I_{1F}(45°, 0°) \\
&= k_1 I_{1F}(45°, 90°)
\end{aligned} \tag{2.27}
$$

Here $k_1 = \sqrt{2}/\mathrm{J}_1\delta_0$ and $k_2 = \sqrt{2}/\mathrm{J}_2\delta_0$ are constants whose values must be determined. $I_{1F}(\eta, \varphi)$ and $I_{2F}(\eta, \varphi)$ mean the first and the second harmonic signals at particular η and φ respectively. From Eqn. (2.15), information of polarization state of sample can be calculated by the PEM signals as below:

$$\phi = \frac{1}{2}\tan^{-1}\frac{S_2}{S_1} \tag{2.28}$$

$$\theta = \frac{1}{2}\sin^{-1}\left(\frac{S_3}{\sqrt{S_1^2 + S_2^2 + S_3^2}}\right) \tag{2.29}$$

$$\gamma = \frac{\sqrt{S_1^2 + S_2^2 + S_3^2}}{S_0} \tag{2.30}$$

$$\gamma_L = \frac{\sqrt{S_1^2 + S_2^2}}{S_0} \tag{2.31}$$

$$\gamma_c = \frac{S_3}{S_0} \tag{2.32}$$

$$\delta = \tan^1(\frac{S_3}{S_2}) \tag{2.33}$$

$$\psi = \cos^{-1} S_1 \tag{2.34}$$

where ϕ represents the orientation of the polarised light. θ means the ellipicity angle. γ, γ_L and γ_C denote the degree of total polarization, linear polarization and circular polarization, respectively. Moreover, from the *Stokes parameters* the retardation of the sample and any information can be obtained. In order to get the four *Stokes parameters* either the PEM or the analyzer should be rotated to get the appropriate η and φ. This is practically difficult to be realized in real experiments. Because it takes long time to calibrate a general PEM system. The Dual PEM system is free from such a problem that results from the component being mechanically rotated. However, if there is no loss of polarization ratio and $S_0 = \sqrt{S_1^2 + S_2^2 + S_3^2} = 1$, above equations are simplified. In this case of the system of setting $\eta = 0$, $\varphi = 45°$ as shown Fig. 2.5, the S_2, S_3 and the absolute value of S_1 can be obtained. As a result, we can measure the birefringence as well as the optical rotation by using Eqn. (2.15). Figure. 2.6 shows that the PEM system used in this thesis consists of a photoelastic modulator combined with a microscope, temperature control system, high-sensitivity photodetector and a specialized light source. A National Instruments data acquisition board is the core part of the

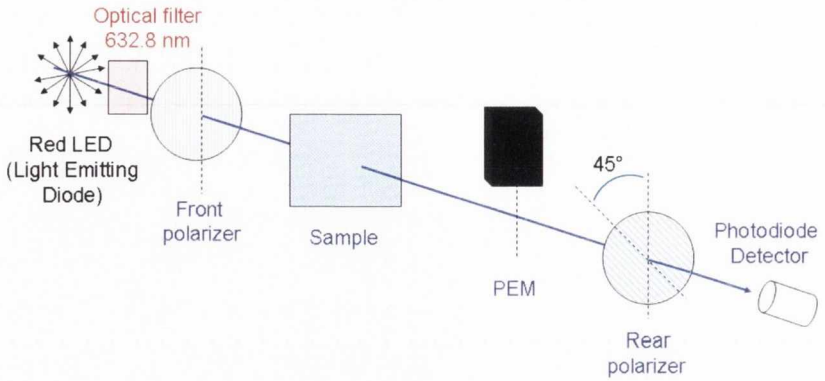

Figure 2.5: The PEM setup used in the thesis. Red LED light source is used with a proper optical filter corresponding to 632.8 ± 0.5 nm. The front polarizer is an accessory of the POM and the PEM is commercially available from the HINDS instruments.

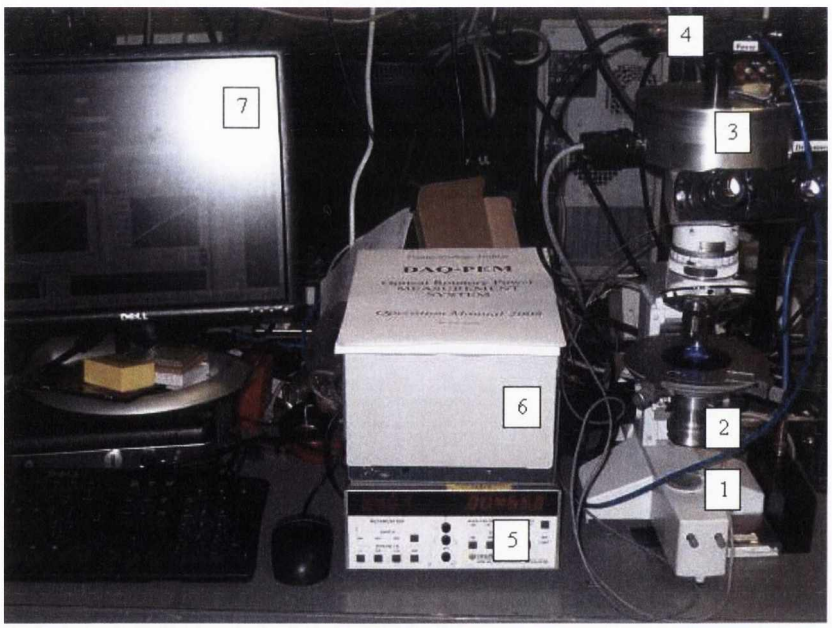

Figure 2.6: Hardware description of PEM. 1) Microscope 2) Monochromatic Linearly Polarised Light Source (LED based, 10 nm bandwidth, several wavelength options) 3) Optical Assembly (PEM head, reference channel etc...) 4) Photodetector (home made) 5) PEM controller (by Hinds Instruments) 6) Electronic Assembly (NI -USB DAQ-mx multifunction data acquisition board and the light source driver) 7) Computer with LabView-based measurement software 8) Eurotherm temperature controller, 10 mK resolution. (not shown)

system. LabView-based software is used for the signal processing. The system automatically measures the optical rotation or the birefringence (with the axis direction) as a function of time, voltage and/or temperature of the sample. The accuracy of the system is tested and calibrated by a quarter wave plate correspond to the optical filter. When the slow axis of the plate is set to either 0° or 45° with respect to the transmittance direction of the front polarizer. The accuracy of the system significantly decreases due to the low harmonic signals, while the repeatability is very high. The retardation (Γ) is measured, when the azimuthal angle (Φ) value lies in the range from 5° to 40°. Ahead of measurements for the valules in the nematic phase, the condition of the PEM system is evaluated in the isotropic phase. The repeatability and stability of the system is monitored by repeating temperature scan at the rate of $0.1°C/\text{min}$.

Part. II

Liquid crystalline materials Phase behavior X-ray patterns The cluster model

Chapter 3

Liquid Crystalline materials and their X-ray studies in the nematic phase

"In this chapter, *the liquid crystalline materials used in this thesis and their phase behavior examined by X-ray analysis is introduced.*

3.1 Introduction

In this chapter, the preceding studies [18] done by the Halle group is introduced in detail. They found that cybotactic clusters are present in the nematic phase of resorcinol derivatives (see Fig. 3.1) and the presence or the size of the cluster depends on the molecular structure of the resorcinol derivatives as well as temperature. So far, most of the substantial results related to the presence of the cybotactic cluster in the nematic phase are based on scattering peaks in the small angle of the X-ray diffraction pattern of the material [18, 24, 45, 46]. However,

this interpretation was criticized by Kumar *et al.* [47]. Therefore, experimental results using different techniques are necessary to settle down the debate regarding the interpretation of the X-ray diffraction pattern. The materials studied by the Halle group show wide spectrum of nematic phases ranging from the usual nematic phase to the nematic phase having cybotactic clusters in terms of X-ray diffraction patterns. We investigate these materials using dielectric and optical techniques. The results from dielectric and X-ray experiments will be compared in Part III.

3.2 Materials

The materials used in this thesis are 4-cyanosubstituted resorcinol derivatives with the same bent-core part and different chains (see Fig. 3.1). From the viewpoint of molecular structure, the bent-core part consists of five phenyl rings and each ring is connected by an ester group. The terminal groups are attached to both ends of the core part. A cyano group is substituted on the central aromatic ring. This plays an important role in forming the nematic phase. When the cyanyl group of resorcinol derivates is replaced by a different functional group such as methyl and chloro, the stability of its nematic phase dramatically decreases. The position of cyanyl group in the central aromatic ring is also important to increase the stability of nematic phase. For example, 5-cyanosubstituted resorcinol derivatives with a symmetric bent-core do not show a nematic phase [48]. The ester group which is more flexible than the C-C covalent bond may give rise to a conformational change in the molecular shape. The phase behavior and the transition enthalpy of the materials were investigated by the Halle group. The results are summarized in TABLE 3.1 [18]. The terminology of phases used in this thesis are taken from [18]. According to their study, all the materials used in this thesis show enantiotropic phase behavior except the material having butyl terminal groups (C4). We found that C4 shows a nematic phase down to $50°C$ under the cooling condition of $1°$/min. It crystallizes after keeping it for about 10 hours. The characterization of the smectic phases and the CybC phase is out of

Table 3.1: Transition temperature (T/° C and the associated enthalpy values in square brackets, Δ/kJ mol^{-1}) of the 4-cyanoresorcinol bisbenzoates.

Comp	n	phase transitions				
C4	4	Cr 117[38.4]			N 107 [0.5]	I
C5	5	Cr 108 [39.6]			N_T^* 108.5 [0.5]	I
C6	6	Cr 98 [37.1]			N_{cybC} 101 [0.5]	I
C7	7	Cr 96 [35.5]	($SmC_{(I)}$ 25 [0.3]	*CybC* 41 [0.2])	N_{cybC} 111 [0.7]	I
C9	9	Cr 98[35.1]	($SmC_{(I)}$ 50 [0.6]	*CybC* 58 [0.3])	N_{cybC} 104 [0.8]	I

Peak temperatures in the first DSC heating curves (10 K min^{-1}), monotropic transitions (enclosed by round brackets) were taken from the second heating run. Abbreviations: Cr = crystalline; I = isotropic phase; N = nematic phase; N_{cybC} = nematic phase having SmC like cybotactic clusters; *CybC* = mesophase composed of elongated cybotactic clusters; $SmC_{(I)}$ = synclinic tilted SmC phase; N_T^* = chiral nematic phase with a pair of molecules. The table and caption are summarized from [18].

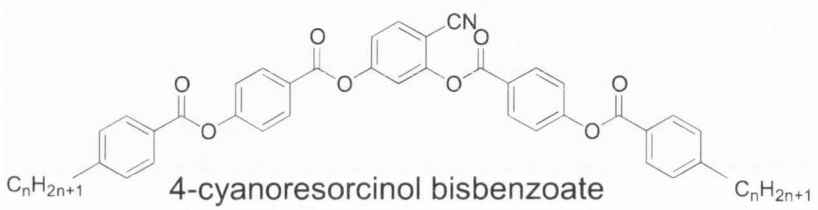

Figure 3.1: Chemical structure of 4'-cyanoresorcinol bisbenzoates.

the scope of this thesis which is limited to the investigation of the nematic phase.

3.3 Structural studies of the materials by X-ray diffraction.

Prior to introducing the experimental results reported by the Halle group, it is helpful to understand the setup and the principle of X-ray technique used in the studies. When light passes through a matter, a interaction between the light and the matter takes place. Specifically, a light with short wavelength such as X-ray interacts with electrons of a volume. As a result, the X-ray is scattered by electrons of the matter leading to a diffraction pattern. The various wavelets from the different electron densities in a volume merge through constructive and destructive

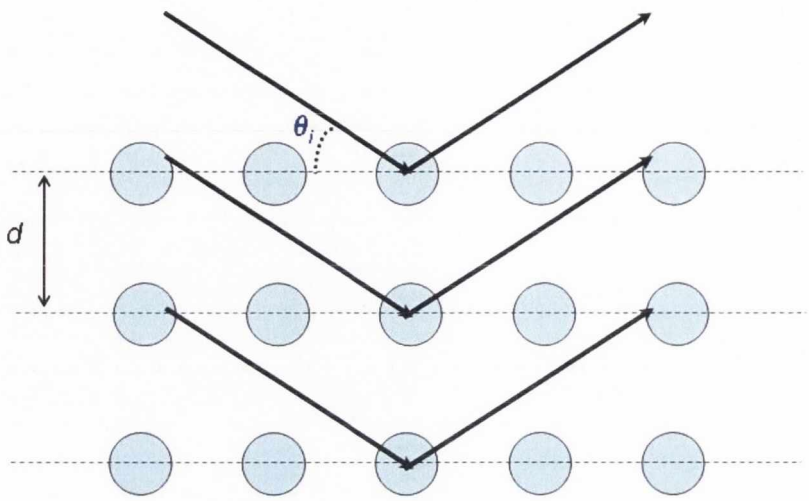

Figure 3.2: Bragg's law.

interference determined by the relative phases of the wavelets. Therefore, the relative phase of the wavelets is associated with the spatial electron density of the volume. Bragg visualized the scattering of X-rays by a crystal in terms of reflections from sets of lattice planes (see Fig. 3.2). For one particular set of planes, constructive interference between rays reflected by successive planes is allowed when the path difference is equal to an integral number of the wavelength. This is known as Bragg's law given by:

$$2d \sin \theta_i = n\lambda \tag{3.1}$$

Where d is the separation of the planes, θ_i is the angle of incidence, n is an integer and λ is the wavelength. This law gives structural information of the matter, while the intensities of the various peaks depend on the total number of scattering centers and their scattering power. $\mathbf{k}_i$ - $\mathbf{k}_f$ is scattering vector with momentum transfer. Since the scattering is elastic, the magnitude of $\mathbf{k}_f$ does not change. Its modulus is given by [7]

$$|\mathbf{Q}| = \frac{4\pi \sin \theta_i}{\lambda} \tag{3.2}$$

For a liquid crystal system, the total scattered intensity at a point in the $\mathbf{Q}$-space is given by averaging over all molecules. This is expressed as a product of two

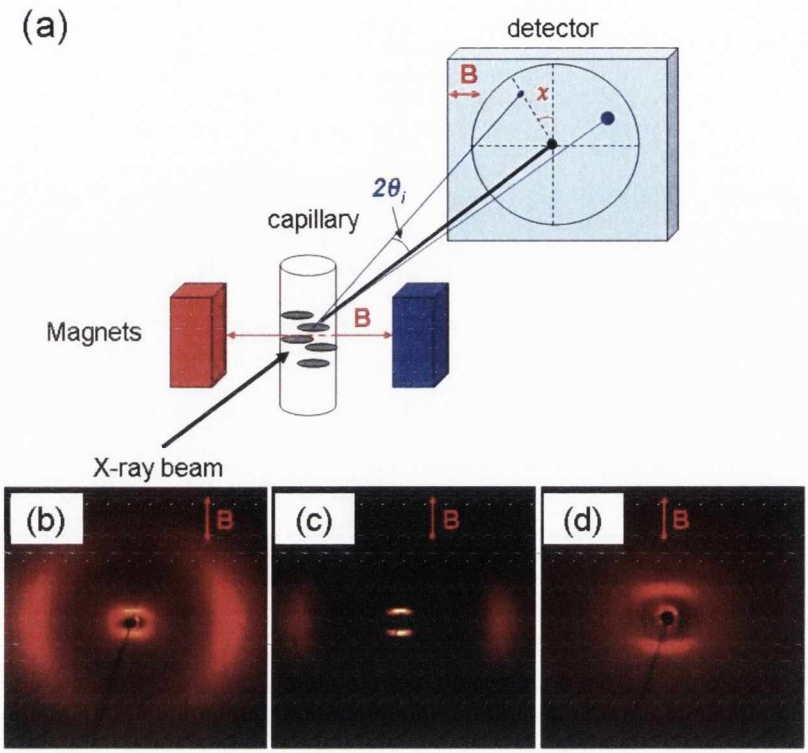

Figure 3.3: (a) Schematic drawing of the experimental XRD setups. (b) is X-ray diffraction pattern of C7 at $100°C$ while the director is aligned by a magnetic field of 1 T. (c) shows the pattern substracted by the pattern of isotropic phase. The part of small angle of (c) is magnified in (d). The X-ray diffraction patterns of C7 are taken from the supplementary information of Ref. [18].

terms.

$$\mathbf{I(Q) = F(q) \times S(q)}. \tag{3.3}$$

The molecular' form factor $\mathbf{F(q)}$ that depends on the molecular structure of a mesogen and the structure factor, $\mathbf{S(q)}$ is determined by both spatial and orientational correlations among the molecules. Either an electric field or a magnetic field can be used for aligning the director in the mesophase. Fig 3.3 (a) shows a typical X-ray setup used for investigating liquid crystals. Figure. 3.3 (b) shows the X-ray diffraction pattern of C7 at $100°C$ when the director is aligned by a magnetic field of 1 **T**. Figure. 3.3 (c)and (d) show the diffraction pattern subtracted by that of isotropic phase in the entire angle and the small angle, respectively. Due to

diamagnetic anisotropy, the molecules in mesophases can be aligned. Therefore, the intensity dependent on χ gives orientational information about the molecule in mesophases. θ_i can be interpreted in terms of the average correlation length among the molecules in the phase. Such a small angle scattering of nematic phase was reported for the first time by de Vries in 1970 [1, 2]. According to the study of the Halle group, there is strong dependence of the intensity of the small angle scattering in the X-ray diffraction pattern on the bent-core mesogen and its terminal group. In general, for a nematic phase, the integrated intensity of small angle scattering is comparable to that of wide scattering angle. The latter is attributed to the transversal correlation among the molecules and the former arises from the lateral correlation among the molecules when the molecules are aligned along the magnetic field. It is natural that the positional order in the nematic phase exponentially decreases with distance. This is given by:

$$D(r) \propto \exp\left[-\frac{r}{\xi}\right] \tag{3.4}$$

And the intensity follows a Lorentzian distribution:

$$I(Q) \propto \frac{1}{1+\xi^2\left|\mathbf{Q}-\mathbf{Q}_0\right|^2} \tag{3.5}$$

where $\mathbf{Q}_0$ is the position of the peak maximum which is reciprocally related to the average separation. ξ is the correlation length. Equation 3.5 implies that the intensity distribution of a scattering peak is related with the correlation length ($\xi = 2/\Delta q$, Δq is the full width at half maximum) [18]. Generally, the integrated intensity of the small angle scattering is less than that of wide angle scattering due to difference between the lateral and the transverse correlation among the molecules in the nematic phase. However, for the bent-core mesogens with long terminal groups, the intensity of the small angle scattering peaks is much larger than that of the wide angle scattering peak while the peaks are sharp (see Fig. 3.3 (c) and (d)). Such a sharp small angle scattering has been observed on

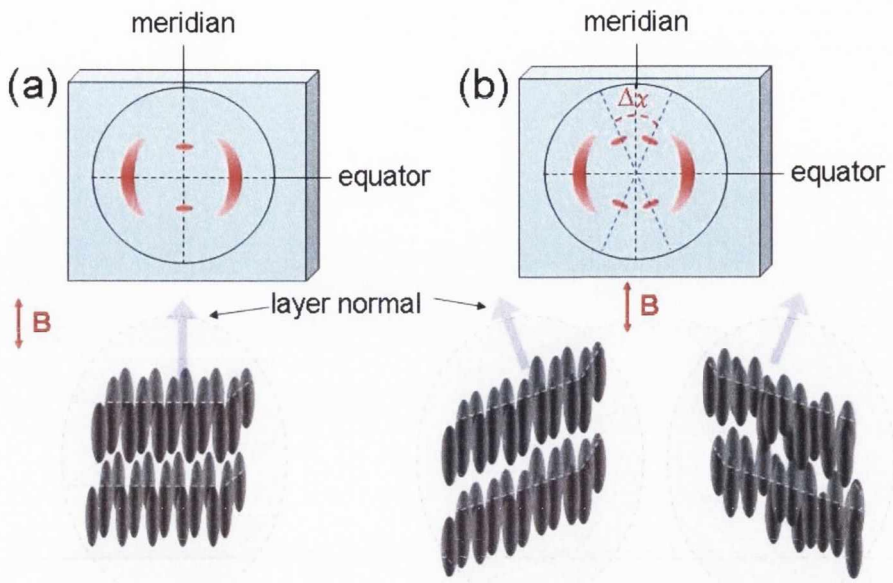

Figure 3.4: Schematic of X-ray diffraction pattern of nematic phases with smectic A type cluster (a) and SmC type (b).

the transition from the nematic to smectic phase as a pretransitional phenomenon of calamitic mesogens [1, 2]. It should be noted that the pattern of the small angle scattering is governed by the types of cluster [7, 18]. Under the magnetic field, the molecules align to be parallel to the direction of the magnetic field due to the diamagnetic property. Since the cluster is smectic A like, the layer normal of the cluster is parallel to the averaged direction of the molecules. Therefore, the small angle scattering is observed along meridian as shown in Fig. 3.4 (a). In the case that the cluster is SmC type, the small angle scattering peak splits into two peaks with a certain $\Delta\chi$ which depends on the the tilt angle of the molecules in the SmC like cluster (see Fig. 3.4 (b). The width of these peaks along meridian and equator are associated with the average correlation lengths of the cluster corresponding to lateral and transverse directions, respectively. The Halle group carried out χ-scans over the small angle regions for the materials. Figure 3.5 shows the relative intensity profiles versus χ at various temperatures. With reduced temperature, the intensity gets larger and shaper. The value of $\Delta\chi$ for the materials also depends on temperature and the molecular structure of the material (see Fig. 3.6 (b)).

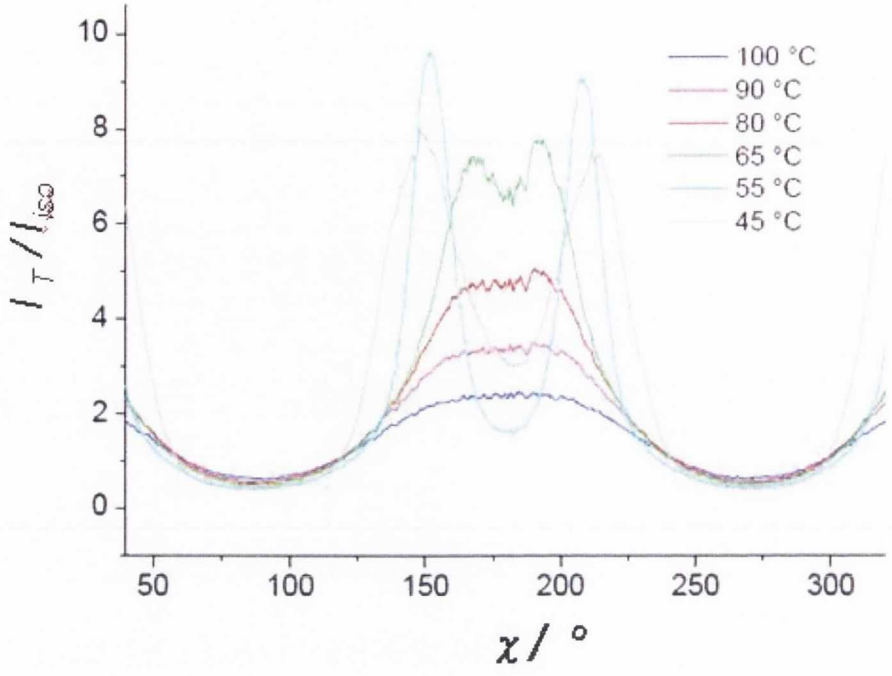

Figure 3.5: Relative intensity profiles versus χ at various temperatures (100, 90, 70, 50, 45°C). The relative intensity defined as I_T/I_{Iso} is taken from the small angle scattering peaks of C9 in the range of $2\theta_i$ between 1.5° and 3.5°.

However, Kumar *et al.* reported that the splitting in the small angle scattering of X-ray diffraction pattern of bent-core mesogens is associated with the angle between two arms of a bent-core molecule [47, 49, 50]. Even though it is clear that the form factor due to the bent shaped molecular structure contributes to the pattern of the small angle scattering in part, it is difficult to understand that such a significant change in the integrated intensity for the bent-core mesogens arises mainly from a small change in nonpolar terminal groups. For the material with long terminal chains (C6, C7, C9), the width of the integrated intensity distribution versus θ_i shows temperature dependence. For C9, the longitudinal ($\xi_{\|}$)and the transverse ($\xi_{\perp}$) correlation lengths calculated from the width of the scattering peaks in the small angle scattering increases linearly in the temperature range of the nematic phase from 14 nm to 40 nm. The longitudinal and transversal cluster size ($L_{\|,\perp}$) of C9 in the nematic phase can also be obtained by fitting the peak

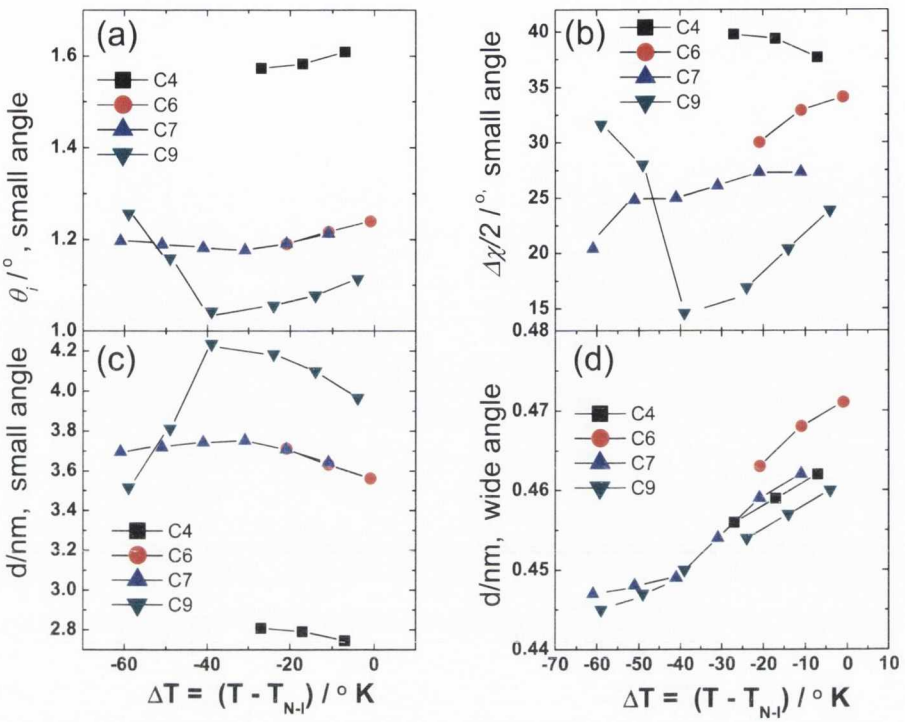

Figure 3.6: Temperature dependence of $\theta_i, d, \Delta\chi$ for C4, C6,C7 and C9. (a) temperature dependence of the small angle scattering peak at maximum. (b) temperature dependence of the splitting angle $\Delta\chi$. (c) temperature dependence of the layer thickness. (d) temperature dependence of the wide angle scattering peak at maximum. Replotted by the data taken from the supplement information of Ref. [18].

along meridian and equator, respectively, to the Scherrer equation given by [51]

$$L_{\parallel,\perp} = K\frac{\lambda}{\Delta(2\theta_i)_{\parallel,\perp}\cos\theta_i} \tag{3.6}$$

here $\Delta(2\theta_i)_{\parallel,\perp}$ can be obtained from the width of the peak at maximum intensity. The transversal cluster size ($L_\perp$) with temperature also increases with reduced temperature. The averaged cluster size of C9 with temperature is shown in Fig. 5.12 where a comparison between the structural size of the cluster and polar correlation length evaluated by a dielectric technique will be introduced. Interestingly, for C9, θ_i, at maximum of the small angle scattering peak significantly shifts with temperature. This indicates that the layer thickness of the cluster increases as temperature decreases. Normally, molecules in SmC phase are tilted

with respect to layer normal and the tilt angle increases with reduced temperature, resulting in the decrease of the layer thickness. Samulski *et al.* [46] reported that SmC like clusters are present in the nematic phase of a bent-core mesogen and the thickness decreases with reduced temperature. Such a temperature dependence agrees with that of SmC phase. They regarded it as an experimental result proving the presence of SmC like cluster. However, for the bent-core mesogens with long terminal chains (C6, C7, C9), the temperature dependence of the layer thickness is similar to that of SmA phase in which more ordered molecules in the layer increase the thickness with reduced temperature. Since the tilt angle represented by $\Delta\chi/2$ also decreases with reduced temperature in the nematic phase of C9 as shown in Fig. 3.6, the temperature dependence of $\Delta\chi/2$ is opposite to the temperature dependence of the tilt angle in the SmC phase. The Halle group interpreted the temperature dependence of $\Delta\chi/2$ in terms of splitting arising from the combination of the form factor and the structural factor. According to the NMR (Nuclear Magnetic Resonace) studies [48], the bending angle (θ_V) made by two arms of the bent-core mesogen is about 140°. For C4 without the cybotactic cluster, $\Delta\chi/2$ slightly increases with reduced temperature from 36 to 38° which agrees with the interpretation that the splitting is attributed to the bent shaped molecule [47]. Therefore, in high temperature range of the nematic phase, $\Delta\chi$ is not directly proportional to the tilt angle of the molecules in the cluster, as $\Delta\chi$ is affected by both the form and structural factor. With reduced temperature, the structural factor mainly governs $\Delta\chi$, since the intensity of the peak in small angle increases. This indicates that the temperature dependent cluster size plays an important role in determining $\Delta\chi$. $\Delta\chi$ also depends on the molecular structure as the cluster size depends on the molecular structure. The interpretation in terms of the cluster size is in agreement with $\Delta\chi$ dependence on the length of terminal chain. $\Delta\chi$ decreases, as the terminal chain get longer (see Fig. 3.6 (b)). For C9, $\Delta\chi/2$ in low temperature range of the nematic phase varies from 15° to 20° with reduced temperature. Meanwhile, $\Delta\chi/2$ immediately after transition to the *CybC* phase jumps up to 28 ° and continuously increases up to 32° in the smectic phase. Tschierske *et al.* interpreted this arising from the enlongated SmC type clusters.

In terms of the cluster model which will be introduced in Chap. 4, the *CybC* phase has clusters large enough to interact with each other. Such an additional interaction among the clusters gives rise to different phase behavior from the cybotactic nematic phase (N_{cybC}) in which this interaction can be neglected. The interaction among the cluster in the *CybC* phase may reduce the thermal fluctuation of layer normal which plays an important role in forming the small angle scattering of X-ray diffraction pattern. From the viewpoint of the microscopic model used for interpreting the splitting of small angle scattering, such a large increase of $\Delta\chi/2$ in the *CybC* phase seems to be extraordinary.

3.4 Conclusion

In this chapter, the phase behaviour of a homologous series of alkyl substituted 4-cyanoresorcinol bisbenzoates has been introduced. The materials exhibit a broad spectrum of the microscopic structure in the nematic phase. The chain length of the materials plays a key role in leading to the structural transformation from the usual nematic phases (C4) to the cybotactic nematic phase (C6, C7 and C9). Moreover the cluster in the N_{cybC} grows with reduced temperature. Such a behavior has been found by the results from the X-ray experiments. The intensity of the small angle scattering in X-ray diffraction pattern for the bent-core mesogens is strongly associated with the cluster size in the nematic phase and this depends on the chain length of the materials as well as on temperature. The change in the cluster size leads to distinct changes in the physical properties of the cybotactic nematic phase. In the rest of this thesis, the relationship between the structural properties introduced in this chapter and the dielectric and the optical properties will be considered. It should be noted that a controversy exists in the literature over the interpretation of the splitting in the small angle X-ray diffraction patterns for bent-core mesogens in the nematic phase. C4 with butyl group exhibits the ordinary nematic phase with only nearest neighbour correlations in terms of X-ray diffraction pattern. The splitting of the small angle in X-ray diffraction pattern of C4 originates from the distinct orientation of the rod-like arms of the

material (form factor), whereas the material with relatively longer terminal chains (C6, C7 and C9) show small angle scattering peaks the intensity of which is larger than that of wide scattering peaks. The splitting pattern in the small angle is attributed to the combination of the form factor and the structural factor arising from the tilt of the molecules in the cluster. Therefore, it will be quite interesting to investigate the N_{cybC} and to determine the influence of the cluster on dielectric and optical properties of the LC in this phase.

Chapter 4

The cluster model.

"In this chapter, *a theoretical model for the cybotactic nematic phase is introduced.*

4.1 Introduction

In Chap. 3, we found that the structural correlation is present in the nematic phase of the bent-core mesogens. The cluster size dependent on temperature as well as on the length of terminal chain can be obtained through analysis of the small angle scattering peaks. Recently, Photinos *al et.* suggested a theoretical model [8–10] supporting the presence of clusters. In this chapter, their theoretical model called the cluster model is being introduced in detail.

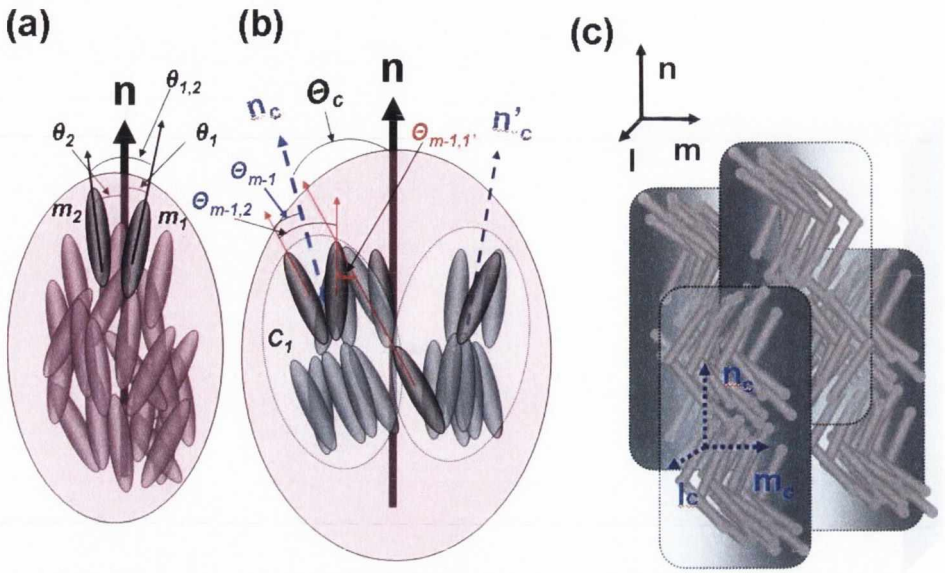

Figure 4.1: Schematics of representation of the internal molecular order in a usual nematic phase (a), a uniaxial cybotactic nematic (b) and a biaxial cybotactic phase (c) with their relative orientations. Thin black arrows represent the long axes of the molecules. Bold black lines represent the direction of the macroscopic directors, **n**. Blue dotted lines mean the cluster directors. m_1 and m_2 denote the molecules in the nematic phase. C_1 indicates a cluster in the uniaxial cybotactic nematic phase. $\mathbf{n}_c$, $\mathbf{m}_c$, $\mathbf{l}_c$ represent the three directors of the biaxial cluster. θ_1 and θ_2 denote the angle that the long axis of m_1 and m_2, respectively, make with the director, **n**. $\theta_{1,2}$ is the angle between the long axes of m_1 and m_2. Θ_c denotes the angle that the director of the clusters $\mathbf{n}_c$ makes with the director, **n**. Θ_{m-1} and Θ_{m-2} denote the angle that the long axis of the molecules in the cluster make with the director of the cluster ($\mathbf{n}_c$). $\Theta_{m-1,1'}$ is the angle between the long axes of the molecules in different clusters. **m** and **l** mean the minor directors of the biaxial nematic phase.

4.2 The extended M-S model for the cybotactic nematic phase composed of unaxial molecules.

In the classical nematic phase, the positional order D(r) falls off exponentially with distance (see Eqn.(3.4)). As a result, the correlation of the phase is limited to just a few neighboring molecules. Such a small correlation would be neglected in interpreting the nematic phase behavior. Maier and Saupe assumed

that all molecules in the nematic phase orient due to a molecular field and neglected the correlation among the neighboring molecules. Such an assumption leads to the molecular field approximation (MFA) which entails N-molecules joint probability distribution $P^{(N)}$ by a product of N effective probability distribution, $f(w_i)$, which is expressed by [10];

$$P^{(N)}(\mathbf{r}_1, w_1, \mathbf{r}_2, w_2, ...\mathbf{r}_N, w_N) \overset{MFA}{\rightarrow} V^{-N} f(w_1) f(w_2) .... f(w_N) \tag{4.1}$$

where N is the number of molecules in the nematic phase, w_i is the orientation of the ith molecule (i= *1,2,. . .,N*) with respect to the macroscopic director $\mathbf{n}$ and $\mathbf{r}_i$ is the position vector of that molecule within the volume, V, of the sample. This is a key concept of the well known M-S model [52–54]. However, as seen in Chap. 3, the considerable correlation exists in the entire nematic temperature range of the bent-core mesogen, resulting in different X-ray diffraction pattern. In order to apply the M-S model to the nematic phase with the cluster, Photinos *et al.* assumed a system of uniaxial molecules to be organized into clusters. In this system, the N molecules are partitioned into a number R of clusters with same order and size. As a result, each cluster is composed of a number n ($= N/R$) of uniaxial molecules. On the basis of this assumption, each individual cluster can be treated as a molecule in the M-S model and the direction of the long axis of the M-S molecule is replaced by the director of the cluster. Photinos *et al.* take two kinds of the Saupe order parameters into account. One is the order parameter of the molecules (S') within the cluster, the other is the order parameter of the cluster directors (S''). These order parameters are given as below [10];

$$S' = \frac{1}{2}\left\langle 3\cos^2\Theta_m - 1 \right\rangle, \tag{4.2}$$

$$S'' = \frac{1}{2}\left\langle 3\cos^2\Theta_c - 1 \right\rangle, \tag{4.3}$$

where Θ_m means the angle that molecular long axis makes with the cluster director ($\mathbf{n}_c$) and Θ_c means the angle between the directors of the cluster and the macroscopic director, $\mathbf{n}$ (see Fig.4.1 (b)). Accordingly, each cluster is characterized not only by the number of molecules taking part in the cluster but also the

ordering of molecules within the cluster and the ordering of the cluster. For the reason, the free energy of the nematic phase includes internal interactions among the molecules in the cluster and the collective energy and entropy of the clusters. Additionally, the exchange of molecules between clusters is possible in this system. For this system, Photinos *et al.* introduced two types of orientational distribution functions. One is a distribution function of the molecular long axis with respect to the cluster director and the other is the distribution of the cluster director. The latter and the former are denoted by $f'(\Theta_m)$ and $f''(\Theta_c)$, respectively. Therefore, the self consistent equation for the M-S model was able to be modified for the extended M-S model by Photinos *et al.* This is expressed as bellow [10];

$$S' \equiv \int_{-1}^{1} f'(\Theta_m) P_2(\cos\Theta_m) d(\cos\Theta_m) \tag{4.4}$$

$$S'' \equiv \int_{-1}^{1} f''(\Theta_c) P_2(\cos\Theta_c) d(\cos\Theta_c) \tag{4.5}$$

where P_2 is the second Legendre polynomial. In general, for molecules interacting in pairs, the effective probability distribution can be related self-consistently to the intermolecular pair potential $u(\mathbf{r}_{i,j},\ w_i,\ w_j)$ by minimisation, at constant density, of the free energy function

$$\frac{F}{N} = \frac{1}{2}(N-1)\int f(w_1) f(w_2) \bar{u}(w_1, w_2) dw_1 dw_2 + k_B T \int f(w) \ln f(w) dw. \tag{4.6}$$

where the positionally averaged anisotropic potential $\bar{u}(w_1, w_2)$ is expressed by;

$$\bar{u}(w_1, w_2) = \frac{1}{V}\int g(\mathbf{r}_{1,2}, w_1, w_2) u(\mathbf{r}_{1,2}, w_1, w_2) d\mathbf{r}_{1,2} \tag{4.7}$$

where $g(\mathbf{r}_{1,2}, w_1, w_2)$ is the pair correlation function between molecules *1* and *2*. In the M-S theory the molecules are assumed to be perfectly symmetric about their long axis (uniaxial molecules) and a crucial approximation is made by putting $\bar{u}$ in the form

$$\bar{u}(\theta_1, \theta_2) \approx -u_0 \frac{a^3}{V} P_2(\cos\theta_{1,2}) \tag{4.8}$$

here, u_0 and a represent, respectively, the effective strength and the range parameters of the anisotropic part of the molecular interaction. The angles θ_1, θ_2 describe the orientations of the long axes of molecules 1 and 2 relative to the director $\mathbf{n}$, $\theta_{1,2}$ denotes the angle of those axes relative to each other (see Eqn. 4.1 (a)). However , the system composed of the clusters, the anisotropic interaction which contributes to the free energy is divided into the interaction between molecules within a cluster and the interaction between molecules in different cluster. Photinos *et al.* used the approximate anisotropic potential similar to Eqn. (4.8) for the cluster system. These are expressed as below [10];

$$\bar{u}'(\Theta_{m-1,2}) \approx -u_0 \frac{a^3 R}{V} \nu' P_2(\cos\Theta_{m-1,2}) \tag{4.9}$$

$$\bar{u}''(\Theta_{m-1,1'}) \approx -u_0 \frac{a^3}{V} \nu'' P_2(\cos\Theta_{m-1,1'}) \tag{4.10}$$

The angles $\Theta_{m-1}, \Theta_{m-2}$ describe the orientations of the long axes of molecules 1 and 2 with respect to the macroscopic director $\mathbf{n}$, $\Theta_{m-1,2}$ denotes the angle that molecule *1* makes with molecule 2 and $\Theta_{m-1,1'}$ denotes the angle that molecule 1 makes with molecule $1'$ in a different cluster (see Eqn. 4.1 (b)). Equations (4.9) and (4.10) correspond to internal and external interaction between molecules. The cluster size determines ν' and ν'' which are the dimensionless factors. For example, when the number of molecules in a cluster is equal to 1, in the absence of cluster, ν' is equal to zero. As the number of molecule, n gets close to N, ν' increases up to 1. On the basis of uniform molecular density , the spatial average of interaction between a pair of molecules should be fixed at a value determined by the M-S model. Therefore $\nu' + \nu'' = 1$. After further application of the M-S approximation, Photinos *et al.* obtained the free energy equation given by [10];

$$\frac{F - F_0}{N k_B T} = \frac{1}{2} b(\nu' + 3(1-\nu')S''^2 - \frac{n-1}{n}\ln(\varsigma'/2) - \left(\frac{1}{n} - \frac{1}{N}\right)\ln(\varsigma''/2) \tag{4.11}$$

where ν' is the dimensionless factor of Eqn. (4.9). ς' and ς'' are the normalisation factors on minimisation of the free energy with respect to $f'(\Theta_m)$ and $f''(\Theta_c)$, respectively. Another condition, from which the cluster size parameter n can be

specified in terms of the temperature variable b, is obtained by minimising the free energy with respect to n, subject to the constraint $nR = N$ = constant >> 1. This yields the equation

$$bS''^2 n \left(\frac{1}{2}(1 - S''^2) n \frac{\partial \nu'}{\partial n} + \frac{R}{R-1}(1-\nu')S''^2 - \frac{\nu' + (1-\nu')S''^2}{n-1} \right) = \ln(\varsigma''/\varsigma') \tag{4.12}$$

On the basis of the above equation, Photinos *et al.* predicted three kinds of phases corresponding to the solution. (i) the molecular isotropic phase (I), in which $S' = S'' = 0$. (ii) the cybotactic-isotropic phase (I′) consists of internally ordered clusters whose orientations are randomly distributed ($S' \neq 0$, $S'' = 0$). This phase is macroscopically isotropic. For sufficiently large n so that $(n\text{-}1)/n \cong 1$, the self-consistency conditions and the free energy for the transition from the I to the I′ phase differ from those of the N-I transition. the I′ phase is stabilized relative to the I phase. (iii) the cybotactic nematic phase (N_{cyb}), in which $S' \neq 0$, $S'' \neq 0$. Its transition behavior depends on the cluster size. the N_{cyb} phase can either evolve from the I phase or the I′ phase depending on b of Eqn. (4.12). According to the definition of the order parameter in Eqn. (1.1), the molecular order parameter S for the macroscopic nematic phase is the averaged orientations of a molecule relative to the macroscopic nematic director **n**. This means that $S = S'S''$.

4.3 The cluster model applied to biaxial molecules

For a system composed of biaxial molecules, the cluster model becomes more complicated. Photinos *et al.* reported [8, 9] that most of the findings related to the biaxial nematic phase are based on microscopically biaxial nematic phases [33, 49, 50, 55]. They interpreted that microscopic biaxiality originates from the biaxial cluster present in the nematic phase and under an action of a transverse aligning stimulus, the macroscopic biaxial ordering can be obtained. They introduced an intermediate nematic phase ($N_{u'}$) between N_u and N_b. The intermediate phase consists of biaxial and possibly polar clusters, the ordering of

which is defined by a set of local directors, $\mathbf{n}_c$, $\mathbf{m}_c$ and $\mathbf{l}_c$ (see Fig. 4.1 (c)). The major directors ($\mathbf{n}_c$) of these clusters can be spontaneously ordered along a common direction $\mathbf{n}$ as a usual nematic phase, whereas their transverse directors ($\mathbf{m}_c$, $\mathbf{l}_c$) are randomly distributed in the absence of external aligning fields or surface anchoring (see Fig. 4.2 (a)). For this reason, the phase is macroscopically uniaxial. This thermotropic phase can undergo a transition, on lowering the temperature, to a spontaneously biaxial macroscopic state (N_b) due to the collective alignment of the transverse directors of the clusters. Photinos *et al.* introduced additional order parameters to the system composed of biaxial clusters. The average internal biaxial order of the clusters is defined as σ and q is used to describe the macroscopic biaxial order of the system. The free energy of the system includes : (i) the internal energy and entropy of the individual clusters; (ii) the interaction energy among neighboring clusters; (iii) the collective entropy associated with the relative magnitudes and orientations of the clusters. Photinos *et al* reported the Landau−de Gennes (L-dG) expansion of the free energy for the system expressed in terms of the order parameters and external electric field, E. This is given by [8, 9];

$$F(T; q, \sigma) = F_0(T) + F'(T, q) + F''(q^2) - e\sigma q^2 - hE^2 q \tag{4.13}$$

where e and h are positive coupling constants, F'' contains at least up to fourth power terms in q and F' contains at least up to third power terms in q and F'. When F', F'' are restricted to their minimal-power form [8] and the first power term of F' carries exclusively the temperature dependence, three distinct phases can exist under no electric field. (i) a macroscopically biaxial phase N_b, with $q \neq 0$; $\sigma \neq 0$; (ii) a macroscopically uniaxial phase $N_{u'}$ of biaxial clusters, with $q = 0$; $\sigma \neq 0$; (iii) a proper uniaxial state N_u with $q = 0$; $\sigma = 0$. The phase sequence with reduced temperature is determined by the relative values of the expansion parameters. This model can accommodate the various mesophases from the N_u phase down a positionally ordered phase such as smectic, columnar or solid phases. According to the model, two optically unaxial nematic phases can be distinguished by magnitude in their response to the applied electric field. In the N_u phase, the electric field cannot align the individual molecules due to thermal motion. In

contrast, for the $N_{u'}$ with the biaxial clusters substantial field-induced biaxial order can be obtained by practical strength of electric field (see Fig. 4.2 (b)). The application of an electric field also elevates the temperature of the $N_{u'}$ to N_b phase transition much more than it elevates the respective temperature for the N_u-N_b transition. They extended the cluster model to include the possibility of local biaxial and transverse polar order. If the biaxial cluster is polar in the transverse directions, the biaxiality as well as polarity are present in the nematic phase [45]. In this case, the primary order parameter ρ of the clusters is defined as the average magnitude squared of the cluster polar vector. The macroscopic polar order is described by the average polar vector $\mathbf{p}$ of the entire sample. Thus, three basic order parameters for this system exist (see Fig. 4.2 (c)): the macroscopic biaxiality order parameter q, the macroscopic polarity order parameter $p \equiv |\mathbf{p}|$ and the cluster polarity order parameter ρ. In this case, the L-dG formulation of the free energy for the system includes the parameter ρ in place of σ in Eqn. (4.13) and the additional terms -e$'\rho p^2$, -e$''\rho p^2$, and -h$'(\vec{E} \cdot \vec{p})$. Here, e', e'', h' are positive constants describing the coupling of the macroscopic polar order to the polar order of the clusters, to the macroscopic biaxial order and to the applied electric field, respectively. The possible nematic phases for this system, in the absence of an external field, are four: a proper uniaxial N_u phase ($\rho = q = p = 0$), a uniaxial $N_{u'}$ phase with local polar order ($\rho \neq 0$, $q = p = 0$)), a biaxial apolar N_b phase ($\rho \neq 0$, $q \neq 0$, $p = 0$)) and a biaxial polar phase N_b^p with $\rho \neq 0$, $q \neq 0$, $p \neq 0$. The cluster compositions of the $N_{u'}$, N_b and N_b^p are depicted in Fig. 4.2.

4.4 Conclusion

The application of the M-S theory for the cybotactic nematic phase was reviewed in this chapter. The extended M-S theory proposed by Photinos *et al.* [10] is also based on the molecular-field approximation which uses the orientation dependence of the effective intermolecular potential. The difference of the extended M-S theory from the M-S model is the possibility for the formation of molecular clusters with internal orientational order. The extended M-S theory predicts two

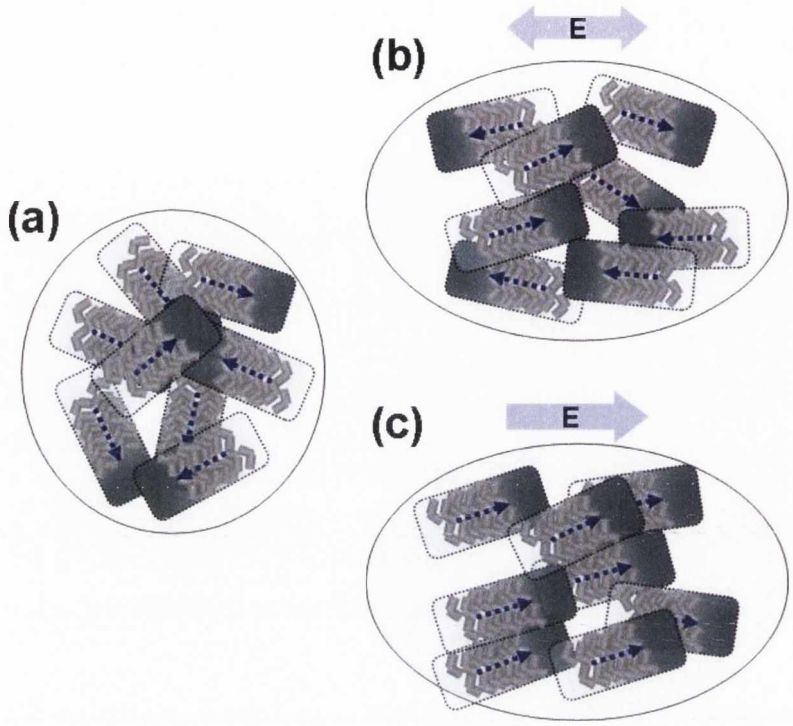

Figure 4.2: Cross-section of a model nematic sample consisting of polar clusters. The directional disposition of the clusters is illustrated for (a) the macroscopically uniaxial phase $N_{u'}$, (b) the biaxial apolar phase N_b and (c) the biaxial polar phase N_b^p. The axis of the assumed perfect molecular alignment is perpendicular to the plane of the figure in all cases. Redrawn from Ref. [9].

macroscopically stable isotropic phases, I and I′. The latter possesses the clusters in which the molecules are ordered. The theory also predicts that the phase transitions from either of these phases to the macroscopically ordered nematic phase, N is allowed. According to Eqns. (4.9), (4.10), (4.11) and (4.12), it is clear that the stability of these phases at a given temperature is associated with the cluster size and it plays an important role in the considerable deviations from the M-S theory. As seen in Chap. 3, the cluster size of the bent-core mesogen can be investigated by a technique using X-ray. It will be quite interesting to investigate the physical properties of the nematic phase with cluster. The extended theory retains the simplicity of the M-S theory, even though it neglects molecular correlations, possible dispersion in the cluster sizes and possible transitions to ordered phases other than the nematic phase. Actually, according to the X-ray results

introduced in Chap. 3 , the clusters have SmC like internal ordering and give rise to macroscopically uniaxial nematic phases. Therefore, a more general formulation was introduced for a system composed of either biaxial or polar biaxial clusters. Additional biaxial phases described by the extended Landau-de Gennes expansion include a macroscopically uniaxial nematic phase composed of either biaxial clusters or polar-biaxial clusters. After all, the cluster model offers new insights into the nature of the phase biaxiality and the related nematic-nematic phase transitions. This broadens the current views on what could be considered as a biaxial nematic LC for the purposes of electro-optic device applications. In terms of this model, the physical properties of the materials introduced in Chap. 3 in the nematic phase will be investigated in the rest of this thesis.

Part. III

Short-range correlation
The observation of the clusters in the nematic phase

Chapter 5

Dielectric spectroscopic studies

"In this chapter,*the dielectric behavior of liquid crystal materials in the nematic phase are investigated in details."*

5.1 Introduction

In this chapter, we focus on the dielectric behavior of the materials confined to planar and homeotropic cells. The dielectric behavior of the materials also shows dependence on the length of the terminal groups. The dielectric data can be interpreted as either the absence or presence of the clusters in the nematic phase. We address the difference between a usual nematic phase and the cybotactic nematic phase in terms of short range correlations due to the presence of cluster. The correlation factors obtained by dielectric measurements can be used for the calulation of polar correlation length in the nematic phase. A comparison between the results of X-ray and dielectric experiments is quite interesting. The polar correlation length obtained by dielectric measurements is found to be reasonably consistent with the structural correlation length deduced from X-ray shown in Chap. 3

5.2 Theoretical background

According to the Maier-Saupe model [56], the occurrence of the nematic phase is attributed to the mean molecular potential due to the anisotropic molecules. The molecules and their permanent dipoles in the nematic phase experience a hindrance to the reorientation around the short axis of the molecule. This reorientation hindrance is expressed in terms of nematic potential which gives rise to additional dielectric dielectric loss bands in the nematic phase. Such bands in nematic phase correspond to molecular rotational modes dependent on the cell configurations [57].

First of all, it should be recalled that the total permittivity is the sum of ϵ_∞ which is the permittivity at optical frequency and the various relaxation strengths. The static permittivity values for the materials thus calculated by summation of all strengths were expressed by Maier and Meier as follows:

$$\epsilon_{\parallel} - n_{\parallel}^2 = \frac{NhF_i g_{\parallel}}{3\epsilon_o k_B T}\left[\mu_l^2\left(1+2S\right)+\mu_t^2\left(1-S\right)\right] \tag{5.1}$$

$$\epsilon_{\perp} - n_{\perp}^2 = \frac{NhF_i g_{\perp}}{3\epsilon_o k_B T}\left[\mu_l^2\left(1-S\right)+\mu_t^2\left(1+\frac{1}{2}S\right)\right] \tag{5.2}$$

$$\langle\epsilon\rangle - n^2 = \frac{NhF_i}{\epsilon_o}\left(\frac{g_N\mu^2}{3kT}\right) \tag{5.3}$$

Here, S is the order parameter. $\mu_l = \mu\cos\beta$ and $\mu_t = \mu\sin\beta$ are the longitudinal and the transverse components of the molecular dipole moment (μ). β is the angle the molecular dipole moment makes with respect to the director $\mathbf{n}$. $n_{\parallel}$ and $n_{\perp}$ are parallel and perpendicular refractive indices respectively. $\frac{NhF_i g_{\parallel}}{3\epsilon_o k_B T}$ and $\frac{NhF-ig_{\perp}}{3\epsilon_o k_B T}$ are the multiplying factors for the two permittivities. N is the number density, ϵ_o is the permittivity of vacuum, k_BT is the thermal energy, F_i and h are the internal field factors for the reaction and the cavity fields. $g_{\parallel}$ and $g_{\perp}$ are the anisotropic Kirkwood correlation factors for the director parallel and perpendicular to the electric field, respectively. g_N is the net dipole correlation factor.

Eqns. (5.1) and (5.2) give relationships between the measured components of the dielectric permittivity and the molecular dipole moment as a function of S. Additionally the density (number of molecules per unit volume) must be specified,

and correction factors (g), F_i and h for the internal field evaluated from the same model. While the qualitative behavior of the permittivity can mostly be explained in terms of these equations, they do not provide a quantitative theory of dielectric behavior. For isotropic fluids, the Kirkwood correlation factor can simply be interpreted as the ensemble average of the cosine of the angle (θ_{pair}) between the dipole moment vectors on interacting pairs of molecules, i.e.

$$g_{isotropic} = 1 + < \cos\theta_{pair} > \tag{5.4}$$

Therefore, in the case that constant g_N, the average permittivity, $\langle\epsilon'\rangle$ ($= (\epsilon'_{\parallel} + 2\epsilon'_{\perp})/3$) expressed in Eqn. 5.3 should vary in a continuous way with decreasing temperature from the isotropic phase to the nematic phase. However, for many liquid crystals, especially those containing strongly polar molecules, the temperature dependence of the dielectric behavior is not as predicted by the above equations, while there is either an increment or a reduction in the mean permittivity at the nematic to isotropic transition due to local dipole-dipole correlations. The net dipole correlation factor (g_N) in the nematic phase is a function of S which in turn is dependent on temperature. This is expressed as below [58].

$$g_N = \frac{g_{\parallel}}{3\mu^2}\left[\mu_l^2(2S+1) + \mu_t^2(1-S)\right] + \frac{2g_{\perp}}{3\mu^2}\left[\mu_l^2(1-S) + \mu_t^2(1+\frac{1}{2}S)\right] \tag{5.5}$$

The short-range angular correlations between the dipolar molecules, which can quantitatively be represented in terms of the Kirkwood correlation factors, are defined by:

$$g_j = 1 + \frac{1}{V}\int G(R)_{(j)}dr \tag{5.6}$$

where V is the volume of the sample, and $G(R)_{(j)}$ is the j-component of the normalized angular correlation matrix [59]. The theoretical evaluation of the angular correlation matrix in the nematic phase requires a detailed microscopic model [7]. It should be noted that $\Delta\epsilon$ ($=\epsilon_{\parallel} - \epsilon_{\perp}$) can be obtained from Eqns (5.1) and (5.2).

This is given by [7]

$$\Delta\epsilon = \frac{NhF}{\epsilon_o}\left(\Delta\alpha - \frac{\mu^2 g_{(\parallel-\perp)}{}^2 (1-3\cos^2\beta)}{2kT}\right) S \tag{5.7}$$

Here, $\Delta\alpha$ ($=n_{\parallel}^2$ - $n_{\perp}^2$) is the anisotropy of polarizability. $g_{(\parallel-\perp)}$ means the anisotropic correlation factor. Interestingly, $\Delta\epsilon$ roughly follows order parameter, if β is constant and the short-range correlations are weak. Thus if the molecular dipole moment is predominantly perpendicular to the alignment axis, then the dielectric anisotropy is negative.

The concept of nematic potential responsible for the occurrence of the nematic phase at low temperatures was included in the theory of the dielectric relaxation of the nematic phases. In particular, compared to the Debye process in the isotropic phase, the M-M model predicts a much slower relaxation process. The relaxation times in the nematic liquid crystals were demonstrated to increase significantly for the longitudinal dipoles, since these reorient together with the molecule around its short axis against the orienting potential [60]. For the nematic phase, each component of the dielectric permitivity in Eqns. (5.1) and (5.2), contains two contributions from the total molecular dipole moment. Each of these components of the permittivity is expected to show at least two relaxation processes at a particular frequency. Figure 5.1 shows possible rotational modes for a molecule in the nematic phase. The parallel and perpendicular axes denote the direction of the electric field with respect to the director. The molecular dynamics can approximately be described by the four rotational modes: (a) the end-over-end rotation ω_1, (b) the precessional motion of the long molecular axis around the director of the phase ω_3 and the combination of precessional and rotational motions around the long molecular axis ω_4 and (c) the rotation around its own long molecular axis ω_2. On the assumption that the molecules are rigid and intramolecular relaxations are forbidden, only a single net dipole moment contributes to the dielectric permittivity. The temperature dependence of the dielectric relaxation strength for each component is primarily determined by the variation of the principal order parameter S with temperature. In order to obtain more information about the

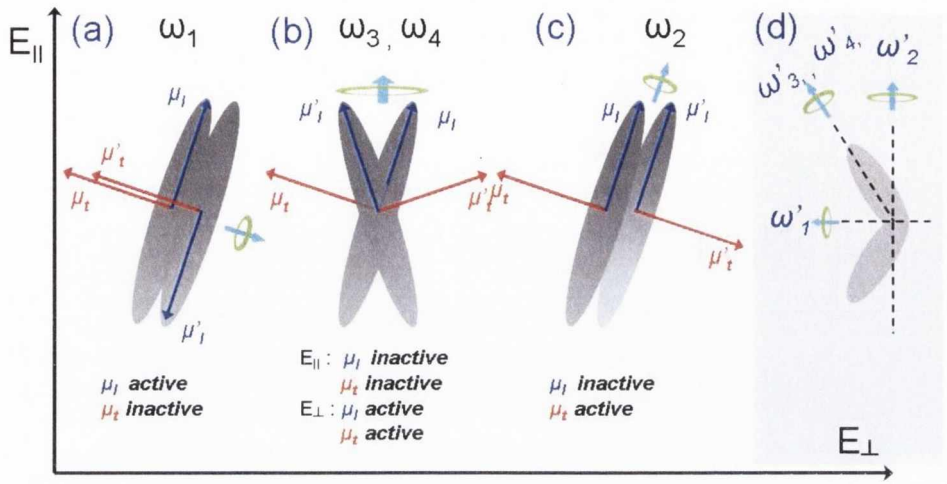

Figure 5.1: Illustration of the mechanisms for the rotational relaxation. The end-over-end rotation, ω_1 (a) and the rotation around its own long molecuar axis,ω_3 (c) are active to $E_{\|}$ under the homeotropic configuration. The precessional motion of the long molecular axis around the director $\mathbf{n}$, ω_2 and the combination of precessional motion and rotational motion around the long molecular axis, ω_4 (b) are active to $E_{\perp}$ under the planar configuration. (d) depicts the molecular rotation of a bent-core molecule and each rotational frequency is similiar to combinational motions of the two arms.

nature of the rotational dynamics in liquid crystals, it is necessary to employ suitable microscopic models. The frequency dependent components of the complex permittivity tensor can be related to the Laplace transform of the time autocorrelation functions for projections of parallel and perpendicular components of the molecular dipole moment to the director. Nordio and co-workers [61] solved this problem in terms of dipole correlation functions. Their result can be compactly expressed in terms of the time evolution of dipole correlation functions parallel and perpendicular to the director:

$$\langle \mu_{\|}(0) \cdot \mu_{\|}(t) \rangle = \frac{1}{3} \left[\mu_l^2 (1 + 2S) \Phi_{00}(t) + \mu_t (1 - S)^2 \Phi_{01}(t) \right] \tag{5.8}$$

$$\langle \mu_{\perp}(0) \cdot \mu_{\perp}(t) \rangle = \frac{1}{3} \left[(1 - S) \mu_l^2 \Phi_{10}(t) + (1 + \frac{1}{2} S) \mu_t^2 \Phi_{11}(t) \right] \tag{5.9}$$

While Eqns. (5.1) and (5.2) give the magnitudes of the components of permittivities, the Eqns. (5.8) and (5.9) express the dynamics of the corresponding relaxations. Each of the time-dependent angular functions, Φ_{mn}, where the subscripts m and n are the indices of the Wigner function, can be expressed as a sum of exponentials in time or frequency of the fluctuating components of the molecular dipole and the time dependence can sufficiently be described by a single correlation time, τ_{mn} for each component. A relation can approximately be established between these times and the four different rotational modes, such that $\omega_1^{-1} \sim \tau_{00}$, $\omega_2^{-1} \sim \tau_{01}$, $\omega_3^{-1} \sim \tau_{10}$ and $\omega_4^{-1} \sim \tau_{11}$, where τ_{00}, τ_{01}, τ_{10} and τ_{11} are the corresponding relaxation times [58] as shown in Fig. 5.2. If the local rotational diffusion coefficient is isotropic, then ω_2 and ω_4 are equal. The relative magnitude of the dipole components and the frequencies of dielectric relaxations indicate precisely the orientation of the dipole with respect to the alignment axis of the molecule. For rod-like molecules the relative frequencies are $\omega_1 << \omega_3 < \omega_4 \leq \omega_2$. However, for BCMs, it is expected that the transverse component of molecular dipole moment will relax at the frequency range comparable to ω_3 because V-shaped molecular structure causes additional hindrance to rotation around the long axis. From the viewpoint of the molecular structure, the BCMs have two arms, the rotation around molecular long axis is similar to the combination of the precessional motion of each arm around molecular long axis. In turn the precessional motion of molecular long axis is similar to the combination of precessional motion of one arm and the rotation around the other arm (see Fig. 5.1 (d)).

Figure 5.2 shows a schematic representation of the components of the real part of permittivity as a function of frequency. The sign of $\Delta\epsilon'$ depends on the range of frequencies as shown in Fig 5.2. In the low frequency range, static $\Delta\epsilon$ is given by Eqn. (5.7). However, in this example $\Delta\epsilon'$ changes sign from $\Delta\epsilon' > 0$ at $f < f_{c1}$ to $\Delta\epsilon' < 0$ at $f > f_{c1}$ as a function of frequency of the applied field, f. The crossover frequencies f_{c1} and f_{c2} are associated with the frequencies corresponding to ω_1 and ω_3 respectively. When an electric field is applied to a LC in a cell, it exerts a torque on the director, $\mathbf{n}$, that depends on the dielectric anisotropy and the sign of $\Delta\epsilon'$ decides the reorientation with respect to the field. The frequency

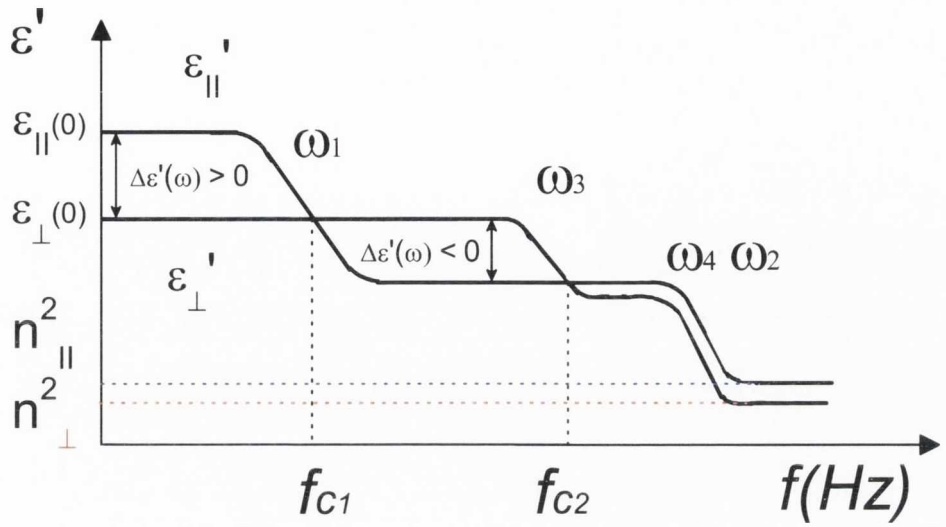

Figure 5.2: A schematic representation of the variation with frequency of $\epsilon'(\omega)$ of a uniaxial nematic and f_c(cross over frequency).

dependent sign of the dielectric anisotropy can be used to align the directors along or perpendicular to the electric field direction by varying the frequency of the driving signal, so called dual frequency nematics (DFNs). This makes it possible to accelerate both the turning-on and turning-off processes by applying a high voltage pulse with different frequencies [62]. In addition to the dielectric reorienting torque, the electric field causes heating of the LC, especially in the dispersion region [63]. It should be noted that Jadzyn *et al* [57] used magnetic field to reorient the director and measured dielectric spectra with angle changing between the probing electric field and the director continuously . They reached the conclusion that dielectric spectra under various angles between the probing electric field and the director should be analyzed in terms of the three relaxations corresponding to the molecular motions. The relative strengths of the relaxations, and hence the corresponding dielectric loss are dependent on the values of the dipole components, i.e., the magnitude of the molecular dipole and its direction with respect to the long axis. This indicates that it is possible to observe molecular rotational modes under imperfect anchoring condition for the planar and the homeotropic arrangement.

5.3 Results

5.3.1 C4: a usual nematic phase

C4 with butyl chains was found to exhibit an ordinary nematic phase without cybotatic clusters (see Table. 3.1, [18]). The dielectric spectra for the parallel and perpendicular components of complex permittivity ($\epsilon^*(\omega) = \epsilon'(\omega) - i\epsilon''(\omega)$) recorded with planar and homeotropic configurations respectively. The parallel components of the permittivity($\epsilon'_{\parallel}$) and dielectric loss ($\epsilon''_{\parallel}$) are shown in Fig.5.3 (a) and (b), for various values of $\Delta T = (T_{N-I}\text{-}T)/^{\circ}K$. The perpendicular components of the permittivity ($\epsilon'_{\perp}$) and the dielectric loss ($\epsilon''_{\perp}$) are shown in Fig. 5.3 (c) and (d) respectively. Compared to the permittivity curves of the isotropic phase at ΔT = -10 (black square), the permittivity curves in the nematic phase (see Fig. 5.3(a) and (c), ΔT = 10, 20, 30, 40, 50) show different values over a wide range of frequencies with the curves shifting to lower frequencies with temperature decreasing. It seems to be a typical behavior for a nematic LC with positive $\Delta\epsilon$. The direction of the molecular dipole moments of the individual molecules are randomized in the isotropic phase, hence the time averaged dipole moment contributes to the permittivity. Meanwhile, in the nematic phase, only the effective molecular dipole moment along the applied field determines the permittivity [57]. After a transition to the nematic phase , the decrease of $\epsilon'_{\parallel}$ at relatively higher frequencies range arises from the nematic order (see Fig. 5.3 (a)). The dispersion, in the dielectric loss $\epsilon''_{\parallel}$ in Fig. 5.3 (b), is related to the nematic order coming from the rotational frequency of the end-to-end rotation around the short axis. Dramatic increases in the permittivity curves observed for frequencies lower than 1 kHz are due to the DC conductivity which makes it difficult to determine the values of the static permittivity at low frequencies. Such increases due to the DC conductivity are also seen in the loss curves as shown in Fig. 5.3(b) and (d). Interestingly, another dispersion f_{10}, is observed in the curve of ΔT = 50 at the frequency of a few hundred kHz (see Fig. 5.3(d)). The temperature, ΔT = 50 lies in a supercooled state and the characterization of the peak is not covered by this

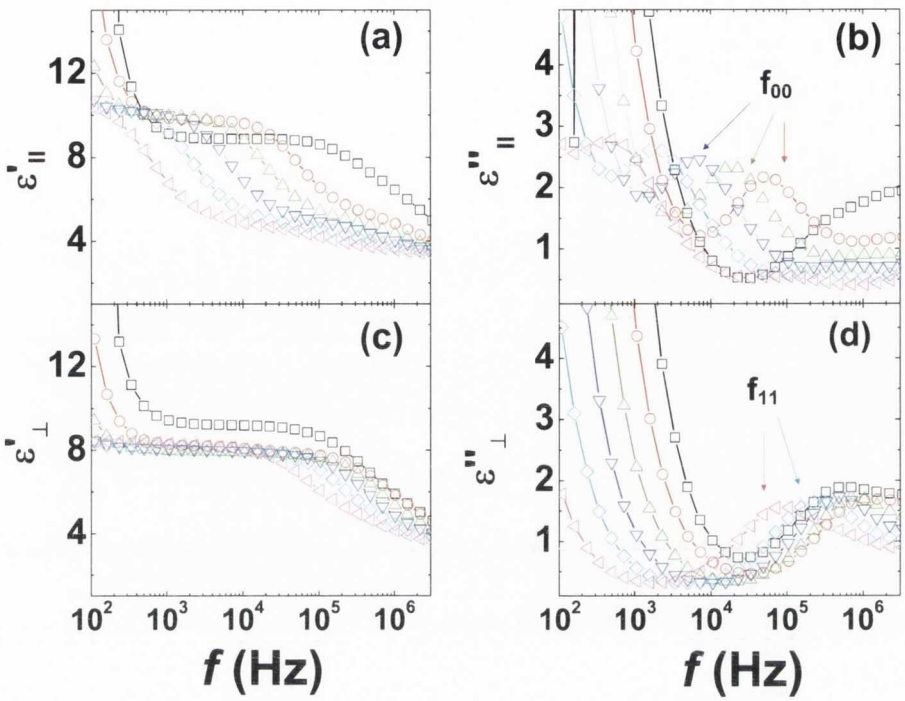

Figure 5.3: Frequency dependence of the real and imaginary parts of permittivity in the nematic phase of C4 for cells of homeotropic and planar configurations. (a) $\epsilon'_{\parallel}$ and (b) $\epsilon''_{\parallel}$ denote the parallel components of the complex permittivity: real and imaginary (dielectric loss) for various temperatures. (c) $\epsilon'_{\perp}$ and (d) $\epsilon''_{\perp}$ denote the perpendicular components of the permittivity and of dielectric loss, respectively for various ΔT (= (T_{N-I}-T)/°K), -10 (black square), 10 (red circle), 20 (green triangle-up), 30 (blue triangle-down), 40 (cyan diamond), 50 (magenta triangle-left) T_{N-I} means the transition temperature from isotropic to nematic phase.

work. Temperature dependence of the permittivity is more clearly seen in Fig. 5.4. $\epsilon'_{\parallel}$ and $\epsilon'_{\perp}$ are plotted versus reduced temperature, T*, at preselected frequencies of 1 kHz, 5 kHz, 10 kHz and 100 kHz. Here, the reduced temperature, T*, is defined as $T^* = T_{N-I}/T$. Immediately after the transition to the nematic phase, $\epsilon'_{\parallel}$ at 1 kHz increases while $\epsilon'_{\perp}$ decreases as shown in Fig. 5.4(a). $< \epsilon' >$ is reduced. Interestingly, with T* increasing, $\epsilon'_{\parallel}$ at 1 kHz does not appear to follow Eqn. (5.1) in the window of temperature. Furthermore, it ends with up falling below $\epsilon'_{\perp}$ which seems to follow Eqn. (5.2). Such a crossover phenomenon dependent on frequency is associated with extraordinarily low f_{00} in Fig. 5.3(b). The sign of $\Delta\epsilon'$ can be determined by an optical method which is insensitive to the DC conductivity and

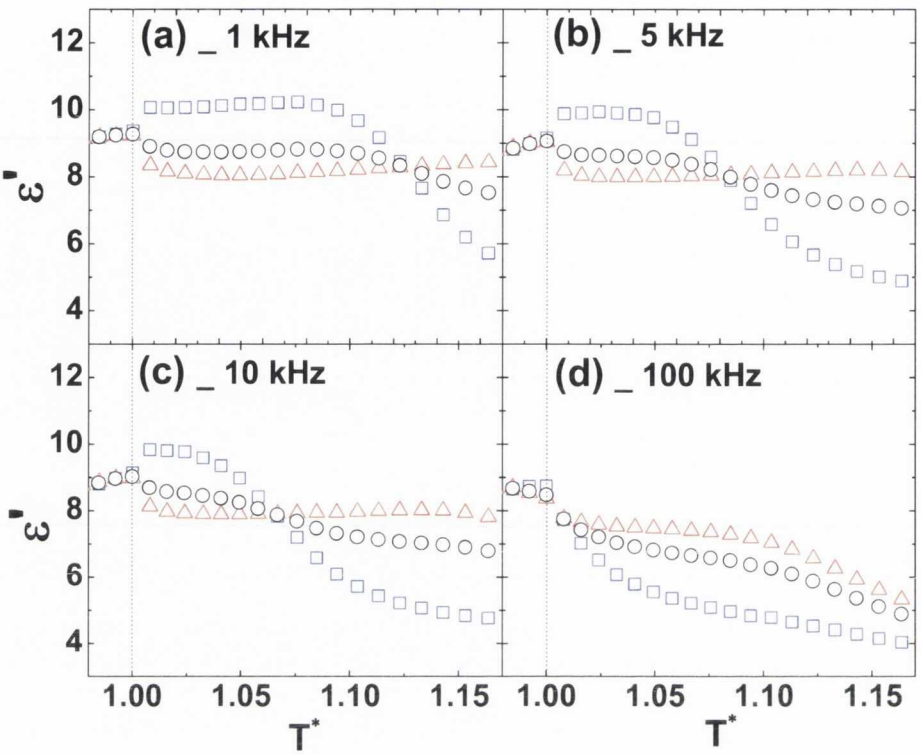

Figure 5.4: Temperature dependence of $\epsilon'_{\|}$ (blue square) and $\epsilon'_{\perp}$ (red triangle) of C4 for the frequencies of 1 kHz, 5 kHz, 10 kHz, 100 kHz, and the average dielectric permittivity (black circle), $< \epsilon' >= (\epsilon'_{\|} + 2\epsilon'_{\perp})/3$. $T^* = T_{N-I}/T$. Black dotted line represents the transitions from the isotropic to the nematic phase.

this will be introduced in Chap. 6.2.1. It is clear from Eqns. (5.8) and (5.9) that the dispersions in Fig. 5.3(b) and (d) are associated with one of the molecular relaxation modes. Total permittivities can be resolved in terms of the strength of each molecular mode. Each relaxation frequency (f_{00} , f_{01}, f_{10} and f_{11}) corresponds to the relaxation time, τ_{ij} expressed as $f_{ij} \approx (2\pi\tau_{ij})^{-1}$ and the rotational motions described in Fig. 5.1. For $\epsilon'_{\|}$ investigated using a homeotropic cell, f_{00} and f_{01} can be recorded. For $\epsilon'_{\perp}$ investigated using a planar cell, f_{10} and f_{11} can also be recorded. According to the M-M model [56], the strength of each mode is a function of the order parameter, in turn, the dependence can indicate what kind of motion it is. The measured dielectric loss of C4 is fitted to the Havriliak-Negami (H-N) equation [64] for the frequency dependent complex permittivity $\epsilon^*(\omega)$ which

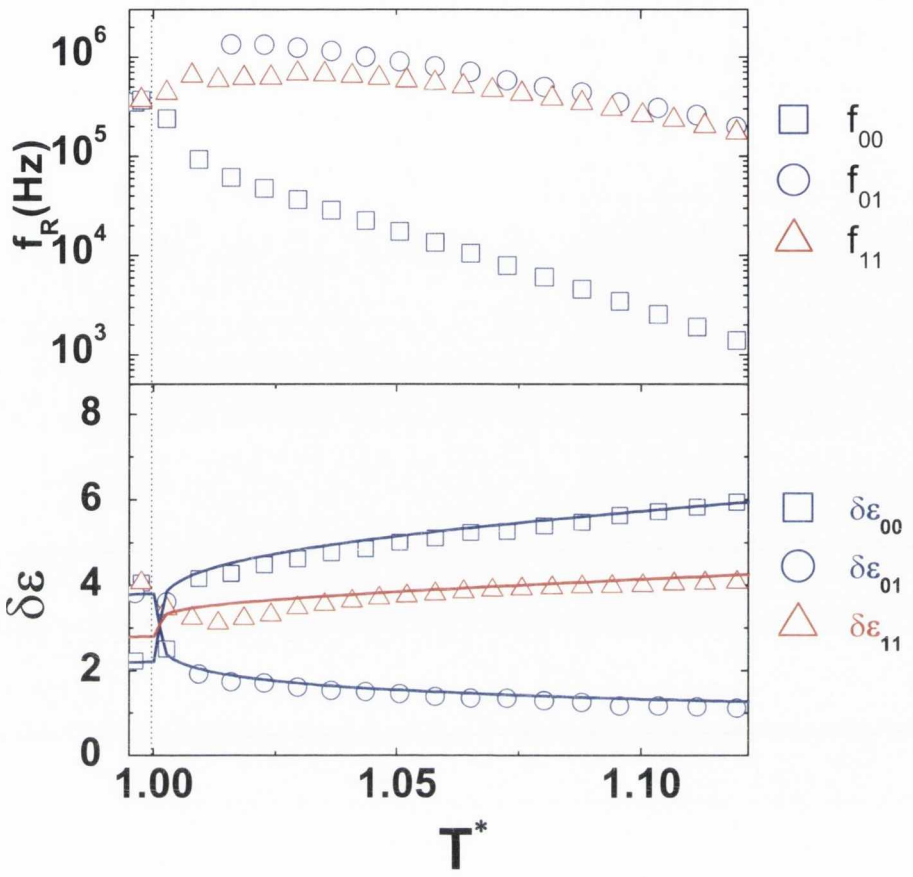

Figure 5.5: Relaxation frequency $f_{ij} \approx (2\pi\tau_{ij})^{-1}$, and the dielectric strength ($\delta\epsilon_j$) obtained by fitting the measured permittivity data to the Havriliak-Negami equation, for planar (red triangles) and homeotropic cells (blue circles and squares) of C4 . f_{ij} and $\delta\epsilon_{ij}$ denote the relaxation frequency and the dielectric strength of the i,j-th mode. $T^* = T_{N-I}/T$. Solid lines indicate fit to M-M model ($\mu_l^2/\mu^2 = 0.368$ and $\mu_t^2/\mu^2 = 0.632$). Black dotted line on the left indicates isotropic to the nematic transition.

is expressed as below:

$$\epsilon^*(\omega) = \epsilon'(\omega) - i\epsilon''(\omega) = \epsilon_\infty + \sum_{j=1}^{n} \frac{\delta\epsilon_j}{[1 + (i\omega\tau_j)^\gamma]^\lambda} \quad , \tag{5.10}$$

where ϵ_∞ is the high-frequency permittivity, j is a variable denoting the number of the relaxation processes up to n, τ_j is the relaxation time of the jth relaxation process, γ and λ are the fitting parameters and $\delta\epsilon_j$ is the dielectric relaxation strength for the jth process. In this fitting γ and λ are found to be larger than 0.8. This means the relaxation is close to Debye type relaxation (see Appendix. A). Fig. 5.5

shows the relaxation frequencies and the dielectric relaxation strengths obtained by fitting the measured ϵ'' data of C4 to the H-N equation. Each frequency is assigned appropriately to: f_{00}, f_{01}, and f_{11}. The dielectric strengths corresponding to f_{ij} are well fitted to the M-M model. Solid lines in Fig. 5.5 indicate ideal curve fitted to the M-M model. Red line shows temperature dependence on 1+2S , while magenta and blue lines show the dependence on functions of 1-S and 1+1/2S, respectively. The order parameter, S, used in the analysis is estimated through the measurements of birefringence which is introduced in Chap. 6.2.2. f_{00} is observed to be much lower than f_{01} which overlaps to same extent with f_{11}. When the frequency range and the dependence of dielectric strengths on S are taken into consideration, the frequencies assigned in Fig. 5.5 are in agreement with molecular motions described in Fig. 5.1. As a consequence, as far as the dielectric behavior is concerned, C4 seems to have a typical nematic phase. Normally, the f_{c1} of a conventional dual-frequency nematic is observed in the range of a few MHz, while f_{00} of C4 is observed in the range of extraordinarily low frequency, as shown in Fig. 5.5. This leads to the sign reversal of $\Delta\epsilon'$ in the window of the experiment. The phenomenon of the sign reversal of $\Delta\epsilon'$ is consistent with the model described in Fig. 5.2. The change in β can also give rise to the sign reversal of $\Delta\epsilon$ which is observable in dimers. Such a possibility will be investigated in Chap. 6 by means of optical techniques.

5.3.2 C9, a cybotactic nematic LC

C9 exhibits the considerable intensity and the splitting of small angle scattering in X-ray diffraction patterns [18] interpreted in terms of the presence of SmC like nanostructre in the nematic phase. Recently, Hong *et al.* [21] demonstrated that the small angle X-ray diffraction patterns recorded in the nematic phases of two related bent-core compounds are consistent with a fluid organized from microscopic molecular clusters possessing short-range SmC-type layering. Francescangeli *et al.* [46] also showed that the change in the splitting angle of the diffuse

four-spot maxima is associated with a change in the tilt angle in the (short-range) layered structure within clusters that constitute the N_{cybC}. The gradual transformation of the four-spot pattern of a bent-core mesogen into the two-spot pattern on increasing temperature reflects the structural change within the cybotactic groups, from a SmC-like to a SmA like supramolecular organization rather than a change in the bending angle (θ_V). However, the splitting has been interpreted in terms of the form factor due to the bent-shape mesogen [47]. Therefore, it is worth studying the role of cybotactic clusters affecting the dielectric behavior of the mesogen in the nematic phase.

Fig. 5.6 shows the frequency dependence of the permittivity and the loss of C9 which has nonyl chains in the terminal groups. The most significant difference from C4 is the magnitude of $\epsilon'_{\perp}$ which is associated with the strong dispersion in the dielectric loss curve at a frequency comparable with f_{11} of C4 (Fig. 5.6(d)).

The temperature dependence of permittivity of C9 at frequencies of 1 kHz, 5 kHz, 10 kHz, 100 kHz are shown in Fig. 5.7. It is should be noted that $\epsilon'_{\perp}$ at 1 kHz drops on the transition to the nematic phase as is observed in C4 and increases significantly in the entire nematic phase with T* increasing, while $\epsilon'_{\parallel}$ at 1 kHz decreases in the nematic phase. This is in contrast with the behavior of C4. Usually, on the transition to the nematic phase, either $\epsilon'_{\parallel}$ or $\epsilon'_{\perp}$ shows larger value than $< \epsilon' >_{N-I}$ due to the orientation of the director under certain anchoring conditions with respect to the applied electric field. However, for C9 both values decrease and show negative $\Delta\epsilon'$ in the entire temperature and frequency ranges. It is difficult to imagine that flexible non polar terminal groups give rise to a large alternation in the molecular dipole moment leading to such a dramatic change in $\Delta\epsilon$. Besides, the contribution of the longitudinal and transverse dipole components to the dielectric permittivity as given by Eqns. (5.1) and (5.2) seems to be different than C4. In order to resolve the contributions of each molecular relaxation mode to the permittivity, a further analysis is being carried out. While frequencies f_{00}, f_{01} and f_{11} are similar to those observed for C4, $\delta\epsilon_{11}$ increases significantly with T* increasing up to a transition to *CybC* phase. It is clear that each molecular rotation occurs in a range of frequencies of C4, however the dielectric strength does not

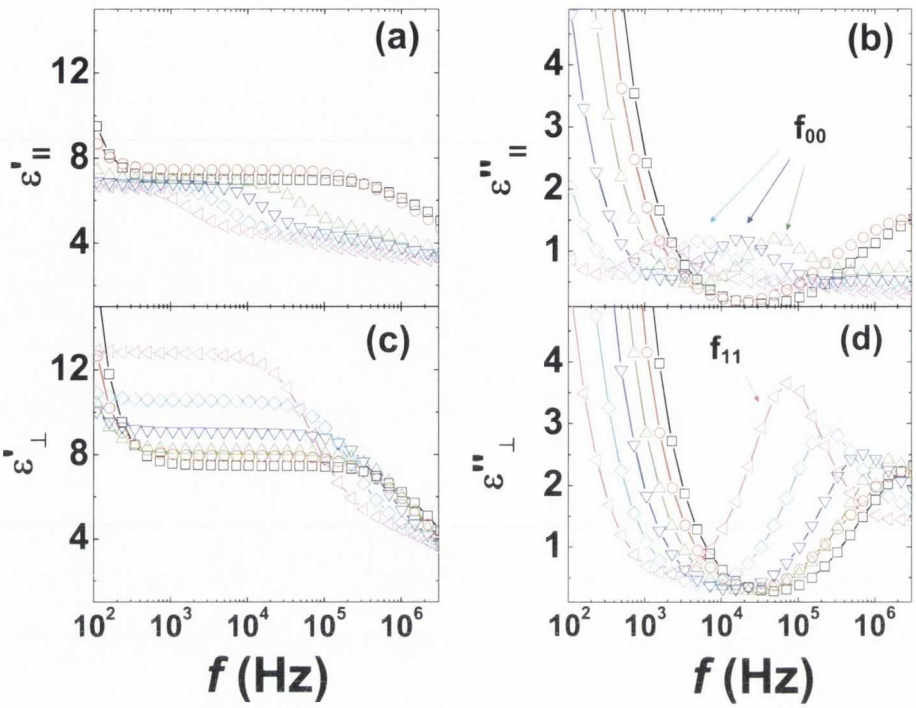

Figure 5.6: Frequency dependence of the real and imaginary parts of permittivity in the nematic phase of C9 for cells of homeotropic and planar configurations. (a) $\epsilon'_{\parallel}$ and (b) $\epsilon''_{\parallel}$ denote the parallel components of the complex permittivity: real and imaginary (dielectric loss) for various temperatures. (c) $\epsilon'_{\perp}$ and (d) $\epsilon''_{\perp}$ denote the perpendicular components of the permittivity and of dielectric loss, respectively for various ΔT(= (T_{N-I}-T)/°K), -10 (black square), 10 (red circle), 20 (green triangle-up), 30 (blue triangle-down), 40 (cyan diamond), 50 (magenta triangle-left) T_{N-I} means the transition temperature from the isotropic to the nematic phase.

follow the M-M model. This disagreement might be associated with strong dipole-dipole interactions which can be interpreted in terms of the Kirkwood short-range correlation factor, g.

5.3.3 C5, C6, C7 with intermediate chains in the terminal groups

The dielectric spectra of C5, C6, C7 are measured as a function of temperature and frequency. For simplicity, we assume $\frac{NhFg_{N-I}}{3\epsilon_0 k_B T}[\mu_l^2 + \mu_t^2]$ to be unity in

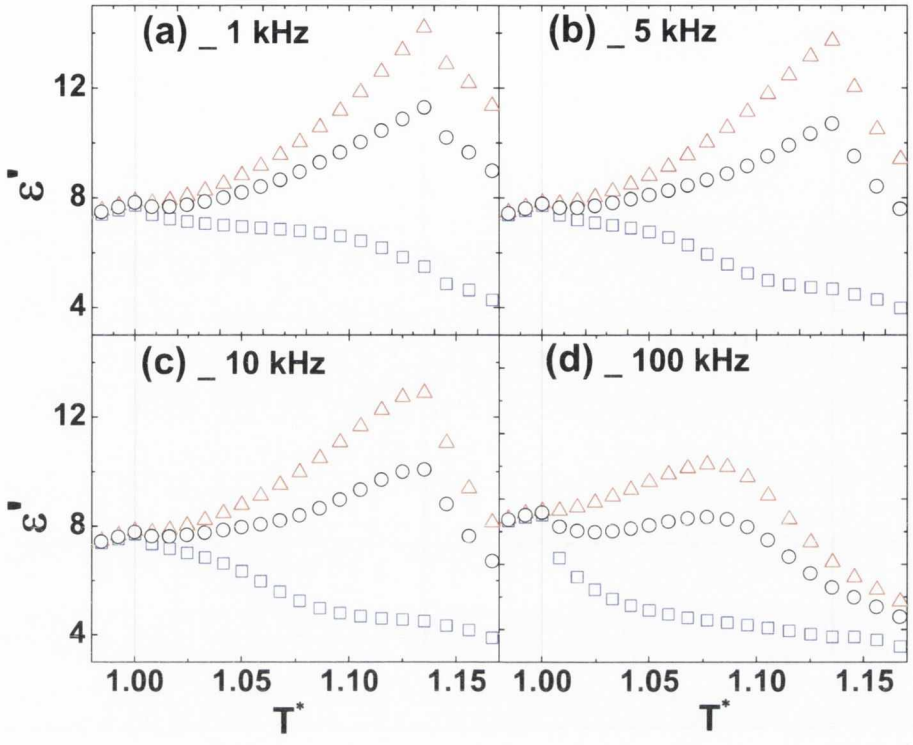

Figure 5.7: Temperature dependence of $\epsilon'_{\parallel}$ (blue square) and $\epsilon'_{\perp}$ (red triangle) of C9 for the frequencies of 1 kHz, 5 kHz, 10 kHz, 100 kHz, and the average dielectric permittivity (black circle), $< \epsilon' > = (\epsilon'_{\parallel} + 2\epsilon'_{\perp})/3$. $T^* = T_{N-I}/T$. Black and red line represent the transitions from the isotropic phase to the nematic phase and the transition from the nematic phase to the CybC phase, respectively.

the temperature range of the nematic phase. The value of $\frac{NhFg_{N-I}}{3\epsilon_0 k_B}\left[\mu_l^2 + \mu_t^2\right]$ can be obtained by fitting the permittivity in the temperature range of the isotropic phase. Then the permittivities due to dipole contributions can be normalized by adjusting the value of Eqn. (5.11) to Eqns. (5.1) and (5.2).

$$A_{N-I} = \epsilon'_{N-I} - n^2_{N-I} = \frac{NhF^2 g_{N-I}}{3\epsilon_0 k_B T_{N-I}}\left[\mu_l^2 + \mu_t^2\right] \tag{5.11}$$

$$\widetilde{\epsilon}_{\parallel} = \frac{\epsilon'_{\parallel} - n^2_{\parallel}}{\epsilon_{N-I} - n^2_{N-I}} = \frac{\widetilde{g}_{\parallel}}{T^*}\left[1 + (3cos^2\beta - 1)S\right] \tag{5.12}$$

$$\widetilde{\epsilon}_{\perp} = \frac{\epsilon'_{\perp} - n^2_{\perp}}{\epsilon_{N-I} - n^2_{N-I}} = \frac{\widetilde{g}_{\perp}}{T^*}\left(1 + \frac{1 - 3cos^2\beta}{2}S\right) \tag{5.13}$$

Here, ϵ'_{N-I} and n_{N-I} are the permittivity and refractive index at the clearing temperature (T_{N-I}), respectively. $\widetilde{g}_{\parallel}$ and $\widetilde{g}_{\perp}$ are defined as $g_{\parallel}/\ g_{N-I}$ and $g_{\perp}/$

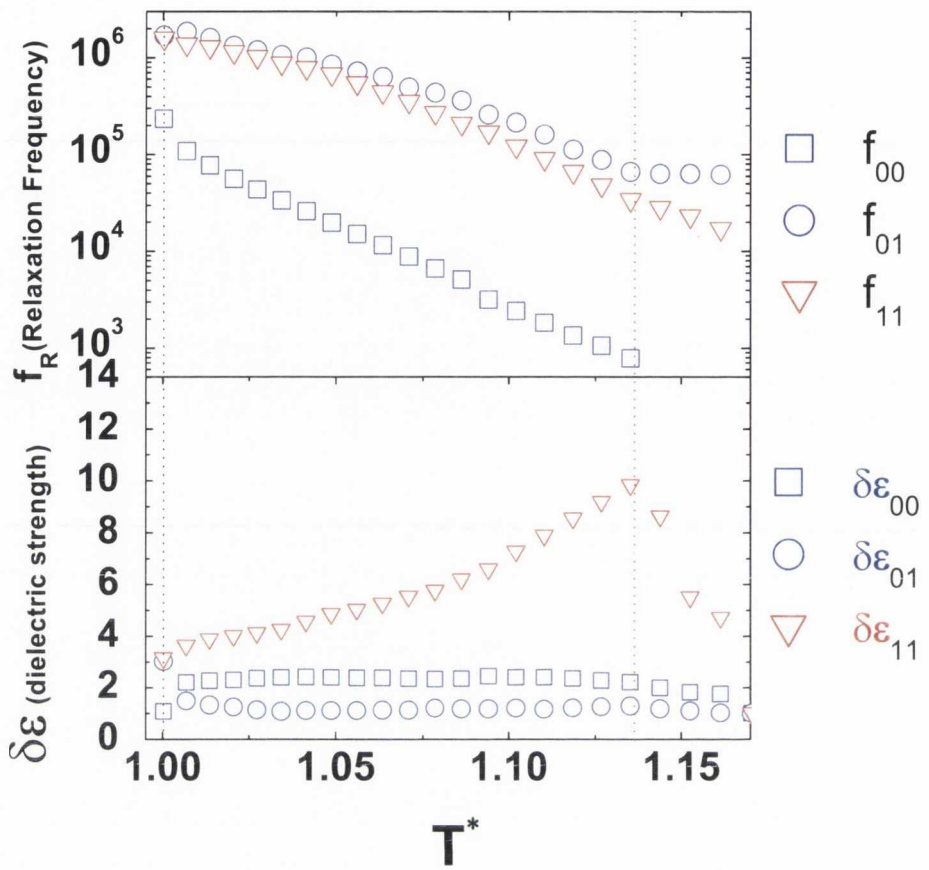

Figure 5.8: Relaxation frequency $f_{ij} \approx (2\pi\tau_{ij})^{-1}$, and the dielectric strength ($\delta\epsilon_j$) obtained by fitting the measured permittivity data to the Havriliak-Negami equation, for planar (red triangles) and homeotropic cells (blue circles and squares) of C4 . f_{ij} and $\delta\epsilon_{ij}$ denote the relaxation frequency and the dielectric strength of the i,j-th mode. $T^* = T_{N-I}/T$. Black and red dotted line indicate the transitions from the isotropic phase to the nematic phase and the transition from the nematic phase to the CybC phase, respectively.

g_{N-I} respectively. Fig. 5.9 (a) and (b) show the normalized values, $\widetilde{\epsilon}_{\parallel}$ and $\widetilde{\epsilon}_{\perp}$ at a frequency of 1 kHz as a function of T^* for parallel and perpendicular configurations, respectively. The permittivities at 1 kHz can be regarded as the static value to the extent that the DC conductivity and the relaxations due to end over end rotation are excluded in the spectra. It is clearly seen from Fig. 5.9 (a) and (b) that as the terminal chains get longer from C4 to C9, $\widetilde{\epsilon}_{\parallel}$ of the materials decreases, while $\widetilde{\epsilon}_{\perp}$ increases in the temperature range of the nematic phase. If the parameter, A and molecular parameter, β are independent of the length of the terminal groups, the

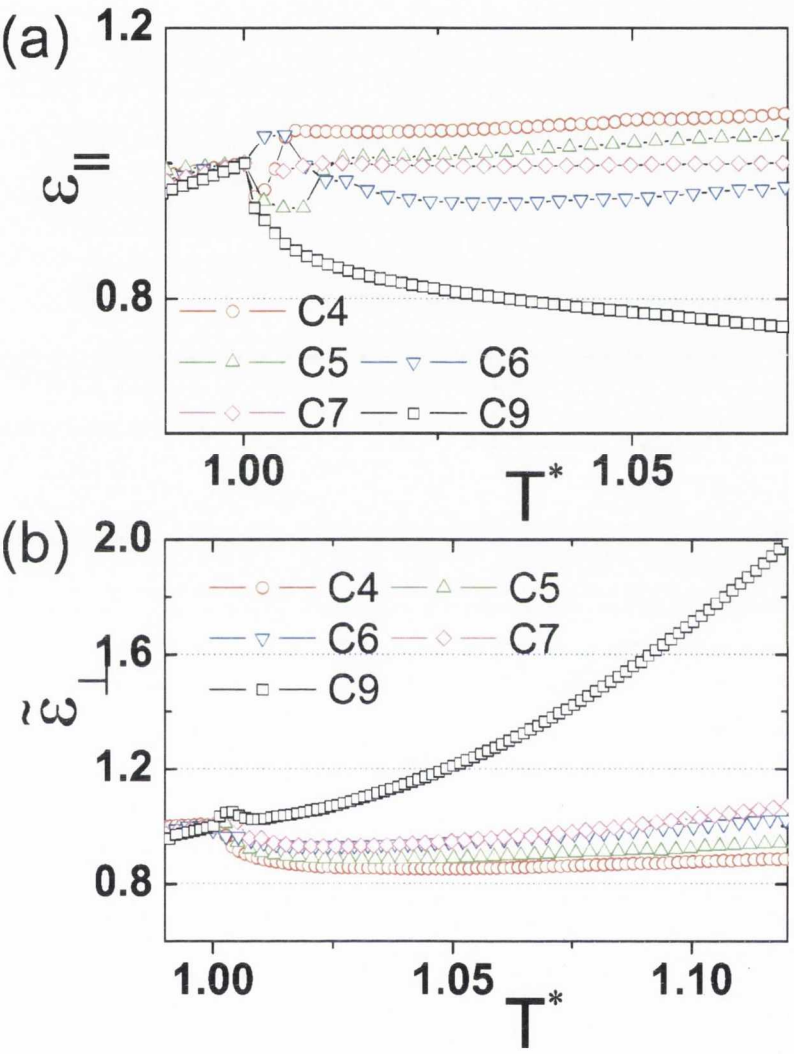

Figure 5.9: Comparison of the normalized permittivities ($\widetilde{\epsilon}_{\parallel}$ and $\widetilde{\epsilon}_{\perp}$)at a frequency of 1 kHz. (a) perpendicular components and (b) parallel components are divided by the value of transition temperature respectively. Here, n_{N-I} is assumed to be 1.6 and temperature independent befringence (Δn_o) is 0.17 which is measured by the PEM. $n_{\parallel}$ and $n_{\perp}$ are calculated to be 1.71 and 1.54 respectively.

disagreement among the normalized values in the nematic phase can be interpreted in terms of the g-factors. As mentioned before, the nematic phase in C4 is found to be consistent with the M-M model with $g_{\parallel} \approx g_{\perp} \approx 1$. If the anisotropic g-factors of C4 are independent of S, the anisotropic correlation factors ($g_{\parallel}$ and $g_{\perp}$) of the other materials are affected by the length of the terminal groups. As the terminal groups get longer, $g_{\perp}$ increases and $g_{\parallel}$ decreases. This means that longitudinal dipoles interact in antiferroelectric order, whereas ferroelectric interaction occurs between the transverse dipoles. The behavior immediately after the transition to the nematic phase might follow from the anisotropy of polarizability ($\Delta\alpha$). Interestingly, $\widetilde{\epsilon}_{\parallel}$ of C6 appears to deviate from the trend of $\widetilde{\epsilon}_{\perp}$ of the other materials (see Fig. 5.9 (a)). It was reported that C6 shows biaxiality under electric field, interpreted as arising from the presence of biaxial clusters [65]. However, the electro-optical behavior is not due to the induced biaxiality but due to the sign reversal of $\Delta\epsilon'$ dependent on temperature as well as on frequency. Recently, Salter *et al.* [66] reported that the flexoelectric coefficient of C6 is greater than that of conventional calamitic LCs.

5.4 Discussion

From the results reported in Chap. 5.3.1, we have found that the dielectric behavior of C4 is consistent with the M-M model based on the molecular-field approximation and the molecular rotational model shown in Fig. 5.1. In these models the short-range correlations in the orientations and positions of neighboring molecules are neglected whereas long-range anisotropic dispersion interactions between the molecules are considered. However, C4 shows the sign reversal of $\Delta\epsilon'$ at quite a low frequency. The conformational change arising from the variation in the anisotropic molecular shape may lead to the change in the magnitude and the angle which the dipole makes with the long molecular axis the molecular dipole moment. Both of these factors may change the dielectric permittivity. Such a dielectric behavior is observed in the liquid crystal dimers which consists of two rigid mesogenic groups linked by a flexible alkyl chain [11]. Stocchero

et al. predicted [12] that dielectric permittivity of a dimer can change the sign of $\Delta\epsilon'$ originating from a conformational change. Nevertheless such a scenario is ruled out for C4 by IR and optical experiments. The core part of C4 consists of aromatic rings and the ester groups. The latter are more flexible than the carbon-carbon bond but are less flexible than the akyl chains. In order to investigate the cause of the sign reversal in C4, we used these two scenarios, one is a comparison between f_{00} and f_c. For determining f_c, we used dielectric spectroscopy as well as an optical method using *Frederiks transition* dependent on the sign of $\Delta\epsilon'$ which was used to confirm the conformational change by Yoon *et al.* [67]. They concluded that two different conformers of a bent-core LC contribute to different slopes of the crossover frequency leading to a biaxial nematic phase. We found that f_c of C4 is comparable to f_{00}, the relaxation frequency due to the end over end rotation around the molecular short axis. This means that so far as the mechanism is concerned, the dual frequency phenomenon of C4 is consistent with the conventional DFNs. Besides, the slopes of f_{00} and f_c against reduced temperature seem to be linear in the window of the temperature range as opposed to works of Yoon *et al.* [67]. In the classical dielectric theory, the macroscopic refractive index is related to the molecular polarizabilty at optical frequencies. The existence of the optical anisotropy is due mainly to the anisotropic optical polarizability of the anisotropic molecular structures. Normally, delocalized electrons not participating in chemical bonds and π electrons play a key role in the optical polarizability. This is the reason that LC molecules composed of benzene rings have higher values of Δn that do the respective cyclohexane counterparts. For more precise evaluation, a different optical technique is applied to investigating the conformation change in Chap. 6. On the basis of the results of the optical and dielectric experiments, we have concluded that C4 has the usual nematic phase and its dielectric behavior can be explained by the M-M-S model. The sign reversal in $\Delta\epsilon'$ in the nematic phase arises from the relaxation frequency of the longitudinal component of the dipole moment which lies at extraordinarily low frequencies.

The static permittivity of cyanoresorcinols with longer terminal chains is gradually shifted from the ideal M-M model as the chain length increases (see Fig. 5.9).

From the viewpoint of the static permittivity, the disagreement can be interpreted in terms of the short-range correlation dependent on the temperature which give rise to a disagreement from the M-M equation. A possibility that this behavior is due to a change in the magnitude and direction of the dipole moment with temperature arising from a conformational change [67] will be ruled out in Chap. 6. As will be shown in Fig. 6.4, the birefringent behavior of C9 is comparable to C4. This implies that there is no significant difference between C4 and C9 in terms of either the molecular flexibility or the conformational change. A most reasonable approach for interpretation of the disagreement in the dielectric behavior is the cluster model: the ordering within the clusters is governed by the short-range anisotropic interactions whereas the macroscopic nematic order is dominated by the long range anisotropic interactions between the clusters. The formation of molecular clusters with internal orientational ordering has been widely reported in a number of nematic BCMs [20–24]. The small angle X-ray scattering pattern in the nematic phase of the material has been reported and this has been interpreted in terms of the presence of clusters [18]. Since C4 does not exhibit any strong small angle X-ray scattering, this cause is ruled out. The temperature dependence of the dielectric relaxation strength for each component of the dipole moment is primarily determined by the dependence of the principal order parameter S on temperature. We find from Fig. 5.10 that results for C4 are well reproduced by the M-M model by assuming $g_{\parallel} \approx g_{\perp} \approx 1$ (see Fig. 5.10). If this assumption is adopted, results between the theory and experiment for C7 and C9 disagree. The only simple appropriate explanation for this disagreement is that both g values are not equal to unity. $g_{\parallel}$ and $g_{\perp}$ are calculated for each temperature with Eqns. (5.1) and (5.2) using the experimental values of $\epsilon_{\parallel}$ and $\epsilon_{\perp}$ and the appropriate scaling factors. We find that $g_{\parallel}$ decreases from unity to 0.7 for C7 and 0.5 for C9, whereas $g_{\perp}$ grows from unity to 1.4 for C7 and up to 3 for C9 as shown in Fig. 5.11. The theoretical evaluation of the anisotropic g requires a detailed microscopic model. One model approach [19] is to think of the clusters as smectic like structures on the assumption that $S = 1$ so that the molecules are constrained to be parallel or anti parallel to the director axis. If a molecular dipole lies at an angle β with

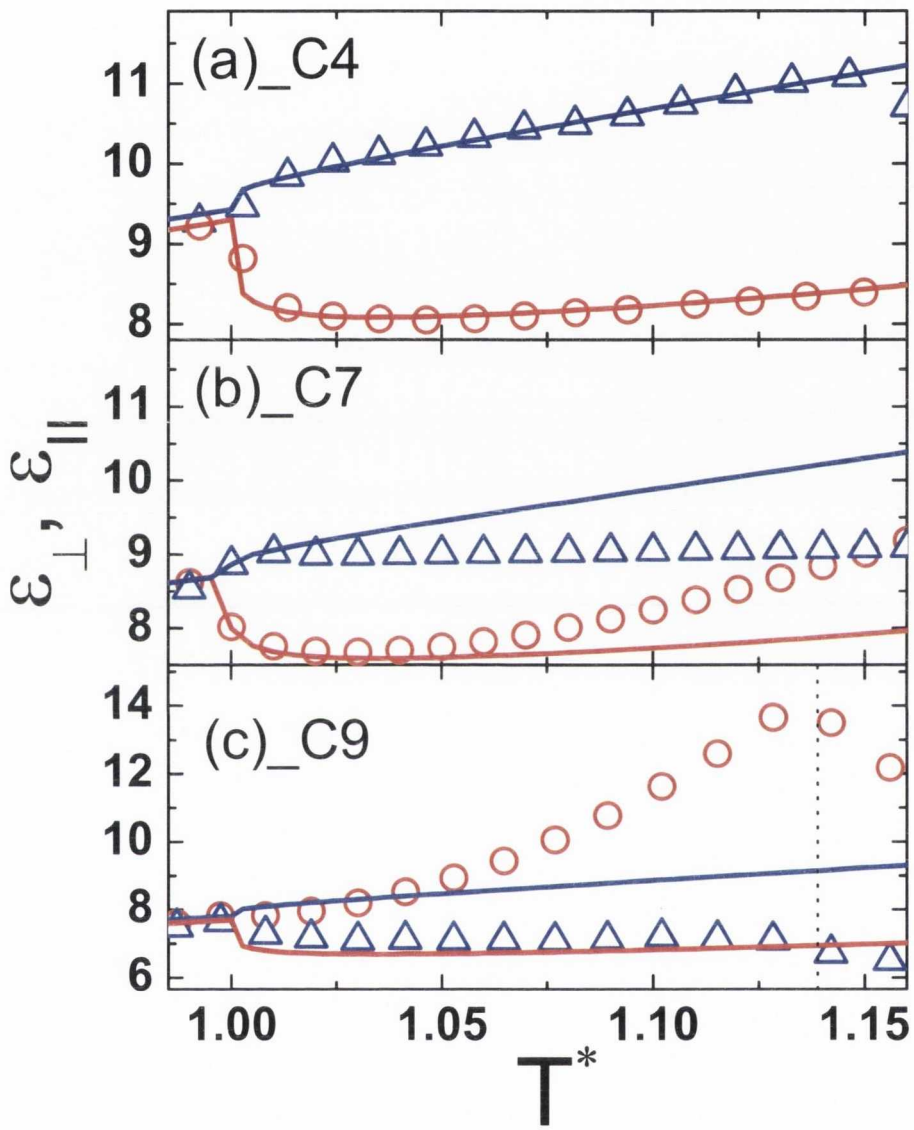

Figure 5.10: Comparison of static and theoretical permittivities of C4(a), C7(b), C9(c) using the M-M model (solid lines). Blue triangles and red circles indicate $\epsilon_{\parallel}$ and $\epsilon_{\perp}$, respectively. These are calculated by adding dielectric strengths for the various processes to ϵ_{∞}. Blue and red lines denote calculated values of permittivity with $\mu_l^2/\mu^2 = 0.368$ and $\mu_t^2/\mu^2 = 0.632$, respectively. Black vertical dotted line in (c) denotes transition from N_{cybC} to $CybC$. We find $\beta = 52.7^o$.

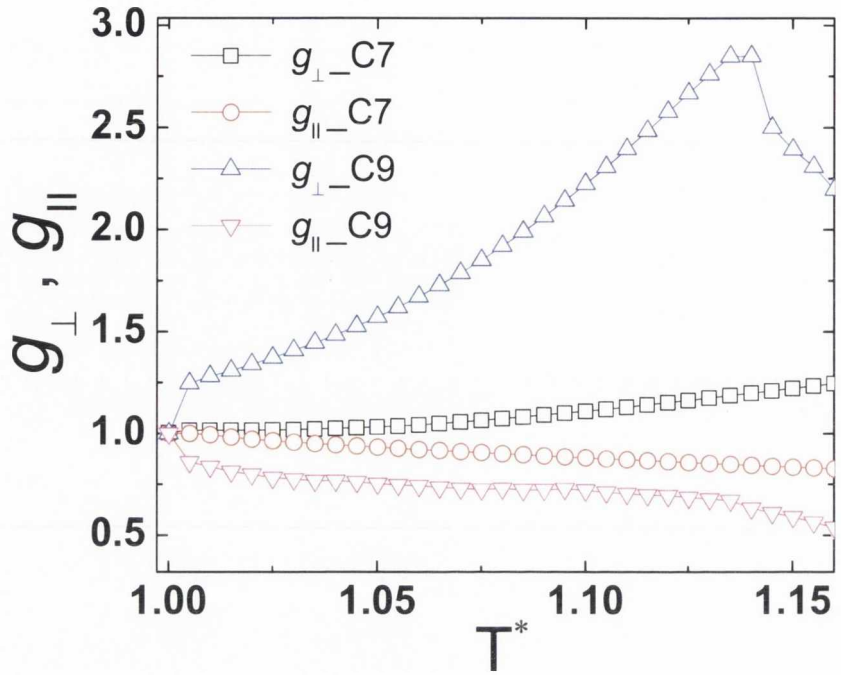

Figure 5.11: Temperature dependence of anisotropic g factors for C7 and C9.

respect to the long molecular axis, the anisotropic dipole-dipole correlation factors can be written as [7]

$$g_{||} = 1 - \frac{n\mu^2 cos^2\beta \left\langle 3\left(\frac{r_z}{r}\right)^2 - 1 \right\rangle}{4\pi\epsilon_o r^3 k_B T} \tag{5.14}$$

$$g_{\perp} = 1 - \frac{n\mu^2 sin^2\beta \left\langle 3\left(\frac{r_x}{r}\right)^2 - 1 \right\rangle}{8\pi\epsilon_o r^3 k_B T} \tag{5.15}$$

here n is the number of neighbors. For a smectic order, the average separation perpendicular to the layers $r_z >>$ in-plane separation, and this results in $g_{||} < 1$. If $\langle r_x^2 \rangle < \langle r^2/3 \rangle$, we get $g_\perp > 1$ indicating a parallel alignment of the polar axes. On using the experimental values of $g_\perp$ and using Eqn. (5.14), we calculate n for a smectic-like order. The average separation values perpendicular r_z and parallel r_x to the individual molecules are taken from the X-ray small angle scattering and wide angle peak positions [18], respectively. We note from Fig. 5.12 that n is increasing significantly versus the reduced temperature T*. The effective volume V of the correlated molecules is estimated by multiplying n by the volume of a single

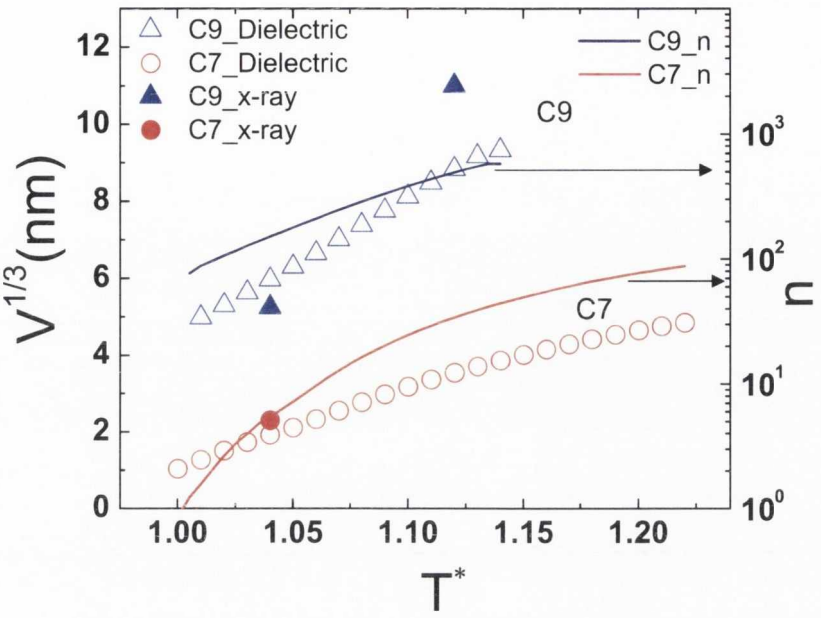

Figure 5.12: Cluster size L=$V^{1/3}$ compared to the x-ray results $V^{1/3} = (\pi/6 \cdot L_{\|} \cdot L_{\perp}^2)^{1/3}$ ($L_{\|}$ and $L_{\perp}$ from [18]) and the line represents n, the number of interacting molecules as a function of reduced temperature (T^*=T_{N-I}/T).

molecule calculated from the molecular weight and density. The polar correlation lengths $l = V^{1/3}$ for C7 and C9 are shown in Fig. 5.12 . It is interesting to compare the above findings with the results from the structural analysis obtained by X-ray scattering [18]. Results agree for C7 and C9 close to the T_{N-I}. However the structural correlation length increases (seen for C9) more rapidly than the polar one. In the structural analysis so far, the splitting in the small angle X-ray diffraction patterns has not been considered yet. The interpretation in terms of the tilt of the SmC type nano clusters will be discussed in Chap. 6.3. The association found from the dielectric results provides information about the polar interactions whereas from X-rays it is really the size and nature of the cluster and the results from the two are broadly in agreement with each other.

5.5 Conclusion

We studied the dielectric behavior in LC cells of homologous series of bent-core liquid crystals with the same mesogenic core but different terminal groups. These materials show different dielectric behavior dependent on the length of terminal groups. As the terminal chains of the materials get longer, the behavior of the devices containing the material deviates from a usual nematic LC consistent with the M-M model. Such a difference has been interpreted in terms of the cybotactic cluster which exists over the entire range of temperatures in the nematic phase rather than a pretransitional phenomenon close to the N-Sm transition. A quantitative analysis has been carried out to find the size of the cluster. The size of the cluster is converted to the number of the molecules in the cluster. The result is compared with that found from X-ray scattering. We find that both results broadly agree with each other.

Chapter 6

Optical studies

"In this chapter, *the optical behaviors of the materials are investigated and interpreted as either the absence or the presence of the cybotactic cluster.* "

6.1 Introduction

An understanding of the relationship between the optical and the molecular properties has been an important topic in the field of liquid crystals. The performance of the electro-optical liquid crystal devices is attributed to the electro-optic properties of materials. In this chapter, we focus on analyzing the difference between the behavior of C4 in which cybotactic clusters are not present and C9 where a nematic phase with cybotactic clusters is found to exist. The macroscopic properties of the materials can be interpreted in terms of cybotactic clusters present in the nematic phase. We use three optical techniques. Firstly, we use an electro optic switching technique dependent on the sign of $\Delta\epsilon$. This is called optical contrast spectroscopy. The results of this method are used to analyze the mechanism of the sign reversal by comparing these results with those from dielectric experiments. In order to find whether sign reversal is caused by conformational change

as was found by Yoon *et al.* [67] or not, the cross over frequency (f_c) is plotted against temperature. Secondly, the birefringence is measured by the PEM for the investigation of the temperature dependence of S. Thirdly, the optical absorbance for the transition dipole moments is measured by the IR spectrometer. This is an indirect investigation for the conformational change with temperature. A brief theoretical background of each technique is being introduced prior to giving the experimental results.

6.2 Results

6.2.1 Measurement of the crossover frequencies using *Frederiks transition*

As a result of $\Delta\epsilon'$, the director can be realigned by an electric field. Thus the reorientation of the director, *Frederiks transition* [68, 69], changes the optical properties of the sample. This phenomenon is used for the commercial LC devices. Normally, the sign of $\Delta\epsilon'$ as well as the magnitude are crucial for the switching of the director. This means that the electro-optic properties of a cell are dependent on the driving parameters such as the frequency of an electric field as well as the temperature. Measurements using optical contrast spectroscopy are carried out in planar cells [31]. While the planar cell used in dielectric measurements is cooled from the isotropic to the nematic phase, the transmittance between crossed polarizers is measured as a function of temperature and frequency. In Fig. 6.1, two transmittance curves with and without the electric field are compared. While an electric field at a frequency of 1 kHz is applied to the planar cell, the *Frederiks transition* is observed. However, below 72° C, *Frederiks transition* is not observed under a field of 2 V/μm applied across the cell. Actually, *Frederiks transition* does not mean exact crossover point of $\Delta\epsilon'$, because it always happens over a threshold voltage which is expressed by $V_{th} = \pi\sqrt{\frac{k_{11}}{\mu_o\Delta\epsilon'}}$. k_{11} denotes the splay elastic constant. Nevertheless, this method is very effective to decide the sign

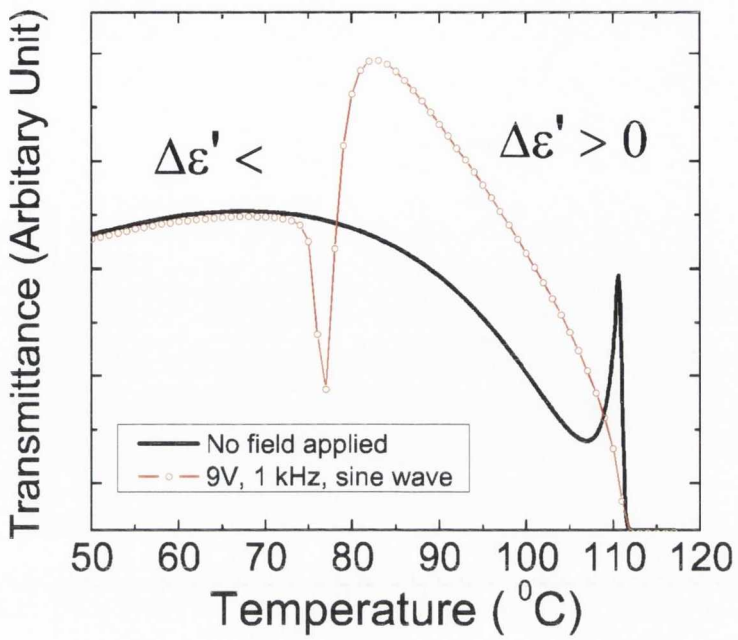

Figure 6.1: For C7, the transmittance curves of the planar cell with and without applied field, thick line denotes without field, thin line with open circles denotes the curve with 9 V, 1 kHz sinusoidal signal. *Frederiks transition* is observed at (72°C).

of $\Delta\epsilon'$ [31, 67]. The sign and magnitude of $\Delta\epsilon'$ are functions of frequency and temperature (see Fig. 5.2). Figure 6.2 shows transmittance change as functions of temperature as well as frequency. The lines mean constant transmittance and the colors represent arbitrary levels of transmittance. The crowed lines are associated with a rapid change in transmittance due to *Frederiks transition*. The slope of the crowded line can represent f_c with the reduced temperature on the assumption that the applied voltage is large enough to reorient the directors with a small magnitude of $\Delta\epsilon'$. By comparing Fig. 6.2 to 6.3, it is clear that f_c of C4 and C5 are comparable to f_{00} of those at the temperature range, while f_c of C7 is in disagreement with f_{00} at low frequency range ($\leq$ 1 kHz). For $T^* \geq 1.12$, the sign of $\Delta\epsilon'$ is alway negative regardless of frequency. This contrasts with the behavior of conventional DFNs. As a result, C4 and C5 are typical for DFNs, while C7 shows dual frequency only at relative higher temperature and higher frequency. At lower temperature and lower frequency, the sign reversal of $\Delta\epsilon'$ for C7 is due to a crossover between the static permittivities ($\epsilon_{\|}$ and $\epsilon_{\perp}$) rather than due to the

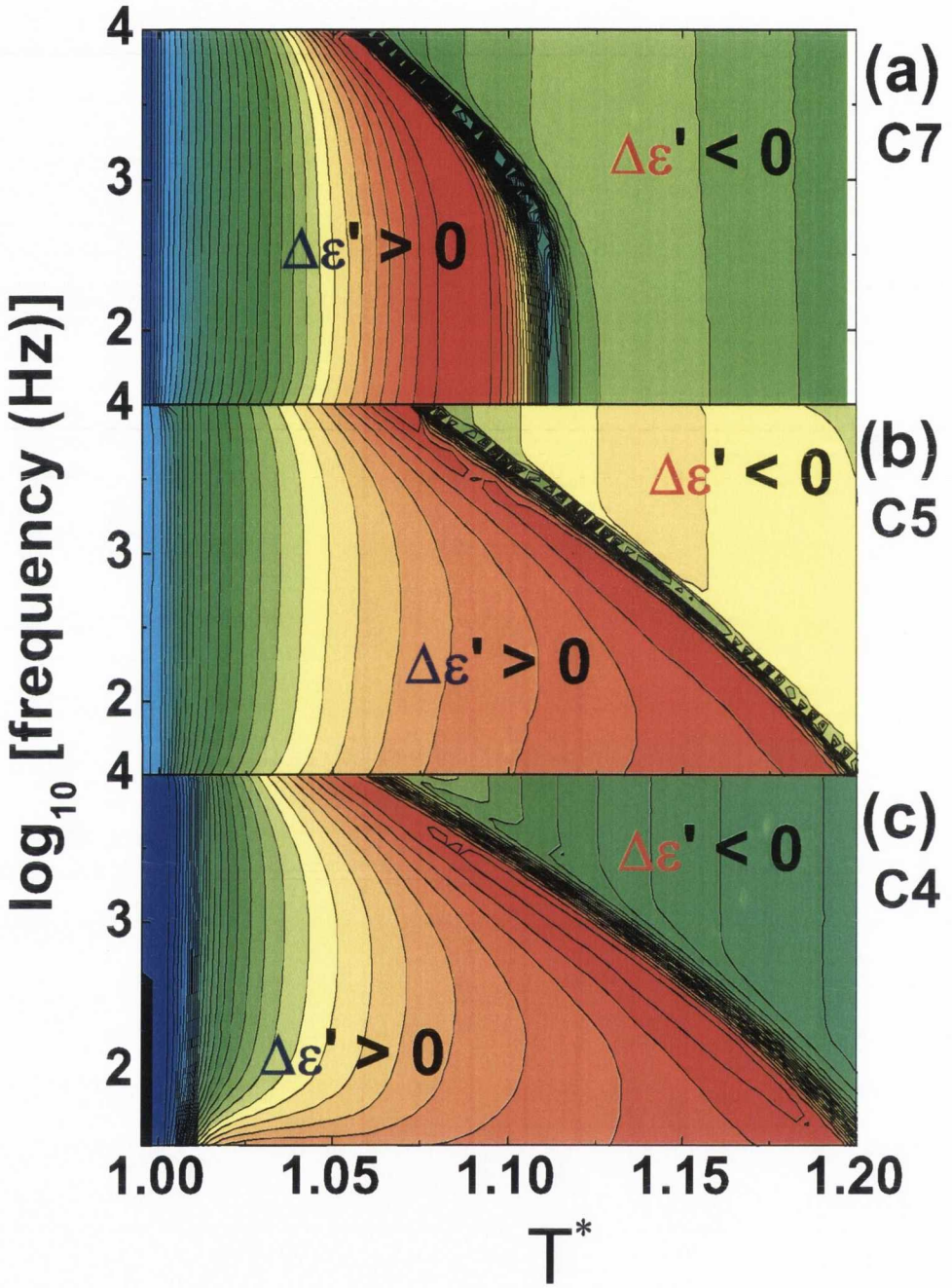

Figure 6.2: Frequency - temperature plot of the transmittance curves of C7 (a), C5 (b) and C4 (c), the contour-line implies a constant value of the transmittance. Slope of the curved crowded lines, f_c as a function of T^* is comparable to f_{00} in a range of limited temperatures.

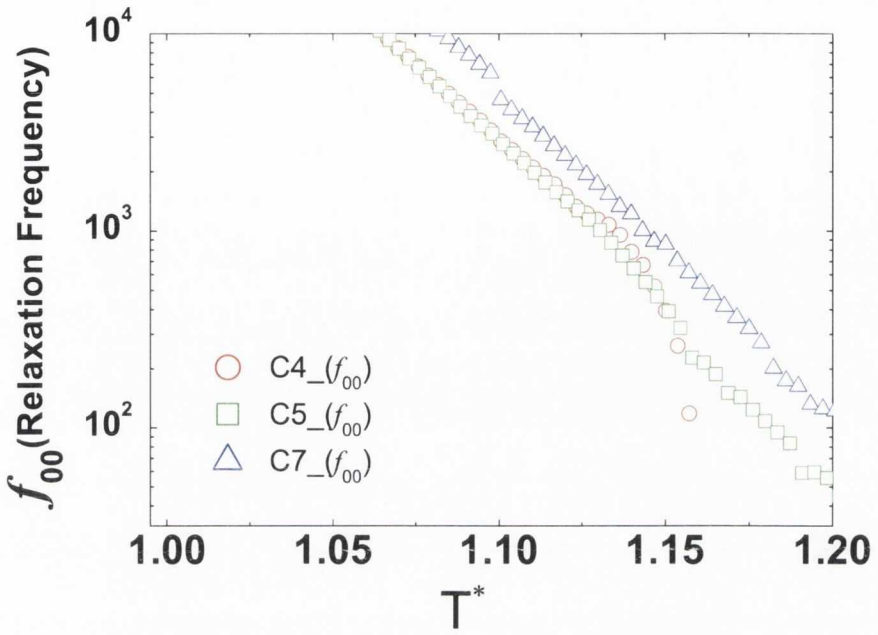

Figure 6.3: Relaxation frequency f_{00} for C4, C5 and C7. $T^* = T_{NI}/T$. For C4, the fall off of f_{00} in the low temperature range of the nematic phase may arise from a supercooled state of the nematic phase. f_{00} of C7 is slightly different from those of C4 and C5. The reason is not clear.

dispersion in f_{00} .

6.2.2 Birefringence and the order parameter

The measurement of birefringence provides a simple method of calculating the orientational order parameter as well as of finding conformational change in the liquid crystalline phase. For the isotropic phase, the Lorentz-Lorenz expression relating the refractive index to the mean polarizability is given by:

$$\frac{n^2-1}{n^2+2} = \frac{N\alpha}{3\epsilon_0} \tag{6.1}$$

where N is the number density, α is the mean polarizabilty, n is refractive index. The above equation means that refractive index of material is governed by a polarizability and the number density of molecules. This model can be adapted to

uniaxial nematic phase for which the formula is given as below:

$$\frac{n_{\parallel}^2 - 1}{n^2 + 2} = \frac{N\alpha_{\parallel}}{3\epsilon_0} \tag{6.2}$$

$$\frac{n_{\perp}^2 - 1}{n^2 + 2} = \frac{N\alpha_{\perp}}{3\epsilon_0} \tag{6.3}$$

where subscripts $\parallel$ and $\perp$ denote the parallel and perpendicular components of refractive indices measured with reference to the director. n is the averaged refractive index. Each component of the polarizability ($\alpha_{\parallel}$ and $\alpha_{\perp}$) can be expressed in terms of the longitudinal and transverse components of the molecular polarizabilties and the order parameter of the phase. The nematic phase of the materials are optically uniaxial. If contributions from the molecular biaxiality are neglected, this macroscopic polarizability can be expressed in terms of the microscopic molecular polarizability and S as given by [7]:

$$\alpha_{\parallel} = \alpha + \frac{2}{3}(\alpha_l' + \alpha_t')S \tag{6.4}$$

$$\alpha_{\perp} = \alpha - \frac{1}{3}(\alpha_l' + \alpha_t')S \tag{6.5}$$

where S is the order parameter and α is the average polarizability. α_l' and α_t' denote the lateral and transverse molecular polarizability, respectively. Combination of above Eqns. (6.2)-(6.5) leads to the following equation [70]:

$$\frac{n_{\parallel}^2 - n_{\perp}^2}{n^2 + 2} = \frac{S\Delta\alpha'}{\alpha} \tag{6.6}$$

where $\Delta\alpha'(= \alpha_l' - \alpha_t')$ is the anisotropy in the molecular polarizabilty. This equation represents the relationship between the birefringence and the anisotropy in the molecular polarizabilty. Conceptually, it is not difficult to connect the anisotropy of the molecular polarizabilities to the anisotropy of molecular shape. The materials under study consist of highly polarizable core part and less polarizable alkyl chains (see Fig. 3.1). It is clear that θ_V significantly affects this molecular polarizabilities as well as the molecular dipole moments. The birefringence and the temperature dependence of order parameter, S can be expressed simply by the

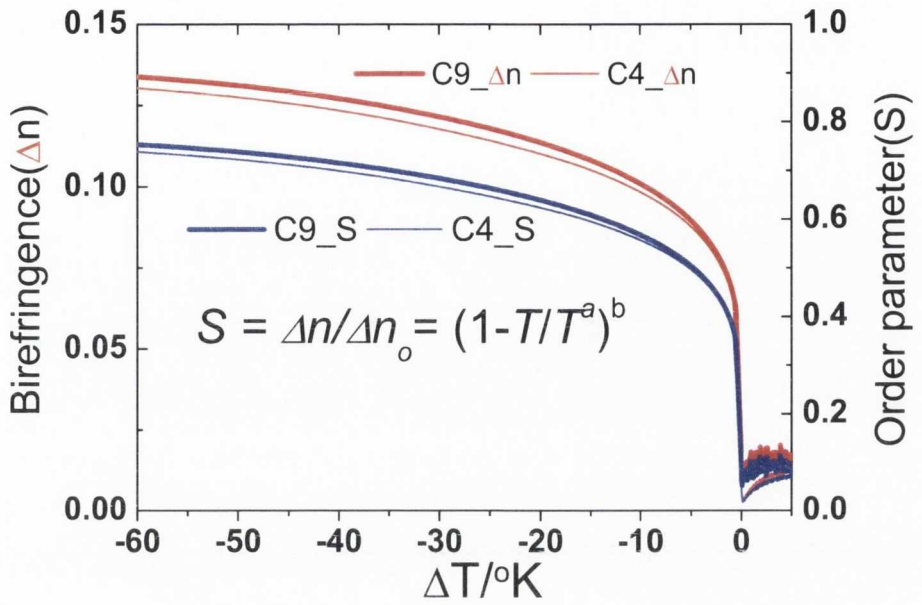

Figure 6.4: Temperature dependence of birefringence (Δn) and S of C4 and C9. Inset equation is relationship between S and birefringence. where a and b are fitting parameters and Δn_0 is a temperature independent birefringence. Fitting parameters of C4 and C9 are $\Delta n_0 = 0.177$, $b = 0.159$ and $\Delta n_0 = 0.178$, $b = 0.153$, respectively.

equation given by:

$$S = \Delta n / \Delta n_0 = (1 - T/T^a)^b \tag{6.7}$$

Here, a,b are the fitting parameters and Δn_0 is the temperature independent birefringence. Birefringence of the materials is measured by an optical technique using the PEM, which is shown in Fig. 6.4. It is clearly seen that the birefringence curve of C4 (thin red line) dependent on temperature is comparable to that of C9 (bold red line) over a wide temperature range. In terms of the optical anisotropy, if there is a conformational change in the bent-core part of C9 compared to C4, it should alter not only the molecular dipole moment or the angle it makes with the molecular long axis but also the optical anisotropy.

6.2.3 IR spectroscopy and the conformational change

IR absorbance spectra due to the transition dipole moment in the LC molecules are dependent on the configuration of liquid crystal phase. At a microscopic level, the IR absorption depends on the angle between the molecular transition dipole moment, μ_i, of the particular absorption band and the polarization of the IR beam. A general biaxial phase of biaxial molecules is described by the four scalar order parameters; S, P, D, and C. The order parameters are defined by a set of equations (Eqn. (1.8)). The order parameter D is a measure of the difference between the distribution of the molecular axes x and y with respect to the laboratory axis Z. If D is positive, the molecular axis x is oriented closer than the axis y to the laboratory axis Z. If the effect of the molecular interactions and the local field can be ignored, then the components parallel and perpendicular to the optical axis can be written down in terms of the components of the dipole moment along the principal axes. Since the components need to be averaged over all possible orientations of the molecules, the averages over the products of direction cosine matrices contains the orientation order parameters, (see Fig. 6.5).

$$A_\perp = A_0 - B\left[\frac{1}{3}S\left\{(\mu_n^i)^2 - \frac{1}{2}\left((\mu_l^i)^2 + (\mu_m^i)^2\right)\right\} + \frac{1}{6}D\left((\mu_l^i)^2 - (\mu_m^i)^2\right)\right] \quad (6.8)$$

$$A_\parallel = A_0 + B\left[\frac{2}{3}S\left\{(\mu_n^i)^2 - \frac{1}{2}\left((\mu_l^i)^2 + (\mu_m^i)^2\right)\right\} + \frac{1}{3}D\left((\mu_l^i)^2 - (\mu_m^i)^2\right)\right] \quad (6.9)$$

$$\frac{A_\perp}{A_0} = 1 + \frac{1}{2}S(1 - 3\cos^2\beta') + \frac{1}{2}D(\sin^2\beta'\cos 2\gamma') \quad (6.10)$$

$$\frac{A_\parallel}{A_0} = 1 + S\left(3\cos^2\beta' - 1\right) - D\sin^2\beta'\cos 2\gamma' \quad (6.11)$$

here, $A_0 = (A_\parallel + 2A_\perp)/3$ is the mean absorbance of the isotropic fluid and μ_l^i, μ_m^i, μ_n^i are the components of the transition moment along the principal axes of the molecule for a particular absorption band. Angles β' and γ' are shown in Fig. 6.5. Then a set of Eqns. (6.8) and (6.9) for absorbance can be converted into angular dependences using the projections of the transition dipole moments on the molecular frame of reference; l, m, and n denote, the molecular frame of

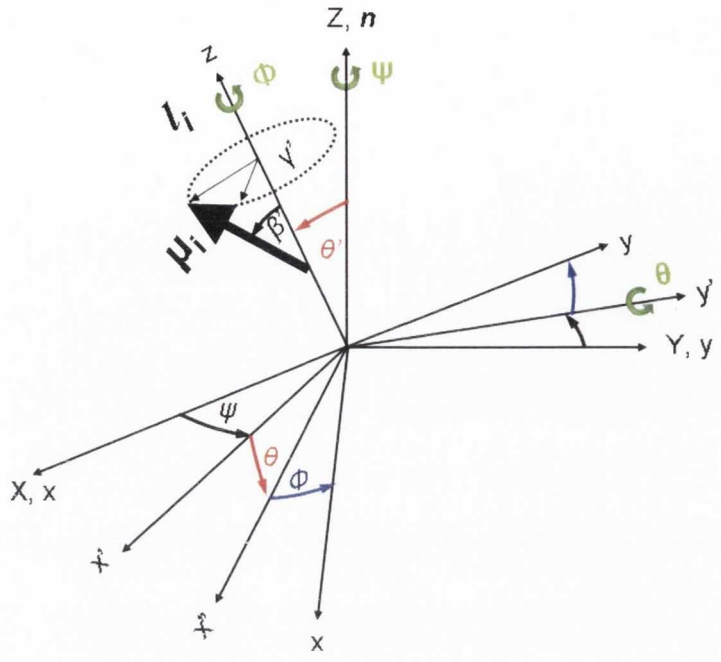

Figure 6.5: Schematics of the orientation of a transition dipole moment within the laboratory X, Y and Z axis system. All possible relative orientations of the two frames are described by ψ, θ and ϕ ; θ is the polar angle, ϕ is the angle between the normal to the z-Z plane and the X axis. The orientation of the molecular short axis x is represented by ψ corresponding to the molecular rotation around z, as the axis of the highest symmetry. γ' is the azimuthal angle of the transition dipole moment (the angle between the projection of the transition moment μ^i on the xy plane and the x-axis). Redrawn from Ref. [71]

reference, x, y, and z molecular axes. This results into the Eqns. (6.10) and (6.11): where β' is the angle between the transition dipole moment and the molecular z axis: γ' is the azimuthal angle of the transition dipole moment (the angle between the projection of the transition moment μ^i on the xy plane and the x-axis). If the correlations of the transition dipoles are neglected, then $B\mu_i^2 = A_0$, where A_0 is a constant [32]. The IR absorbance measurements are carried out in the transmission mode for the homeotropic orientations of C4 and C9 under cooling. Figure 6.6(a) and (b) show the temperature dependence of the absorbance for the representative stretching bands, for C4 and C9, respectively which are aligned in the homeotropic configuration. In this case, the normalized aborbances are independent of the direction of polarized IR beam. For liquid crystals phases of uniaxial symmetry,

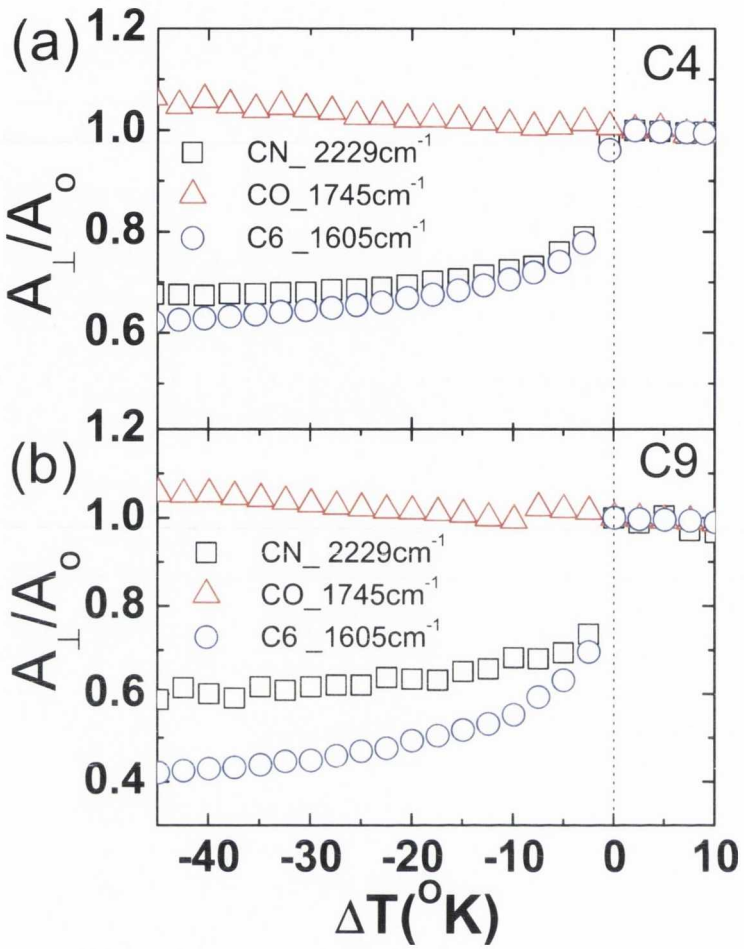

Figure 6.6: Normalized IR absorbance of the representative stretchings: phenyl at 1605 cm^{-1} (blue circle),cyanyl group 2229 cm^{-1} (black square) carbonyl groups at 1745 cm^{-1} (red triangle) for C4(a) and C9(b), respectively. A_o means the absorbance at T_{N-I}. ΔT = T- T_{N-I}. $A_\perp$ for the materials is measured in the homeotropic cells.

the optical axis coincides with the average alignment of the molecules so that it is parallel to the director. Usually, the Z axis is chosen to be parallel to the optical axis. Therefore, the independence of the normalized absorbance on the direction of the polarized IR beam means that the molecules have equal probability distributions around the laboratory X and Y axes. The biaxiality of the phase described by the order parameters C and P is neglected. For simplicity, we also neglect the molecular biaxiality. Throughout the entire temperature range, a linear increase of the absorbance is observed for the carbonyl stretching corresponding to 1745 cm^{-1}. Meanwhile, the absorbance curves of cyanyl (2229 cm^{-1}) and phenyl

stretching vibrations (1605 cm^{-1}) appear to be affected by S and β' in the nematic phase, while the curves of the two stretching bands deviate from each other.

6.3 Discussion

The optical anisotropy of the two representative resorcinols (C4, C9) are investigated here. As shown in Fig. 6.4, the temperature dependence of Δn for the two mesogens appears to roughly coincide with each other over a wide temperature range. Δn_0 represents temperature independent birefringence. These values for C4 and C9 are 0.177 and 0.178, respectively. This means that both C4 and C9 having the same core part do show the same optical anisotropy as this is determined by the molecular shape. To exclude the possibility of a conformational change, we used IR spectroscopy. If the conformational change would have been the likely cause of the reversal of dielectric anisotropy then the angle that a transition dipole moment makes with the long molecular axis, β', should change with temperature. Based on the IR absorbance measurements for the stretched phenyl group, we found that the temperature dependence of the normalized aborbance is similar to S obtained by the measurements of birefringence. This is being discussed later where a comparison of β's between C4 and C9 will be made. If β' would not change with temperature, then there would not be any significant change in the bending angle, θ_V with temperature. Thus a conformational change with temperature is ruled out as the cause for the sign inversion in $\Delta\epsilon'$ for C4. Furthermore the dielectric strength for $\epsilon'_{\parallel}$ is greater than for $\epsilon'_{\perp}$ (see Fig. 5.5). This explains the observed behavior of the cross-over temperature in $\Delta\epsilon'$ is frequency dependent. It is clear from Eqn. (6.8) that the IR aborbance is associated with the angle, β' and the order parameters, S and D. D is assumed to be zero for simpilcity. The normalized absorbances are expressed in terms of β' by adjusting S obtained by the measurement of birefringence to Eqn. (6.8) on the assumption that D is zero. Figure 6.7 shows temperature dependence of β's of the cyanyl and the phenyl stretching vibrations. Interestingly, for C4, β' of the cyanyl stretching is found to be close to 30°. This is in agreement with that expected from the

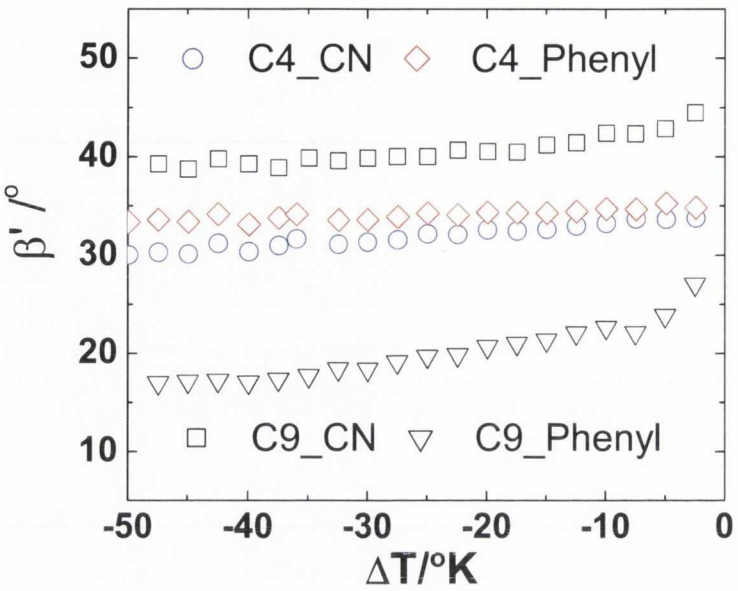

Figure 6.7: Temperature dependence of β' of the representative transition dipoles of C4 and C9. ΔT = T- T_{N-I}.

molecular structure of the material (the angle between the molecular long axis and the stretching of cyanyl group in the central aromatic ring is approximately 30°. see Fig. 3.1). Meanwhile in the case of the phenyl stretching vibration, at least 5 chemically different phenyl stretching vibrations participate in the absorbance. Even though β' of the individual phenyl stretching vibration cannot be evaluated, the averaged β' of the phenyl stretching bands for C4 is found to be approximately 35° (see Fig. 6.7) as expected from the molecular structure. As a result, results from IR spectra also means that C4 has a usual nematic phase without cybotactic clusters. However, β' of the cyanyl and the phenyl stretching vibrations for C9 show different values from C4. The cyanyl stretching band of C9 exhibits higher β' ranging from 40° to 43° with temperature increasing. As mentioned before, the cyanyl group is attached to the central ring containing the symmetry axis. β' of the cyanyl stretching dipole moment is not affected by a conformational change in the molecular shape. Therefore such a higher value of β' may be associated with the presence of the clusters. It should be noted that the splitting of small angle scattering can be interpreted as the synclinic effect of the cluster with respect to the layer normal (see Fig. 3.4 (b)). We also observed an increase in $\epsilon_\perp$ with temperature decreasing. This implies ferroelectric interaction among the molecules

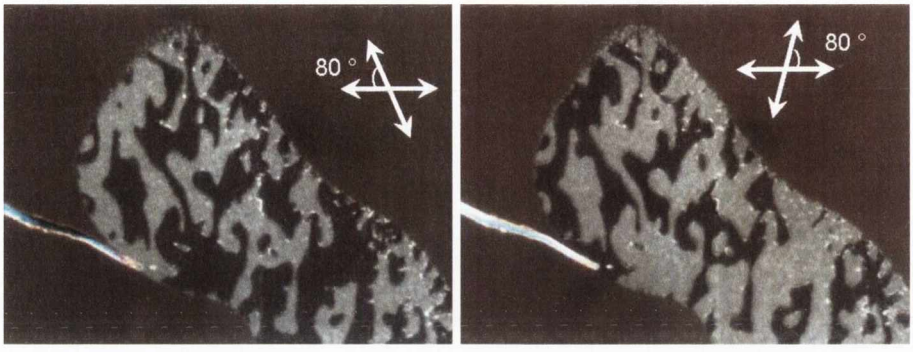

Figure 6.8: Chiral domains observed on the transion from the nematic phase to *CybC* phase in a homeotropic cell of C9. The opposite handedness of the chiral domains is confirmed by rotating one of polarizers to the opposite direction. Two chiral domains are surrounded by optically uniaxial nematic phase which is independent of the direction of the rotation of the the polarizer. The chiral domains are thermally stable, while domain boundary and the size of each domain is dependent on temperature. The arrows indicate the direction of polarizers.

in the layer which indicates that molecules align ferroelectrically. As a result, the species of the cluster of C9 is SmC_SP_F like in which C_S and P_F mean synclinic tilt and ferroelecric polar ordering, respectively [5]. Another important fact that needs to be pointed out is that a lamellar structure has identical chirality in adjacent layers. These leads macroscopically to homogeneous chiral states as mirror images. In macroscopic samples both enantiomeric organisations can be found in distinct regions [4, 5]. Even though C9 seems to be an optically uniaxial nematic phase over the entire temperature range in the nematic phase. This can be interpreted as the chirality of the clusters, which degenerates and results in racemic mixture of two different chiral clusters. Interestingly the homogeneously chiral domains of comparable area are observed on transition to the *CybC* phase (see Fig. 6.8). If the *CybC* phase results from the expansion of the clusters, the origin of the N_{cybC} for C9 should be similar to the *CybC*. Therefore the occurence of the chiral domains is in line with the origin of the cluster.

6.4 Conclusion

In this chapter we have reported measurements on birefringence and the IR absorbance for C4 and C9 in their nematic phase. These optical properties are dependent on the length of the terminal groups. This results of C9 are different from C4. This is due to the presence of clusters in C9 as opposed to C4. The results of the optical experiments agree with the results of the dielectric experiments given in Chap. 5. C4 shows the typical behavior of a usual nematic phase, meanwhile the material with the cybotactic clusters shows different response under electric field. Interestingly, it is seen that the molecules in the cluster are tilted to the layer normal of the cluster with a certain tilt angle. Quantitative analysis of the tilt angle of the molecule in the cluster will be given in Appendix. A.

Part. IV

Chirality

Biaxiality.

Chapter 7

Chirality of C5

"In this chapter, *chirality of C5 is investigated and is interpreted in terms of a new mechanism for the chirality of achiral bent-core."*

7.1 Introduction

The chirality of liquid crystals (LCs) has been a topic of enormous interest especially in phases such as blue and twist grain boundary (TGB) phases. The chirality arises either from the molecular asymmetry of the LC or from the formation of supra-structure in the mesophase [5]. Recently, a number of achiral bent-core liquid crystals (BCLCs) are reported to show chirality in a mesophase [4, 5, 72, 73]. Such a phenomenon of chirality formed from achiral molecules is scientifically intriguing as most commonly the chiral phase with chiral structures arises from the organization of chiral liquid crystalline molecules. Dynamically, standard organic molecules can have an infinite number of different chiral conformations which may exist in fast equilibrium under various experimental conditions. Exceptionally, some molecules, with a large rotational barrier along a covalent bond that

connects the two moieties, have a stable chiral structure. These stable chiral conformers are used as a ligand for an asymmetric synthesis to create new chiral materials [74]. Flexible achiral BCLCs can also form transient chiral conformations which may lead to chiral nucleation. This is a possible interpretation of the chirality of achiral BCLCs [75]. In a system consisting of racemized conformers, chiral conformers instantaneously form a homochiral cluster with the same handedness via a self-assembly process. A local chiral phase can thus build up through additional packing of molecules so as to lower the free energy. As a result, mostly two domains with opposite handedness are observed or in some cases a single homogeneously chiral domain in the phase [73, 76] is also observed. Recently, a computational study [77] has shown that chiral superstructures can arise from rigid achiral molecules by self-assembly. A consistent twist sense can be also induced by the chiral dopants in which the chiral nucleation otherwise is not possible. In both interpretations, the chirality of the BCLCs in a mesophase is associated with either local clustering of molecules or via the self-assembly of molecules. The presence of cybotactic clusters of smectic-like structures in the nematic phase has been reported by several groups [10, 18, 21–23, 25, 45, 46, 78, 79]. It should be noted that a possibility of the short-range order of C5 cannot be excluded from the Kirkwood correlation factors (see Fig. 5.9) compared to the C4 homologue even though N_{cybC} occurs when $n \geq 6$). This indicates that the phase behavior of C5 in the nematic phase is an intermediate between N and N_{cybC} (see TABLE. 3.1). Interestingly, only C5 in the materials shows chirality in the nematic phase. Therefore it is unclear whether the chirality of C5 is due to the presence of the cluster. Basically, a V-shape molecule has C_{2v} symmetry which is achiral. A bent shaped molecule of such a symmetry leads to complicated molecular quadrupolar and octupolar interactions [14]. In a simpler system that comprises two BCMs, combining two molecules yields various symmetries [80, 81]. Such symmetries created through a pairing of the two BCLCs, with nonzero quadrupolar and octupolar interactions, can create additional order parameters such as the biaxiality of mesophase and the chirality via spontaneous symmetry breaking. In this chapter, the chirality and the phase behavior of C5 is investigated and interpreted in terms of the pairing of

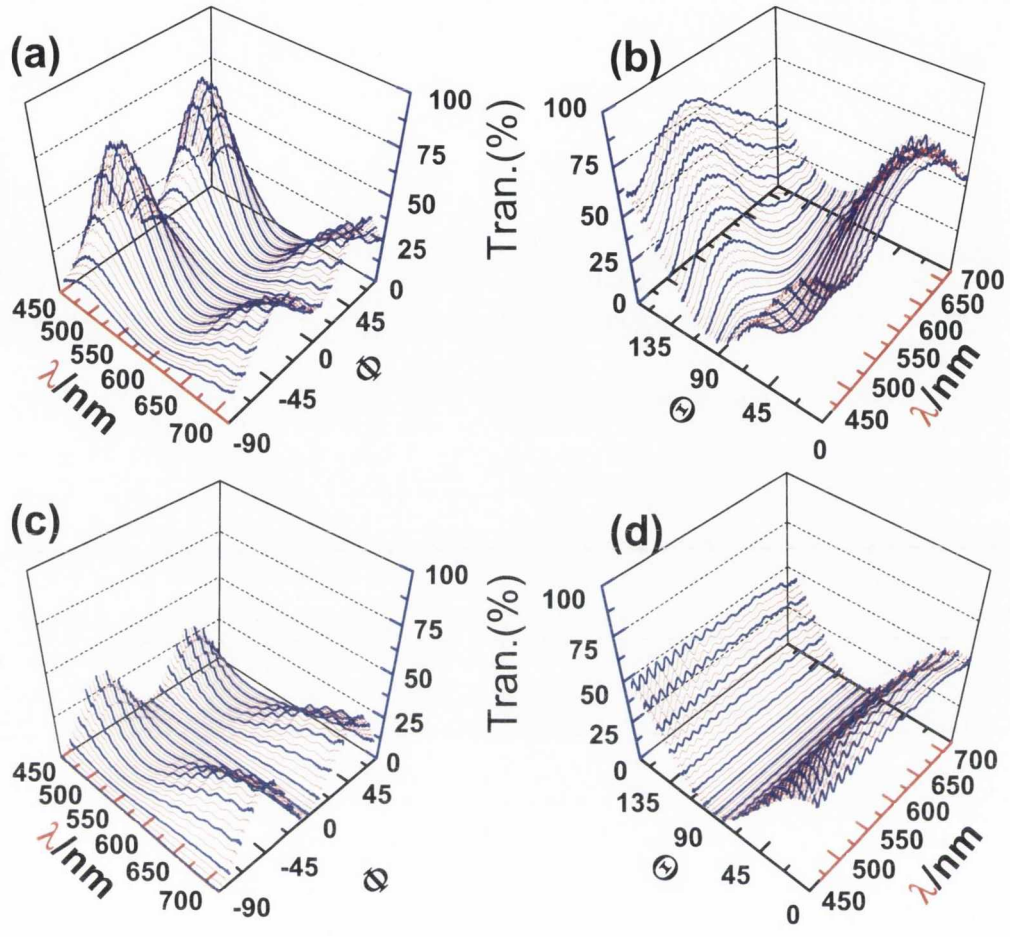

Figure 7.1: (a), (b) are the transmittances of the cell made of C5 measured for various values of Φ (the angle between the rubbing direction and one of polarizers) and Θ (angle between the polarizers), respectively. (c), (d) are those for C6, at $\Delta T = 5$. $\Delta T = (T_{N-I}\text{-}T)/^{\circ}K$. $\Delta T = (T_{N-I}\text{-}T)/^{\circ}K$. (c),(d) show typical behavior of a planar cell. (a), (b) show those of a twisted cell.

two molecules.

7.2 Results

The transmittances of two cells containing C5 and C6 are compared for different angles between the front and the rear polarizers and by changing the azimuthal angle. The angle between the two polarizers is denoted as Θ. Φ is the angle between the polarizer and the rubbing direction and is called as the azimuthal

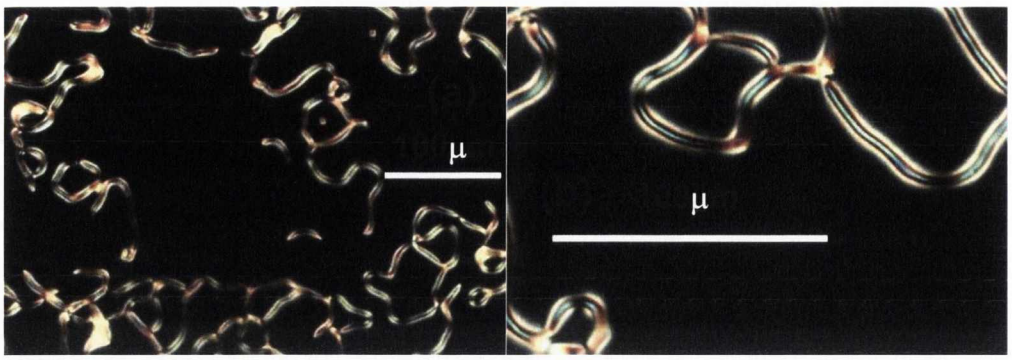

Figure 7.2: Fingerprint texture of C5 under hometropic anchoring condition. The cell gap is 8.7μm at $\Delta T = 1$.

angle. Figure 7.1(a) and (c) show the transmittances of C5 in a 10μm cell gap and those for C6 in a 5 μm cell gap under planar surface condition as a function of the wavelength and the azimuthal angle. Figure 7.1(b) and (d) show the transmittance when the polarizers are decrossed for C5 and C6, respectively. In a 10 μm cell containing C5, the dark state of a typical planar cell under the condition that rubbing direction is parallel to one of the polarizers cannot be observed as shown Fig. 7.1(a). Meanwhile, the minimum transmittance as a function of wavelength is dependent on the angle between the polarizers Θ in Fig. 7.1(b). Such a behavior of the planar nematic cell of C5 is reminiscent of a twisted nematic cell. Subsequently, we checked out the spontaneous twisting of materials with homeotropic anchoring condition. A typical helical structure of chiral nematic LC is observed as shown in Fig. 7.2 (a), (b). Interestingly, these results are found only in the cells containing C5. The cells containing C6 and other compounds of this series do not show chirality up to the cell gap of 35 μm. In order to measure the pitch length, P_l, of C5, a *Grandjean-Cano wedge cell* with a thickness between the two confined glass substrates varying up to 50 μm is used. The planar alignment is achieved by using a polymer layer. The cell with planar anchoring shows several disclination lines; these lines are orthogonal to the direction of the increasing layer thickness (assumed as the spacer thickness), shown in Fig. 7.3. The disclination lines correspond to a change in the twist angle across the layers as π and these occur when the cell thickness, d is related to the pitch length. This is expressed

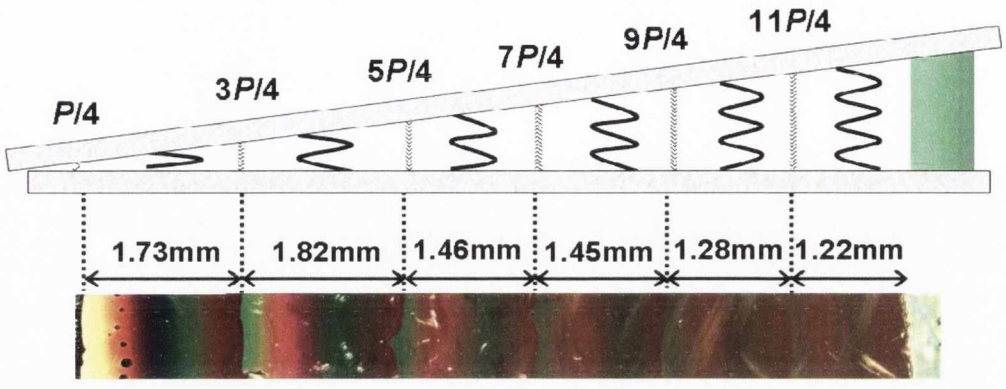

Figure 7.3: Due to a limited filed of view of the microscope used in the study, each domain is taken individually and combined to be a panoramic view. A 50 μm film type spacer was used for the gradually increasing cell gap and the other side was grinded for the flat edge. The spacing of each domain range from 1.22 mm to 1.82 mm. The disclination lines in the wedge cell, so called *Grandjean-Cano wedge cell*, correspond to a pitch of $\frac{1}{4}$, $\frac{3}{4}$, $\frac{5}{4}$, $\frac{7}{4}$, $\frac{9}{4}$, $\frac{11}{4}$ sequentially from left to right in the figure.

as below [82].

$$d_n = (2n-1)\frac{P_l}{4}, n = 1, 2, 3, ... \tag{7.1}$$

The distance between disclination lines gradually decreases as the cell gap increases. This might arise from an uneven edge of the substrate or a distorted glass substrate. It is very difficult to estimate an accurate structure of the wedge cell due to gradually changing cell gap. For more accurate determinations of the pitch length, we carried out a qualitative comparative experiment. Figure 7.4 shows color comparisons between the second domain (2π twisted) of the wedge cell and a 2π twisted cell of 10.1 μm cell gap under the same experimental conditions. We can decide on a position which shows the same color property dependent on Θ (the cell gap gradually increases from the left to the right side of the figure). This positional information indicates that the pitch length of C5 is approximately 9 μm ($P+\frac{P}{8} = 10.1\mu$m). Subsequently, a comparison between the first domain and a π twisted cell of 5 μm cell gap was also carried out. Interestingly, any position with the same color property could not be determined. This might indicate that the π twisted cell of 5 μm cell gap has the opposite handness to that of the wedge

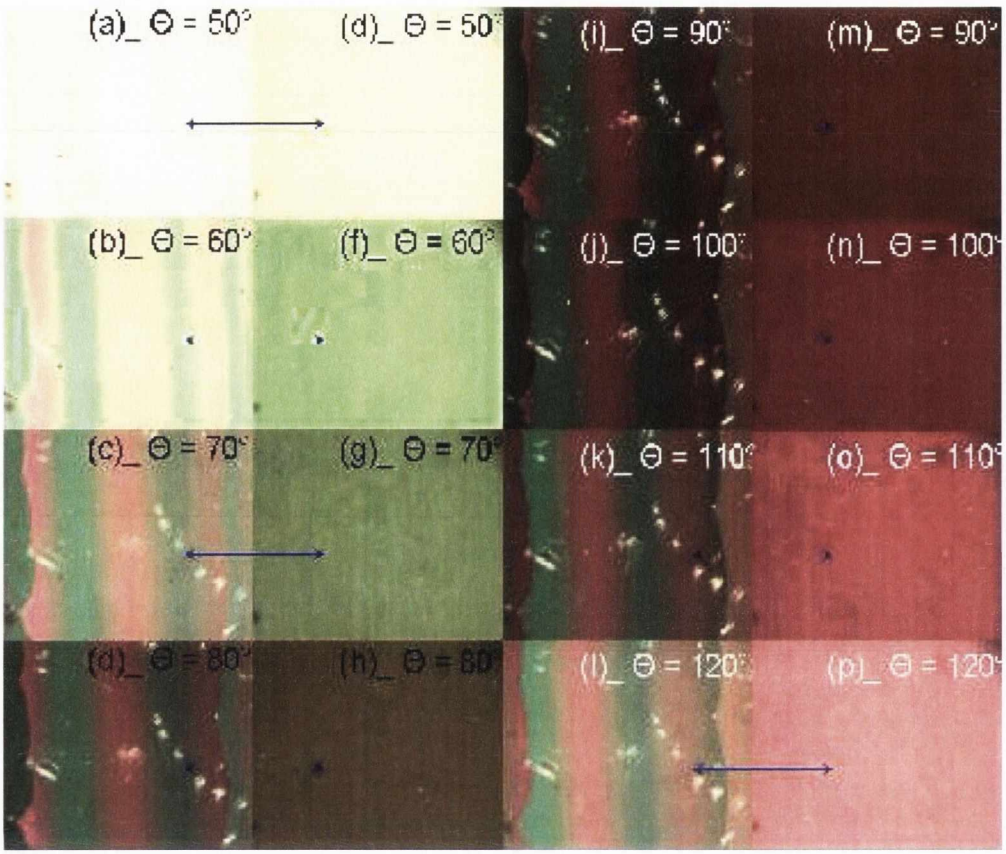

Figure 7.4: The color of the 2nd domain for various Θs (angles between the two polarizers) are compared with a planar cell of 10.1 μm cell gap at $\Delta T = 25$. $\Delta T = (T_{N-I}\text{-}T)/^{\circ}K$. (a)-(d),(i)-(l) were taken from the second domain of the wedge cell with a analyzer rotated, (e)-(h),(m)-(p) are taken from the planar cell of 10.1 μm under same condition, respectively. Θ means the angle between the polarizers, the arrows indicate the position with same color, in which two cells have the same cell gap.

cell. In general, chiral materials with a pitch length of 200 μm are used in many commercial twisted Nematic cells to reduce twist degeneracy and the materials with 20 μm pitch length are used to induce the higher twist angles found in Super Twisted Nematic cells [82]. A comparison between the pitch length of the commercial materials and that of C5 indicates that C5 has quite a strong helical twisting power which is inversely proportional to pitch length (P_l). Even though we did not measure the twist elastic constant k_{22}, we can guess that C5 has a larger k_{22}. This is associated with the pitch length.

It is conceivable that the twisting power could possibly have been induced with a

contamination from a chiral impurity for the case when homochiral phase is observed. If we are able to make two cells with opposite handedness, it would be a proof for excluding the chiral contamination. However, under practical experimental conditions, it was very difficult to reproduce cells with the same handedness and cell gap. In order to exclude the possibility of contamination, we investigated the chirality with two C5 samples, synthesized separately. One is based on using pentanoic acid and the other is based on using pentanol/pentylbromide. Both samples show the compatible chirality. Therefore there is no special reason for having a chiral impurity. We cannot completely exclude that traces of chiral material could have been present in the starting materials, since the synthesis started from the alkanoic acids. However the probability of chiral contamination is not especially any higher for C5 than C4, C6, C7 and C9, (the other members of this homologue series). It is known that in an ideal planar cell, a right handed twisted domain has exactly the same free energy as the left handed one which means that the two states are degenerate. As a consequence, the two domains with opposite handedness can coexist [73, 76] in the mesophase. However, the rubbing direction of one of the substrates used in the cell can most likely deviate from the second rubbing direction in the device. In such a case, due to a deviation angle (ψ_R) between the two rubbing directions in a planar cell, the twist angle of one state is different from the other. The twist energy F_t per unit volume of a layer of thickness d and twist angle ϕ is known from the continuum equation:

$$F_t = \frac{k_{22}}{2}\left(\frac{\phi}{d} - \frac{2\pi}{P}\right)^2 \tag{7.2}$$

$$\Delta F_t = \frac{k_{22}\psi_R}{d}\left(\frac{\phi}{d} - \frac{2\pi}{P}\right) \tag{7.3}$$

ΔF_t is the energy difference between the two states. When the deviation angle between the rubbing direction on each glass plate ψ_R is taken into consideration, the energy difference ΔF_t in the nematic phase between the two states of opposite handedness can be expressed in terms of Eqn. (7.3). ΔF_t is dependent on the cell gap (d), the deviation angle (ψ_R) and k_{22}. In a wedge cell different domains are observed while the sample is cooled from the isotropic to the nematic phase. In a

part of the cell with smaller cell gap, we may get homochiral domains that can be stabilized over a shorter period of time. Meanwhile in a thicker part of the cell, it takes a considerable time for the domains to get stabilized. Besides, as the energy difference between the domains of opposite handedness is small, it is extremely difficult to distinguish one domain from the other with opposite handedness by rotation of a analyzer using the method of color comparisons. The color change brought about by a rotation of the analyzer is too insensitive to confirm the handedness. A 2π twisted cell was made with a cell gap of 8.2 μm. Figure 7.5 (a) shows a couple of domains immediately after the transition to the nematic phase. With the passage of time, the two domains merge into a single one as seen in Fig. 7.5 (b). Two of the domains have opposite handedness. This is confirmed by decrossing the polarizers in the opposite direction as shown in Fig. 7.5 (c), (d). If the twist of the directors were to be induced by a chiral impurity, the domain with one chirality can only occur on the transition to the nematic phase. Therefore the presence of the domain with opposite handedness is incompatible with an explanation of a sample contamination. Recently, Kim *et al.* reported a nematic phase (N_T^*) [83] to appear along with an earlier discovered isotropic nematic phase (N_T) of a BCLC [16]. The ferrocene derivatives with the free rotation of the cyclopentadienyl rings can adopt chiral conformations and these can be interlocked and stabilized with a coupling from the neighboring conformers of the same handedness into tetrahedral dimers. The symmetry breaking arises from the interlocked conformers with the same chirality and (N_T^*) is generated as well as a chiral smectic phase. In the case of BCMs, such an interlocking through transient chiral conformers is possible under specific conditions that the transitional freedom of LC is limited to the nearest neighbors where the two bent-core molecules form a tetrahedric dimer. As mentioned above, C5 forms a nematic phase whose nature is intermediate in between the usual nematic phase and N_{cybC} phase. So far, the small angle scattering in X-ray diffraction pattern has been interpreted in terms of the clusters. A weak small angle scattering can be interpreted as follows: either the size of the clusters is small or the number of molecules participating in the cluster is small. While most of the molecules take part in forming a typical nematic phase, nevertheless

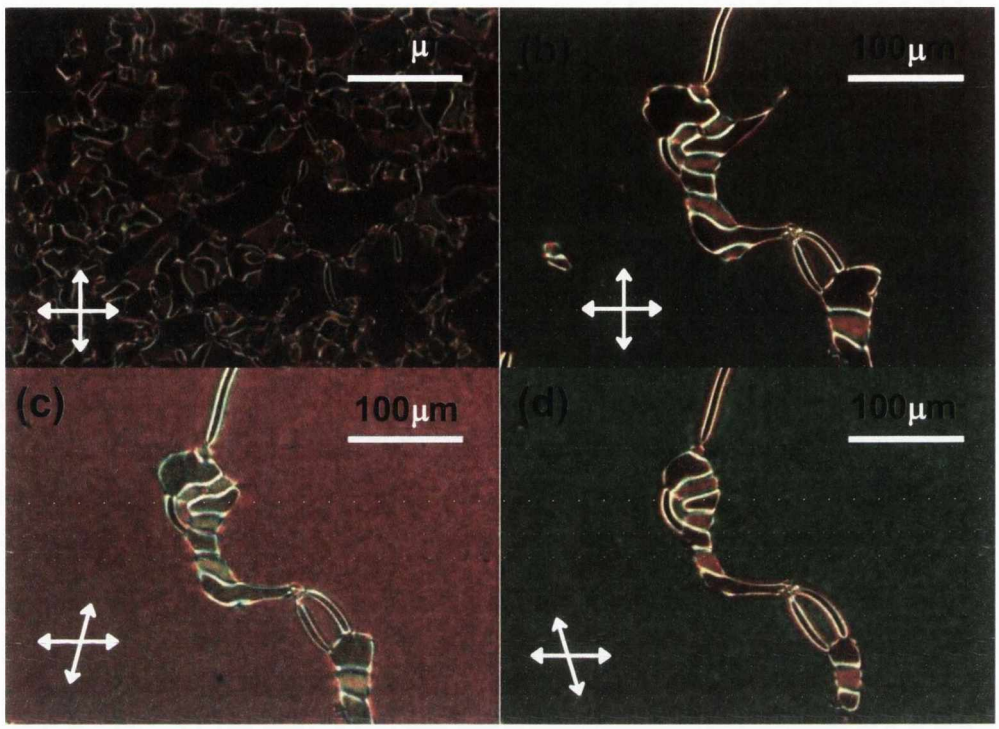

Figure 7.5: The domains with opposite chirality coexist over a very short time and merge into one most stable domain of a single handedness in a planar anchoring condition. (a) taken 15 seconds after transition to the nematic phase at a cooling rate of 1°/sec at $\Delta T = 11°K$, (b)-(d) taken subsequently, between the crossed and de-crossed polarizers, respectively.

some of the molecules form a simple interlocked cluster that is composed of two bent-core molecules and these behave like a chiral dopant. The other molecules with longer terminal chains build up larger clusters. These behave like a biaxial particle in uniaxial nematic phase referred to in the cluster model. And the lateral correlation observed by the dielectric measurement is not negligible in terms of the Kirkwood correlation factors (see Fig. 5.9). This indicates the presence of a certain short-range correlation in the nematic phase.

The most plausible scenario is a coupling of the two BCLCs to form a simplest cluster (see Fig. 7.6). A preliminary theoretical interpretation of such a system has been given at macroscopic and microscopic scales [17, 80, 81, 84]. According to these theoretical models, such a pairing can form a simplest cluster

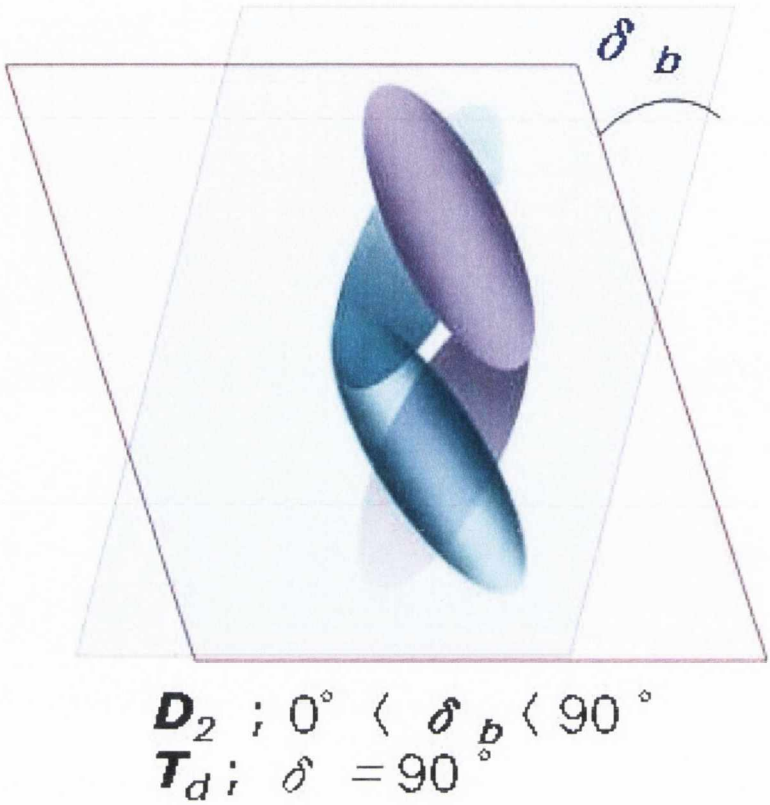

Figure 7.6: A pair of two bent-core mesogens. when $0 < \delta_b < \frac{\pi}{2}$), N_T^* phase takes place.

which can generate not only the usual nematic phase but also new types of nematic phases such as the biaxial nematic (N_b), tetrahedratic nematic phase (N_T), chiral tetrahedratic nematic phase (N_T^*) through higher order molecular interactions (quadrupolar, octupolar) . According to the computational study carried out by Longa *et al.* [81], the phase transition from the isotropic to N_T^* phase is not allowed except through the *Landau point* where all possible phases can coexist under a specific condition. In order to construct the phase diagram, we investigated the transition behavior of the material under extreme slow cooling. Figure 7.7 shows four optically different domains. The left side of the figures is at slightly lower temperature than the right side due to a temperature gradient in the cell. This is shown by a gradual change in the color of the major domains on the left side of Fig. 7.7 (a), (b). Single and twin arrows indicated on the figures denote the direction of rubbing and of the polarizers, respectively. Black regions on the

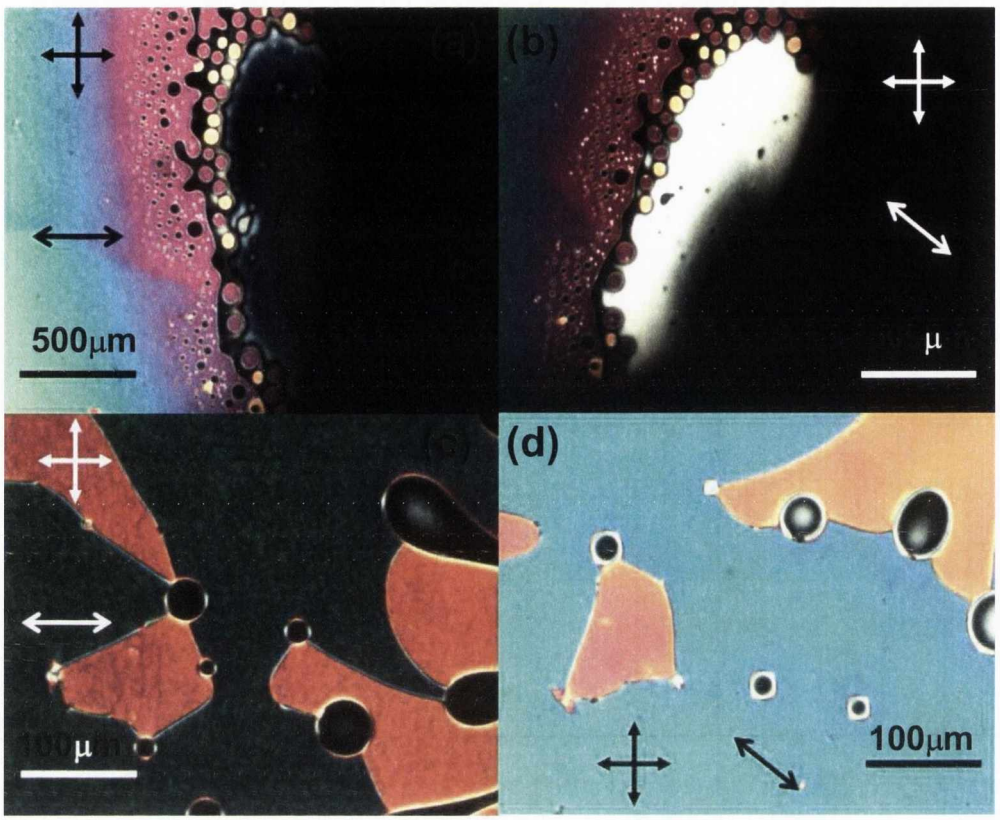

Figure 7.7: Transition behavior of C5 on slow cooling with the rate of which is 0.5° / hour.

right side of Fig. 7.7 (a), (b) are the non-transparent parts of the sample holder, and the white domain in Fig. 7.7 (b) is the uniaxial nematic phase with the planar anchoring condition. This is confirmed by rotating the stage of the microscope (see Fig. 7.7 (a)). A bright big domain on the left side of Fig. 7.7 (a), (b) is assigned to the chiral nematic phase. Between the two main domains, domains with black and yellow colors are observed. The former appears to be the chiral nematic phase with either a different handedness or helicity and the later is optically isotropic under planar anchoring condition, confirmed by a rotation of the stage (Fig. 7.7 (c), (d)). This optically isotropic nematic phase can be interpreted as a tetrahedratic nematic phase (N_T). On the basis of the temperature gradient in the cell, the phase transition of C5 can be assigned as follows: isotropic, uniaxial nematic, N_T, N_T^* phases seen upon cooling optically. This result is consistent with the theoretical prediction of Longa *et al.* [81]. Interestingly, a clear phase boundary

is not observed between the uniaxial nematic and N_T in Fig. 7.7. The microscopic structure of C5 in the nematic phase is still elusive. However the macroscopic behavior of C5 is well explained with the model of a possible tetrahedric dimer consisting of two molecules.

7.3 Conclusion

It has been shown that planar and homeotropic cells under certain boundary conditions containing achiral bent-core C5 liquid crystalline material show chirality. In terms of the phase behavior, the nematic phase of C5 is intermediate between the usual nematic phase and the cybotactic nematic phase. Even though short-range correlation between the molecules of C5 is not as strong as for molecules with longer terminal groups, C5 shows a considerable twisting power in the entire nematic phase. It is interesting that the chirality is not directly proportional to the formation of the clusters in the nematic phase. The stability of such chiral domains in a planar cell depends not only on temperature but also on the device parameters such as the cell gap and the relative directions of rubbing on the substrates. The energy difference between the two states with different twist angle between the rubbing directions is expressed in terms of the device parameters. The chirality of C5 with a pitch length of 9 μm is discussed in terms of the molecular symmetry created by the formation of a pair of the two bent-core molecules. Such a pairing of molecules acts as a chiral dopant. The experimental results on the device containing the material are compared with a prediction from a theoretical model with higher order molecular interactions in the bent-core system and it is suggested that the observed nematic phase is tetrahedratic chiral nematic phase of D_2 symmetry as recently predicted by Longa *et al.* [81].

Chapter 8

Optically biaxial nematic phase

"In this chapter, *Optically biaxial nematic phase is reported which is confirmed by texture behavior and quantitative measurements using the PEM system.* "

8.1 introduction

Since the first prediction of a biaxial nematic phase (N_b) (see Fig. 1.2) made by Freiser in 1970 [85], N_b phase has continued to attract significant interest among scientists during the last decade for reasons of advancing fundamental science and especially for its potential of use in new types of displays. The switching mode in N_b is more likely to realize faster response [15, 86] and wider viewing angles. In modes such as VA (Vertical Alignment), IPS (in plane switching), TN (Twisted Nematic), OCB (Optical Compensation Bend) using conventional N_u phase to achieve wider viewing angle displays, it is necessary to use expensive optical compensation films [87, 88]. However the intrinsic biaxiality of N_b is versatile in reducing the light leakage for oblique viewing angle [89]. The most plausible structure for N_b device able to realize both fast response and wider viewing angle is the homeotropically aligned cell with in-plane switching of the minor director

[15]. To achieve a fast response, the minor director should be driven without involving the major director **n**. If both the major and minor directors take part in the reorientation of molecules under electric field, the response time of LC would be dominated by the slower motion. Besides, in terms of its application to displays, this structure is advantageous in forming a normally black state in which the initial state without electric field has the darkest grey level. However the development of such a system has been hindered by a lack of materials possessing N_b and by difficulties of alignment. In this chapter, we experimentally demonstrate the possibility to produce this type of device. In spite of attention already given to the phase [33, 49, 50, 55], little is known about driving of the minor director. Lee, *et al.* reported fast switching of the minor director [90] with bent-core LC, ODBP-Ph-C7, which had already been confirmed by NMR and x-ray experiments [55], but their study was strongly criticized by Stannarius for incorrect interpretation of the results [91]. Recently Le *et al.* reported optical study of the bent-core LC, A131, which had already been confirmed as showing biaxiality in nematic phase [50]. However Le *et al.* did not find any evidence of optical biaxiality in this material [92]. Therefore, from the optical point of view, no material with N_b having large optical biaxiality has been confirmed as yet.

8.2 Results

The material under investigation, PAL1 possesses a bent-core structure and asymmetric terminal groups. Its molecular structure and refractive indices are shown in Fig. 8.1 . It shows negative dielectric anisotropy due to the strong short-range correlation (see Fig. 8.2). The homeotropic and planar aligned cells are shown in Fig. 8.3. For the in-plane switching in a homeotropic cell, the ITO electrodes are also deposited on the top plate, for electrostatic screening of the cell. Both glass plates of the cell are spin-coated with a polymer layer for homeotropic alignment. We prepared two types of homeotropic cells with and without rubbing. The rubbing direction is at an angle of approximately 45° with respect to those of the electrodes. Standard commercial cells (E.H.C Co.,LTD) with a thickness of 5

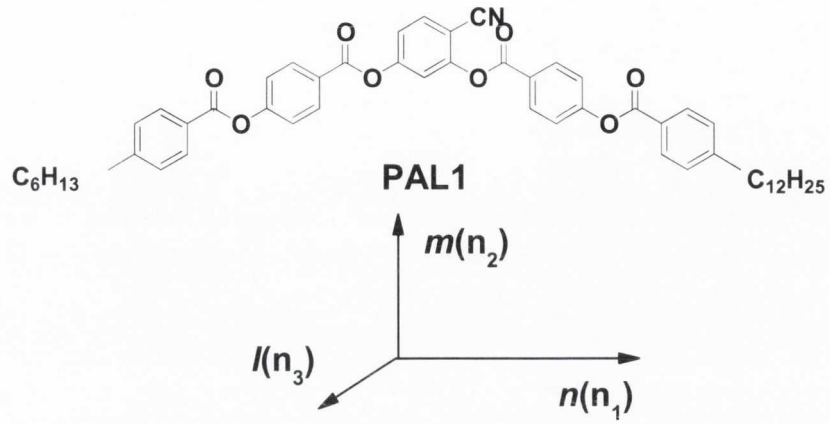

Figure 8.1: Molecular structure of PAL1. The three directors and their refractive indices for the biaxial phase are denoted by $\boldsymbol{l}$ (n_3), $\boldsymbol{m}$ (n_2), and $\boldsymbol{n}$ (n_1). The phase transition was investigated by the dielectric and optical technique. I 116°C N 65 °C N_b 54.5°C SmX. SmX is an unidentified smectic phase.

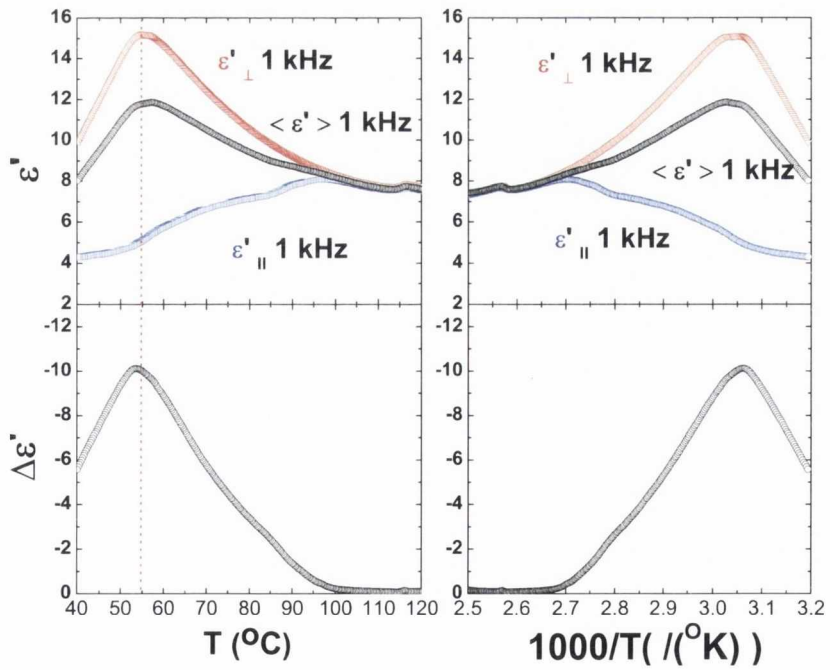

Figure 8.2: Temperature dependence of $\epsilon'_{\|}$, $\epsilon'_{\perp}$ and $\Delta\epsilon'_{\perp}$ of PAL1 at the frequency of 1 KHz.

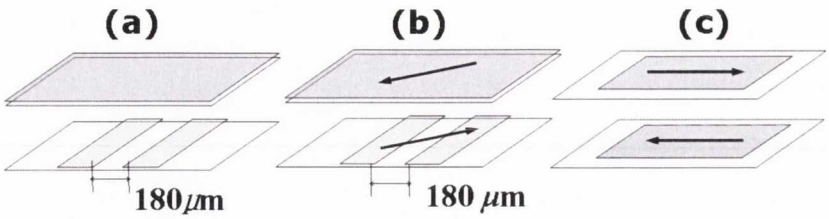

Figure 8.3: The configuration of three cells used in optical study (a) homeotropic cell, cell gap =7.2 μm, (b) homeotropic cell, anti-parallel rubbing, cell gap = 7.6 μm. (c) planar cell, anti-parallel rubbing, cell gap =5.0 μm,(E.H.C. Co.,LTD). Arrows mean rubbing direction.

μm and both sides antiparallel rubbing are used to carry out experiments in the planar geometry. Three LC phases are observed in an unrubbed homeotropic cell by scanning with temperature as shown in Fig. 8.4. Due to the negative dielectric anisotropy of PAL1 in the N_u phase, the director stands right up on the application of an in-plane field. Moreover, in between the N_u and smectic phases we observe another nematic phase where the minor director is switched by an electric field of 1 V/μm as shown in Figs. 8.4 (b) and (c). In order to align the minor director, we slightly rub the homeotropic cell. By observing a 7.2 μm-thick cell in a polarising microscope, we find a small deviation of the major director, here called the pretilt angle, from the normal position towards the rubbing direction in the temperature range of the N_u phase (Fig. 8.5 (a), (b)). On applying the electric field of (1 V/μm) the space between the electrodes gets darker and is independent of the cell rotation angle (Fig.8.5 (e), (f)). This indicates that the director stands right up normal to the in-plane electric field and consequently to the surface of the electrodes. The transmittance of the biaxial phase in the temperature range from 56° to 64° is larger than that of the uniaxial phase due to a contribution of optical biaxiality arising from aligned minor directors. In the absence of an electric field, the minor director aligns along the rubbing direction (Fig. 8.5 (c), (d)). On the application of an electric field of 1 V/μm, a rotation of the minor director in the biaxial nematic phase towards the direction of the field is observed (Fig. 8.5 (g), (h)). Just below a temperature of 65°C in the nematic phase the cell shows behavior similar to the IPS mode. Therefore we can clearly see a qualitative difference between the two different nematic phases. For an accurate measurement of the birefringence, the

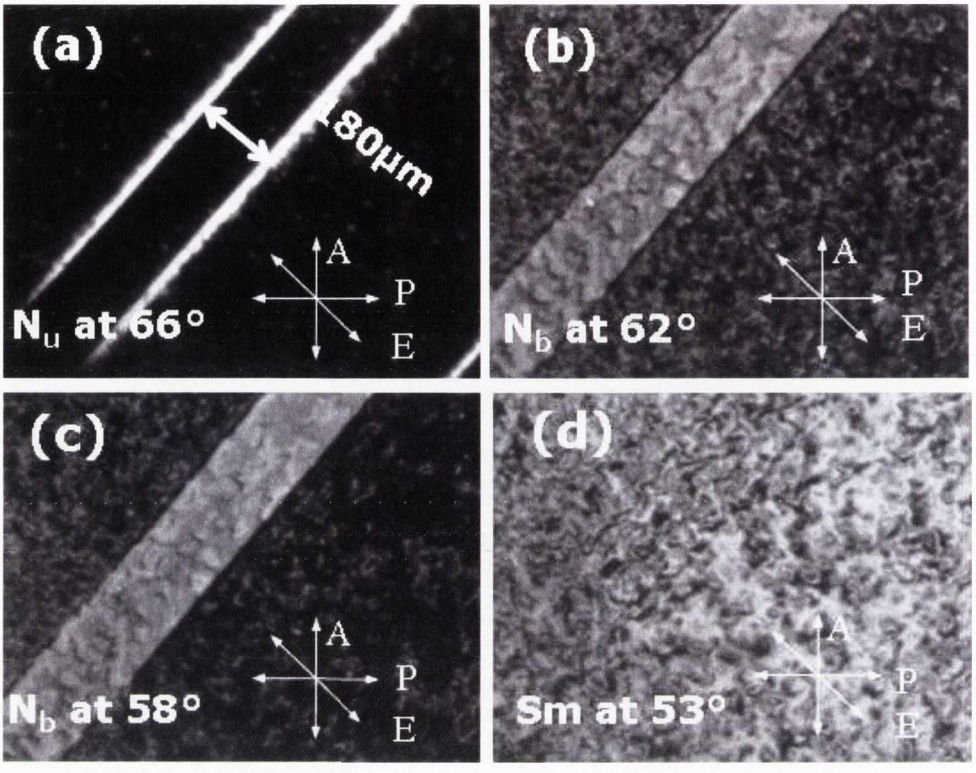

Figure 8.4: Texture of the unrubbed homeotropic cell for temperatures of (a) 68°C, (b) 62°C, (C) 58° and (d) 53°C. Cell gap = 7.6 μm, E =1.0 V/μm , 120 Hz square wave, a. A denotes the direction of the analyzer, P is the Polarizer, R the rubbing direction, E the Electric field.

PEM based system is used. It can provide simultaneous measurements of both the retardation (Γ) and the azimuthal angle (Φ, defined as the angle between the retarder axis of the cell and the polarizer). The temperature dependence of the retardation and of the azimuthal angle in homeotropic cell in the absence of the field is shown in Fig. 8.6. The cell was cooled at the rate of 0.1°C/minute. The microscope based PEM system acquires a throughput of light from an area of approximately 150x200 μm^2 of the cell in between the electrodes. The observed values of azimuthal angle and the retardation correspond to the average values over several domains. This is why at low fields the absence of a particular direction in the unrubbed cell causes significant deterioration in the accuracy and the data in this region should be disregarded. Higher fields cause a gradual alignment of the minor director in the unrubbed cell and a corresponding increase in the

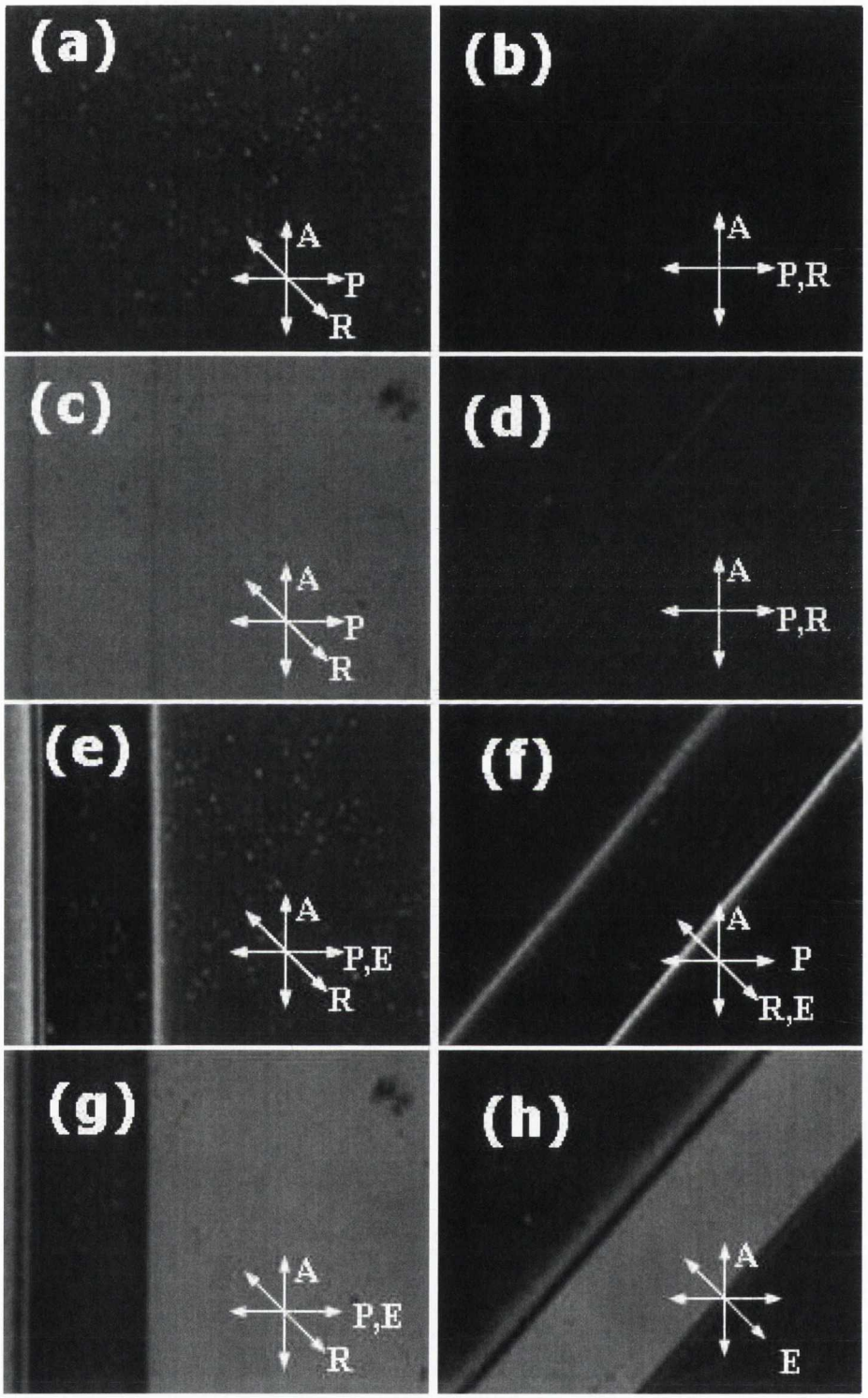

Figure 8.5: Texture of a rubbed homeotropic cell. cell gap 7.2 μm. (a), (b) N_u at 66°C , without applying field. (c) ,(d) N_b, at 64°C without applying field. (e), (f) N_u, with 1.0 V/μm applied. (g), (h) N_b, with 1.0 V/μm applied. 120 Hz square wave is used to drive the cell, distance between the electrodes is 180 μm.

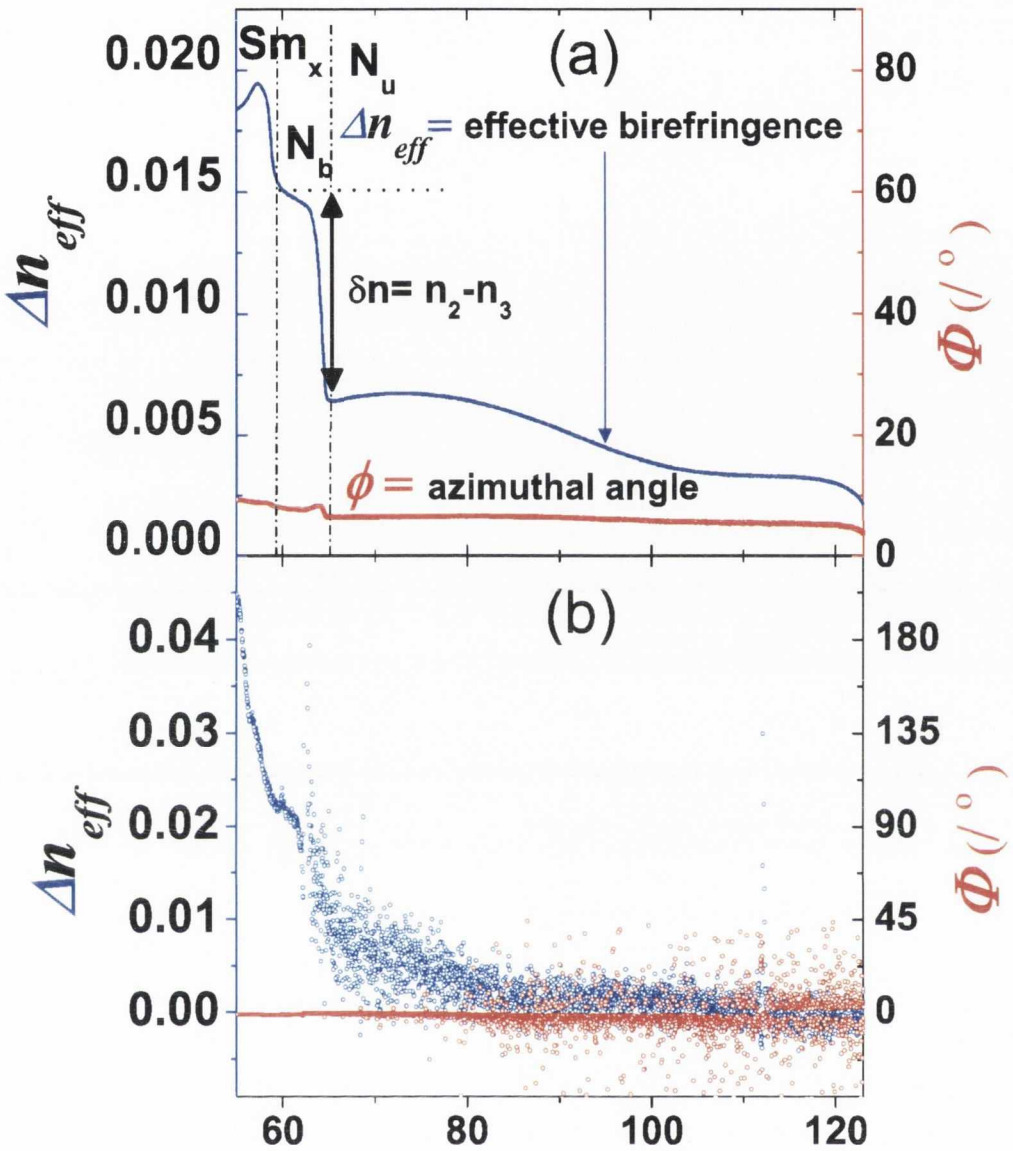

Figure 8.6: Temperature scan of PAL1 by PEM. (a) rubbed homeotropic cell. (b) unrubbed homeotropic cell.

apparent retardation (see Fig. 8.6 (b)). In the N_u phase the measured retardation is close to zero as it should be for a classical homeotropic alignment. However for a rubbed homeotropic cell, one can clearly see a jump in the retardation at a temperature of approximately 65 °C accompanied with a negligible change in the azimuthal angle (Fig. 8.6 (a)). The minor director coincides with the rubbing direction as observed in the microscope. This increase in the retardation results from a transition to the N_b phase which corresponds to a biaxiality, δn (=n_2 -

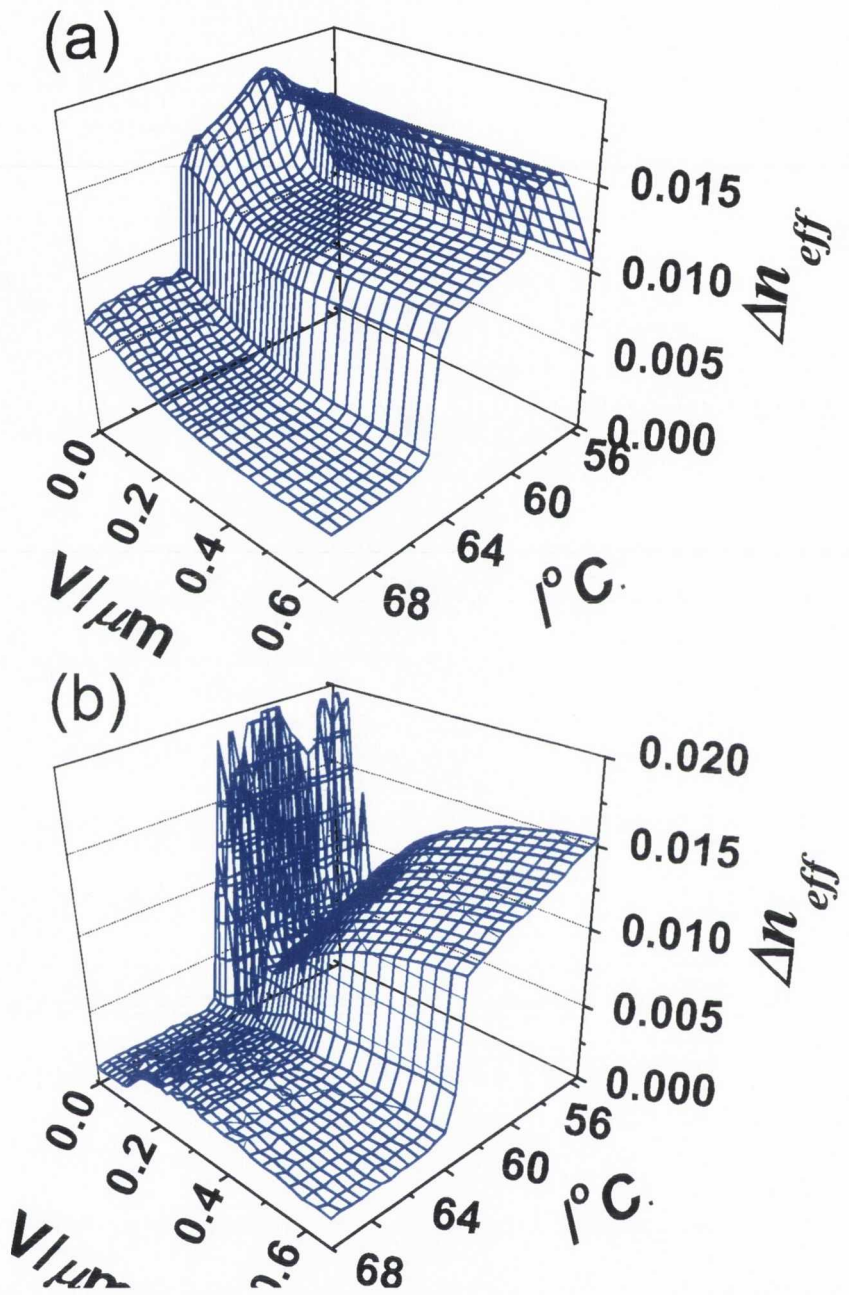

Figure 8.7: Three dimensional temperature and voltage plot of PAL1 by PEM. (a) rubbed and (b) unrubbed homeotropic cell.

$n_3) \approx 0.01$. To investigate the electro-optic switching, we applied 120 Hz square wave electric field with an amplitude up to 0.7 V/μm. Fig. 8.7 (a) represents the plot of retardation as a function of temperature and the electric field. One observes that by increasing the electric field in both nematic phases results in a decrease of the retardation of the rubbed homeotropic cell. This is easily explained

by a typical tilt of the major directors to the position of a perfect homeotropic alignment by the electric field in the nematic phase as the material has negative dielectric anisotropy. However the angle between the retarder axis of the cell and the polarizer with electric field is found to rotate in the N_b phase. We thus find that the surface induced tilt can be eliminated by the application of an in-plane electric field. This makes it possible to measure the optical biaxiality of the phase and avoid the problems related to the surface-induced birefringence [92]. In order to confirm the biaxial nematic N_b phase, we must observe an optical signal in a planar cell as well. Our PEM measurements with a commercial planar cell also show a similar jump in the retardation in the nematic phase (see Fig. 8.8). In the N_b phase in a planar cell, the minor director has so far been reported as parallel to the substrate [49, 50]. However in our experiment we observe an increase in the retardation at the transition temperature which means that the minor director is aligned perpendicular to the substrate. On applying 2 V/μm to the planar cell, we do not observe any measurable change in the retardation in either of the two nematic phases. This is because the minor director of the phase is already parallel to the electric field and the N_b with negative dielectric anisotropy will preserve its planar alignment under the electric field.

We find n_2-n_3 from the homeotropic cell as 0.01, whereas from the planar cell, $\frac{\sqrt{n_2^2+n_3^2}}{2} - n_3 \approx n_2 - n_3 \approx 0.004$. This discrepancy can possibly be explained by a difference in the surface conditions in the two cells. However, it is reasonable that the value found in the homeotropic cell is closer to biaxiality in reality. The most striking result is that in a planar cell the minor director is normal to its surface. This is favored by the fact that the transverse dipole moment being parallel to the minor director is normal to the surface. However there is a competing effect due to packing of the molecules favoring the minor director to be parallel to the substrate.

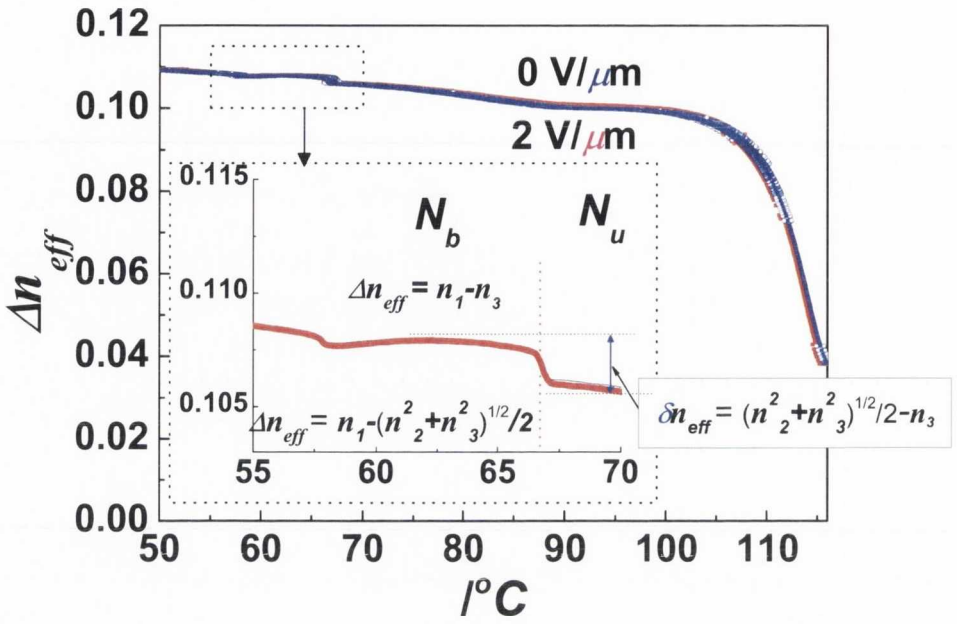

Figure 8.8: Temperature dependence of the effective birefringence in a planar cell using PEM with and without voltage.The inset shows a magnified view of the dotted rectangle in the figure.

8.3 Conclusion

A bent-core mesogen with asymmetric end groups has been studied for different surface conditions in both planar and homeotropic cells using both qualitative and quantitative optical techniques. A biaxial nematic phase observed in between the uniaxial nematic and the smectic phase is accompanied with a sharp increase in the biaxiality in a homeotropic cell. The material in this phase is also found to be switchable through the minor director by applying an in-plane electric field. We can distinguish between the biaxial nematic (N_b) phase and the anchoring transition of a uniaxial nematic (N_u) phase by retardation measurements using the PEM. In a planar cell, the optical change resulting from the transition is also observed. We realize the most plausible device configuration for display applications. Even though further understanding is required to interpret the difference in δn (= n_2 - n_3) results obtained from homeotropic and planar cells. Nevertheless, this is the first substantial observation of the optical biaxiality in the N_b phase using a quantitative technique.

Part. V

Applications and Conclusion .

Chapter 9

Application to displays

"In this chapter, *applications of the phases introduced in previous chapters are treated.* "

9.1 Introduction

Nematic liquid crystal displays (LCDs) have revolutionized the display industry. A liquid crystal display (LCD) consists of three basic units as shown in Fig. 9.1. These systems are driving circuit, LCD panel and backlight systems. Each unit plays an essential role in reproducing an image and color. Compared to other displays, the key feature of the LCD is the presence of a liquid crystal layer between two glass substrates in which liquid crystals are aligned under certain surface conditions. Its initial configuration and the structure of electrodes on the substrates determine the types of LC-modes such as TN, PVA, IPS. Even though each mode has been improved under the name of either advanced or super, from the viewpoint of the optical configuration, the basic concept of each mode has not significantly changed. Figure 9.2 shows three representative LCD modes that are commercially used. In order to understand the merits of a new mode, it is very

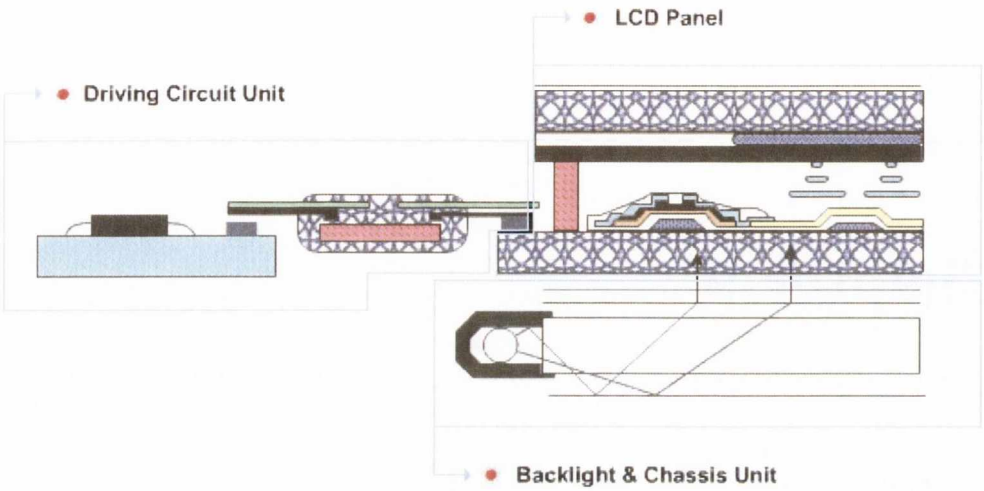

Figure 9.1: The structure of LCD.

helpful to understand the principle and the properties of the conventional modes. In this chapter, firstly, three representative modes are reviewed in terms of the optical properties. Secondly, applications of N_b is discussed.

9.2 The LC modes commercialized in a mass production.

Each mode in Fig. 9.2 has its own unique electro-optical property and advantages that lead to being commercially exploited. It is notable that the different configurations of the directors in each mode lead to different conversions in the polarization state of the light passing through the liquid crystal layer of the LCD mode. As a result, different transmittance equations in terms of the cell parameters such as the cell gap and the wavelength, λ are encountered. Usually, either the Müller matrix or Jones matrix for each mode is used to express a quantitative transmittance behavior of LC cells. However, in this chapter , the expression using the *Stoke parameters* on the *Poincare sphere* is used for the investigation of the changes in the polarization states of the light (see Chap. 2.2) As mentioned in Chap 2.2, this method makes it possible to intuitively understand the behavior of the LC modes.

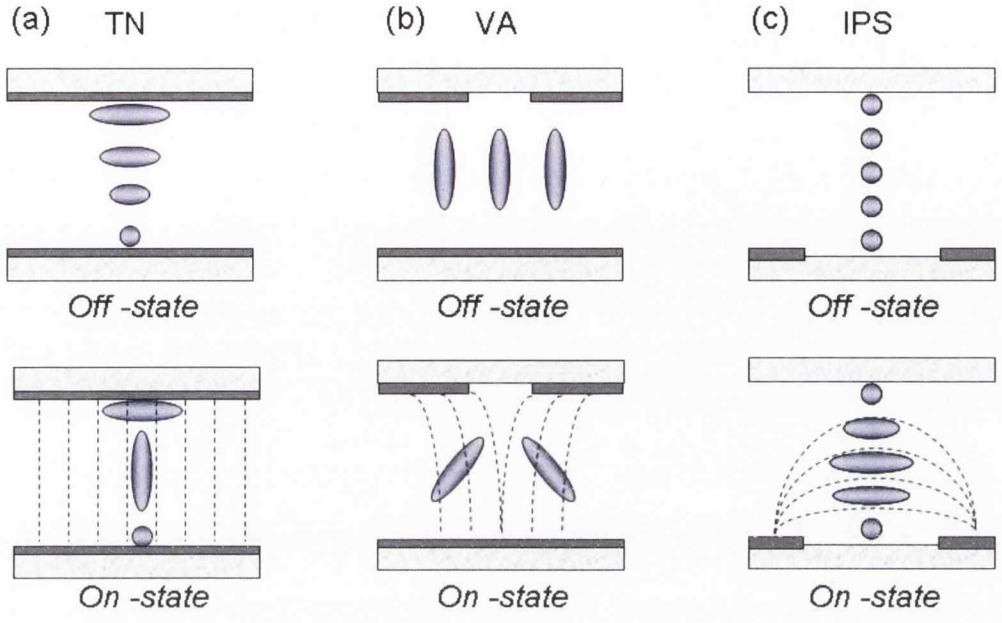

Figure 9.2: Commercialized LCD modes.

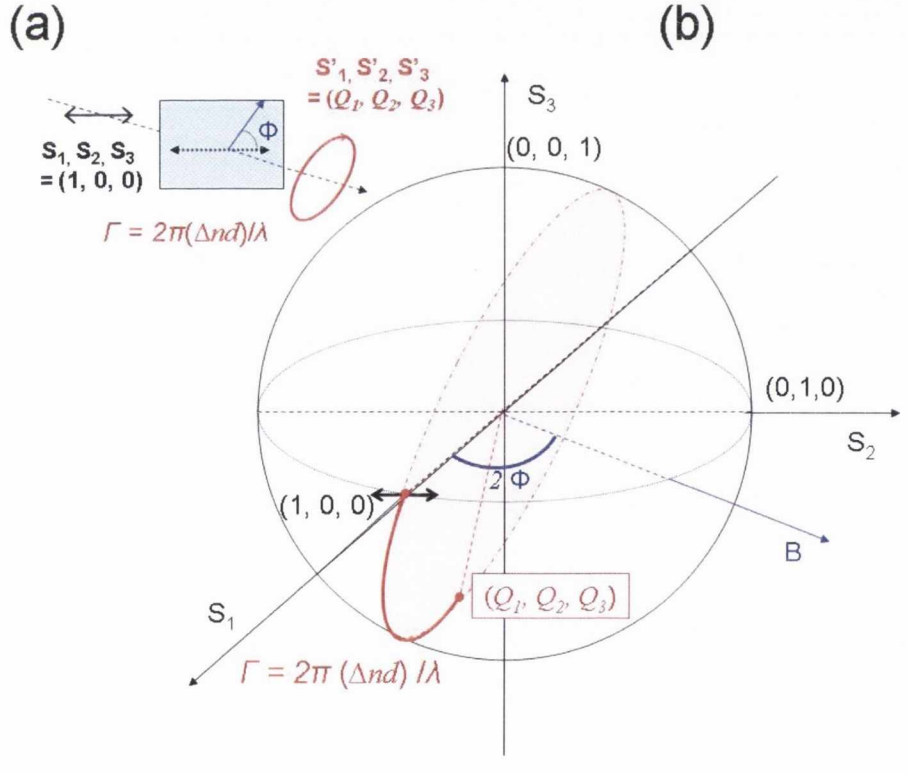

Figure 9.3: Polarization conversion using a general birefringent wave plate. (a) optical configuration of the system. (b) points of the polarization states on the *Poincare sphere*. $\Gamma = \frac{2\pi}{\lambda}\Delta nd$. ϕ is the azimuthal angle of the slow axis of the retarder

Figure 9.3 (a) shows an example that describes the states of a polarized light passing before and after a wave plate with a phase retardation $\Gamma(=\frac{2\pi}{\lambda}(\Delta nd)$. These two polarization states are described in Fig. 9.3 (b). The output polarization state on the *Poincare sphere* can be obtained from the initial state on this sphere by the rotation of the angle by Γ around the B-axis. Therefore, we can design an optical system to obtain a state of polarized light by setting values of Φ and Γ. Moreover the above method can be employed for the analysis of polarization evolution in the LC modes.

9.2.1 TN mode

We can assume that TN mode consists of a number of LC layers with a continually varying Φ, (see Fig. 9.4 (a)). When $\frac{\lambda}{2} << \Delta nd$, the wave guiding occurs as a light beam propagates in the LC layer. The inequality is also know as the *Mauguin condition* for a 90° TN cell. The state of the polarized light can be expressed on the *Poincare sphere* as shown in Fig. 9.4 (b). Basically, this is consistent with the optical rotation which alters only S_1, S_2 but S_3. TN mode exhibits maximum transmittance when no electric field is applied. As the electric field between the sandwitched electrodes increases, the directors exert a reorientation which is determined by free energy density induced by distortion which is before, the free energy of a LC system is given by [93, 94]

$$g = \frac{1}{2}\left[k_{11}(\nabla \cdot n)^2 + k_{22}(n \cdot \nabla \times n)^2 + k_{33}(n \times \nabla \times n)^2\right], \tag{9.1}$$

where k_{11}, k_{22} and k_{33} are the elastic coefficients for splay, twist and bend deformations, respectively. The energy expression depends on the deformation structure. Under the electric field, the directors in each mode exert a reorientation by minimization of the free energy. The threshold voltage of each mode is given in TABLE. 9.1. The dark state of TN mode can be obtained under an electric field strong enough to align most of the directors vertical to the substrates as shown in Fig. 9.4 (a). However, the directors on the surface cannot be aligned to be normal to the surface due to a strong surface anchoring. As a result, TN mode

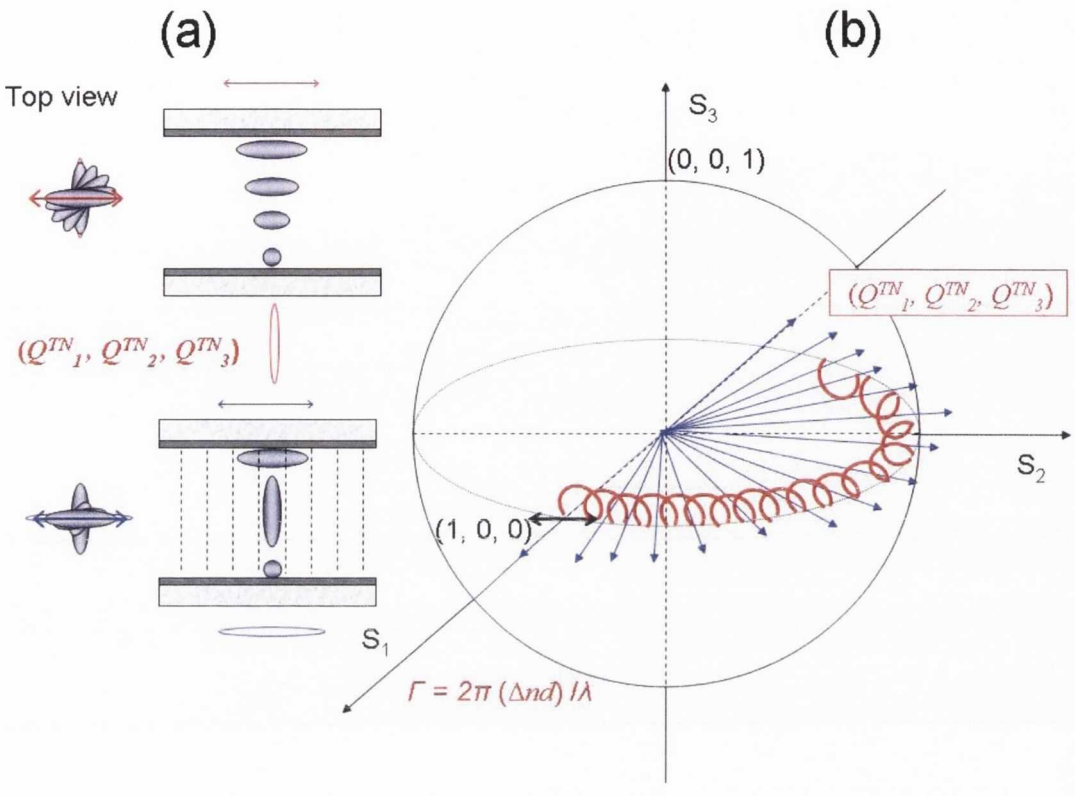

Figure 9.4: Polarization conversion in TN mode. (a) optical configuration of the TN mode. (b) the points of the polarization states on the *Poincare sphere*. $\Gamma = \frac{2\pi}{\lambda}\Delta nd$.

shows relatively lower contrast ratio among the three LC modes due to a residual retardation arising from the orientation of the directors close the surface.

9.2.2 VA mode

The directors in the VA cell are vertically aligned under zero electric field. This leads one to realize an ideal dark state. As the electric field increases, the vertically aligned directors fall down due to the negative dielectric anisotropy. The transmission of the VA cell at normal incidence depends on the applied voltage. A state of the polarized light can be expressed as shown Fig. 9.5 (b). The transmittance dependent on the applied voltage is attributed to an effective Δn at normal incidence.

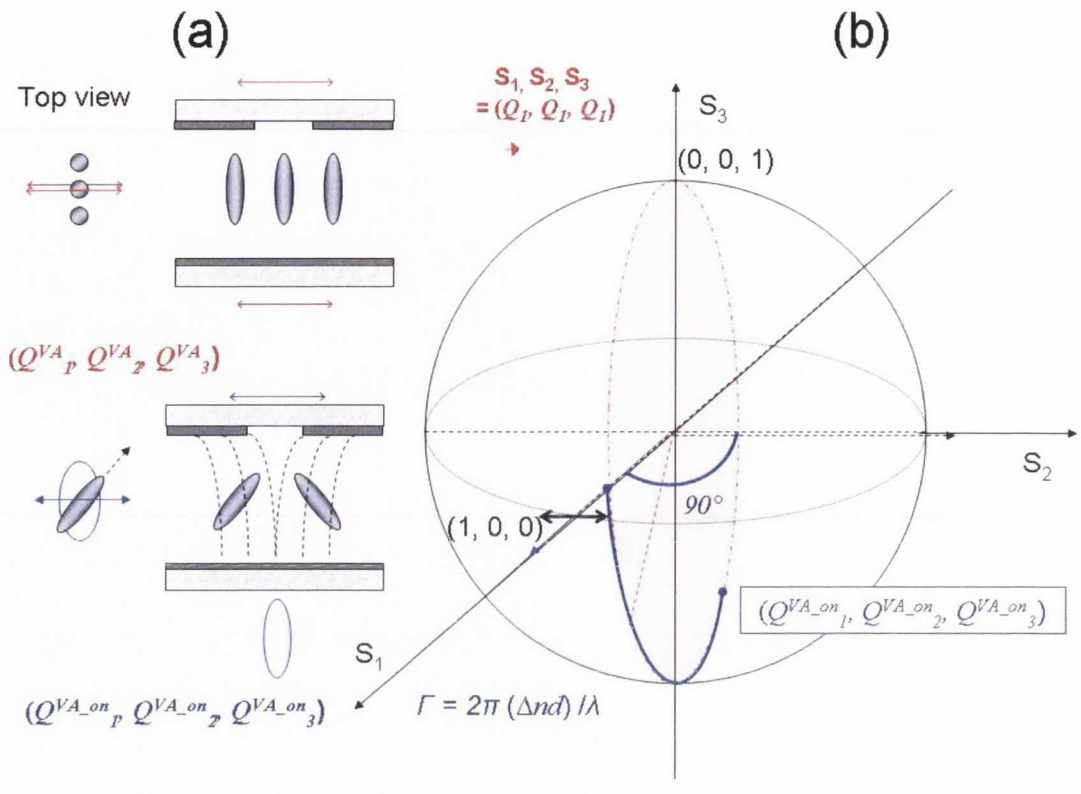

Figure 9.5: Polarization conversion in VA mode. (a) optical configuration of the TN mode. (b) the points of the polarization states on the *Poincare sphere*. $\Gamma = \frac{2\pi}{\lambda}\Delta nd$.

9.2.3 IPS mode

For the IPS mode, the dark state of the IPS mode is obtained by aligning the rubbling direction of the cell so as to be parallel with one of two polarizers. A azimuth angle Φ controlled by the electric field plays a major role in determining a transmittance of the cell. The polarization conversion in a IPS mode is shown as Fig. 9.6 (b). Each mode undergoes different polarization conversions, resulting in different transmittance equations in terms of λ, d and Δn. Actually, the light source used in LCD is polychromic. The color quality of the LC mode depends on the transmittance of a polychromic light, therefore the color properties and image quality of the LCD are mainly governed by the selected LC mode.

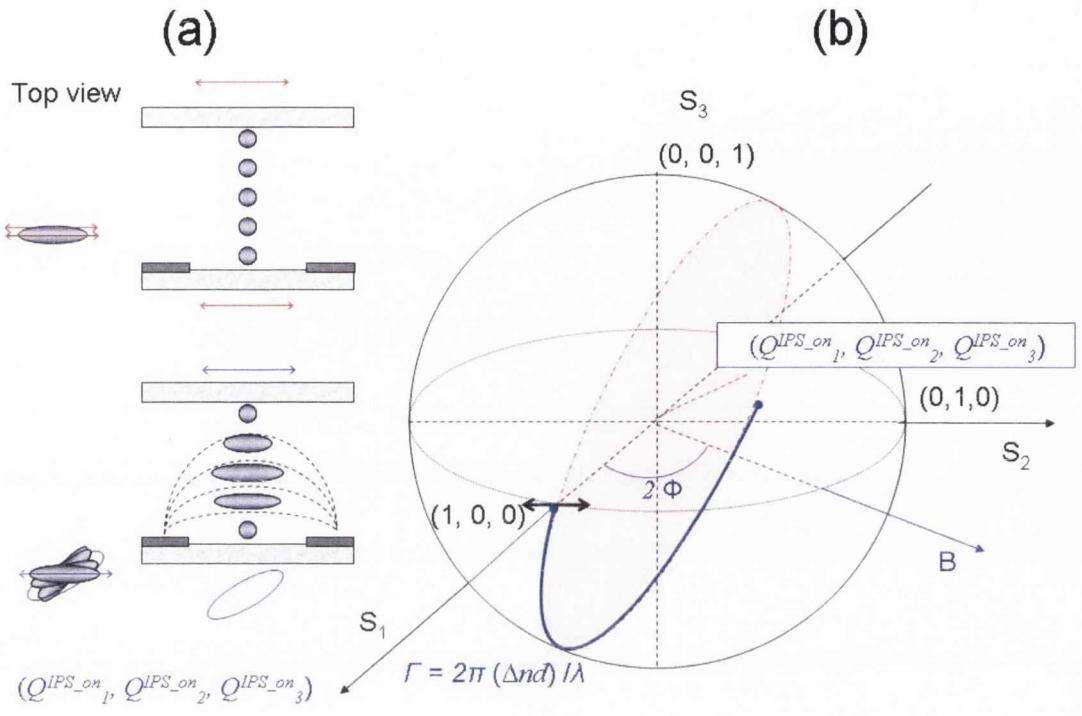

Figure 9.6: Polarization conversion in IPS mode. (a) optical configuration of the TN mode. (b) the points of the polarization states on the *Poincare sphere*. $\Gamma = \frac{2\pi}{\lambda}\Delta nd$.

Table 9.1: Transmittance and dielectric anisotropy of the LC modes.

Modes	TN	VA	IPS
$\Delta\epsilon$	positive	negative	positive
Eqn. of trans.	$\frac{1}{2} - \frac{1}{2}\frac{\sin^2\left[\frac{\pi}{2}\sqrt{1+u^2}\right]}{1+u^2}$	$\frac{1}{2}\sin^2\frac{\Gamma}{2}$	$\frac{1}{2}\sin^2 2\Phi \sin^2\frac{\Gamma}{2}$
Anchoring	planar	homeotropic	planar
V_{th}	$\pi\sqrt{\frac{k_{11}}{\Delta\epsilon}}\left[1+\left(\frac{k_{33}-2k_{22}}{4k_{11}}\right)\right]^{1/2}$	$\pi\sqrt{\frac{k_{33}}{\Delta\epsilon}}$	$\pi\sqrt{\frac{k_{22}}{\Delta\epsilon}}$
Dark gray	*On* state	*Off* state	*Off* state

$u = \frac{2\Delta nd}{\lambda}$. k_{11}, k_{22}, k_{33} are the splay, twist and bend elastic constants, respectively.

9.2.4 Viewing angle

So far, we have considered only transmissions at normal incidence. However, the transmission property at oblique angles is equally important to that of the normal incidence. One of the most important specifications of LCDs is viewing angle which represents the transmission property at general incidence expressed by

$$Contrast_{\theta_i,\Phi} = f(\frac{T_{max}}{T_{min}}, \theta_i, \Phi). \tag{9.2}$$

The viewing angle is defined in terms of the contrast at an off axis angle of θ_i and Φ. θ_i is the angle between the incidence direction and the normal direction to LCD plane and Φ is the azimuthal angle of incidence direction measured with respect to the polarizer orientation. Originally, the VA mode and the IPS mode were developed to improve the viewing angle of the TN mode which is the most serious drawback of the latter. Practically, wider viewing angle displays are realized by using expensive optical compensation films [87, 88].

When two independent modes of propagation are given to a direction of propagation in an anisotropic medium. The two modes dubbed the ordinary mode and the extraordinary mode are mutually orthogonal. The eigen indices of refraction of these two modes depend on the direction of propagation. In uniaxially birefringent media, the refraction index of the ordinary mode is independent of the direction of propagation, whereas the refractive index for the extraordinary mode depends on the direction of propagation. Thus the phase retardation may depend on the direction of propagation. For a normally incident beam, the phase retardation is given by

$$\Gamma_0 = \frac{2\pi}{\lambda}(n_e - n_0)d. \tag{9.3}$$

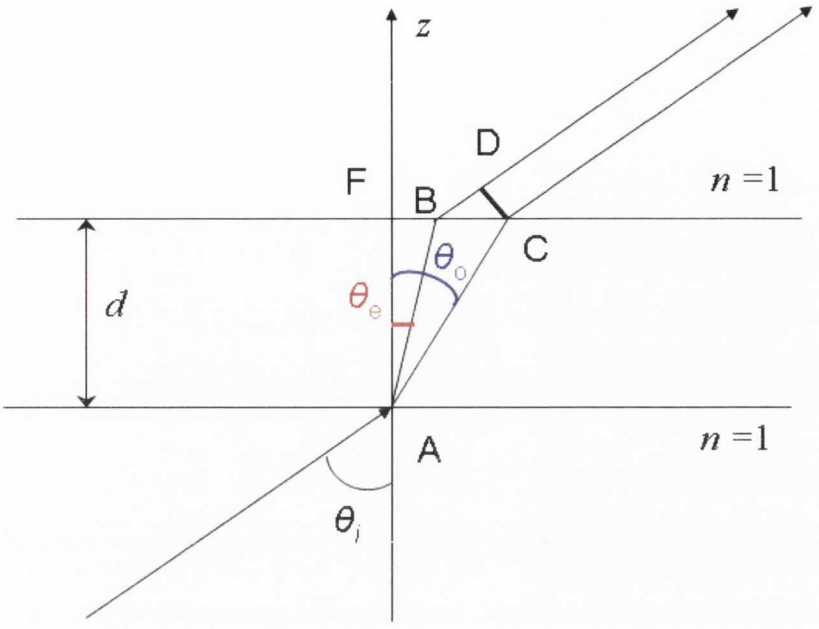

Figure 9.7: Phase retardation at oblique incidence. CD is perpendicular to the direction of propagation in air. Redrawn from Ref. [95].

A general expression for the phase retardation is given by

$$\Gamma = (k_{ez} - k_{oz})d \tag{9.4}$$

$$\Gamma = kn'_e AB + kBD - kn_0 AC \tag{9.5}$$

$$\sin\theta = n'_e \sin\theta_e = n_o \sin\theta_o \tag{9.6}$$

$$\Gamma = k(n'_e \cos\theta_e - n_o \cos\theta_o)d \tag{9.7}$$

here, k_{ez} and k_{ez} are the z components of the wave vectors, n'_e is the refractive index dependent on the incident angle. The phase retardations of the LC modes are given as below [95]:

$$\Gamma_{VA} = \Gamma_0 \frac{n_o + n_e}{2n_o n_e} \sin^2\theta_i \tag{9.8}$$

$$\Gamma_{IPS} = \frac{2\pi}{\lambda} d \left[n_e \sqrt{1 - \frac{\sin^2\theta_i \sin^2\Phi}{n_e^2} - \frac{\sin^2\theta_i \sin^2\Phi}{n_o^2}} - n_o \sqrt{1 - \frac{\sin^2\theta_i}{n_o^2}} \right] \tag{9.9}$$

The above retardations give rise to light leakage leading to a poor contrast at an oblique viewing angle (see Fig. 9.8). Moreover, even with a pair of crossed

polarizers and no LC layer, a light leakage still occurs [43]. When a light is passing between two crossed polarizers with an oblique angle θ_i, the angle between the transmission axes of the polarizers is dependent on θ_i (see Fig. 9.8 (b)). The deviation angle from 90° for transmission axes of the crossed polarizers is given by:

$$\frac{\pi}{2} - 2\Phi' = \arcsin \frac{\sin^2 \frac{1}{2}\theta_i'}{\sqrt{1 - \frac{1}{2}\sin^2 \theta_i'}} \tag{9.10}$$

here, $\sin\theta_i' = n \sin\theta_i$, n is the refractive index of the optical element. θ_i is the oblique angle of incident light. Φ' is defined in Fig. 9.8 (b). Basically, in the case of VA-mode, a negative c-plate ($n_e < n_o$) with a comparable retardation value can be used for the compensation of Γ_{VA}. But the light leakage due to the decrossed transmission axes of the polarizers at an oblique angle still remains.

9.3 Limitation of a LCD using the biaxial nematic phase

A biaxial system is versatile in reducing the light leakage arising from a retardation of the LC layer as well as a deviation of transmission axes of the polarizers [89]. Figure 9.8 shows how a biaxial medium change the states of a polarized light on the *Poincare sphere*. In order to reduce the transmittance at an oblique angle, the state of the polarized light should be converted to the opposite point of the rear polarizer on the *Poincare sphere*. This point is called the extinction point as shown in Fig. 9.8 (c). Actually, the rotational axis (denoted by the green dotted arrow in Fig. 9.8 (c)) on the *Poincare sphere* is determined by $\frac{n_x - n_z}{n_x - n_y}$. A biaxial film with the appropriate refractive indices can minimize the transmittance at an oblique angle (see Fig. 9.9). Therefore. N_b with the appropriate refractive indices can replace the expensive compensation films for wider viewing angle. In the system, the biaxial LC layer can play a role in reducing the light leakage at oblique angles, leading to a wider viewing angle.

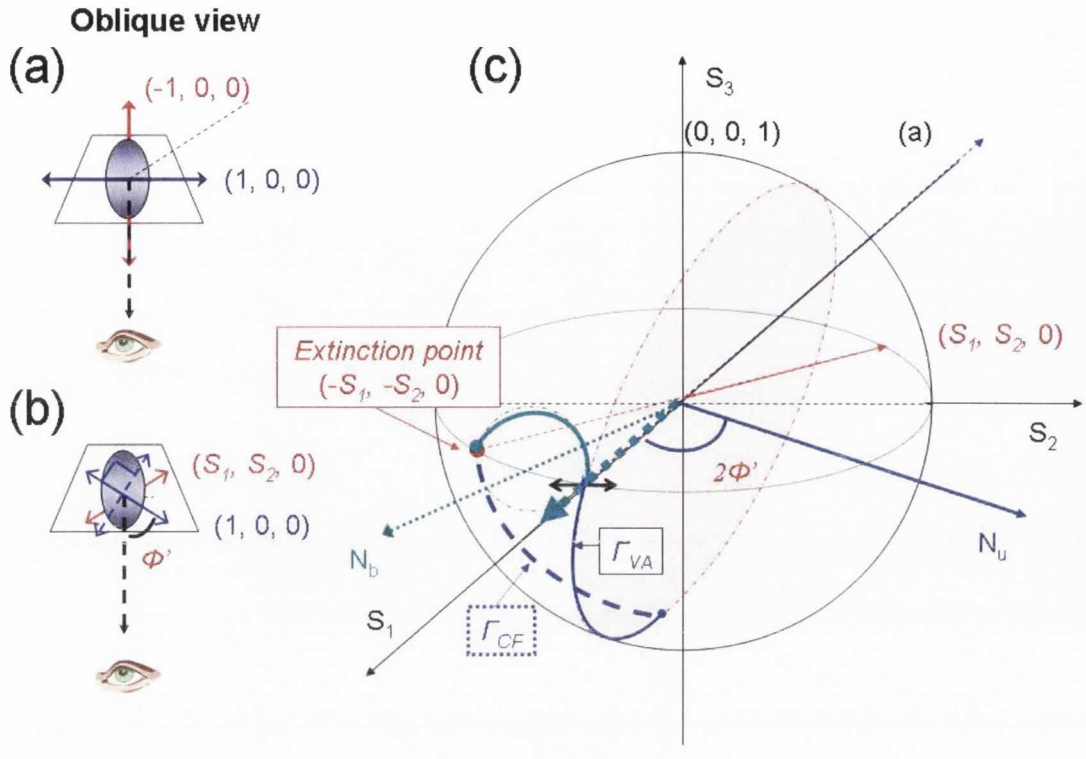

Figure 9.8: Schematic representation of viewing angle and polarization conversion on the Poincare sphere. (a) viewing from the direction along with the transmission axis of the polarizer. (b) viewing from the direction between the transmission axes of the polarizers (c) the points of the polarization states on the *Poincare sphere*.

Another advantage of N_b arises from the reorientation of the minor director under an electric field. This was expected to show a faster response than that of the major director due to the lower elastic constants [15, 86]. A LC mode in which biaxial nematic LCs are homeotropically aligned on in-plane electrodes was suggested for switching the minor director [15]. Such a system was realized and its optical behavior was investigated in Chap. 8. The response time, τ_r $(= \tau_{on} + \tau_{off})$ of the system is a few minutes to so that conventional techniques for measuring τ_r are not applicable. According to the cluster model, the biaxiality of N_b results from the alignment of the biaxial clusters (see Fig. 4.2). When the biaxial clusters reorient under an electric field, the response time would be not so short as predicted by Berardi *et al* [86]. Moreover, when the electric field is off, it takes

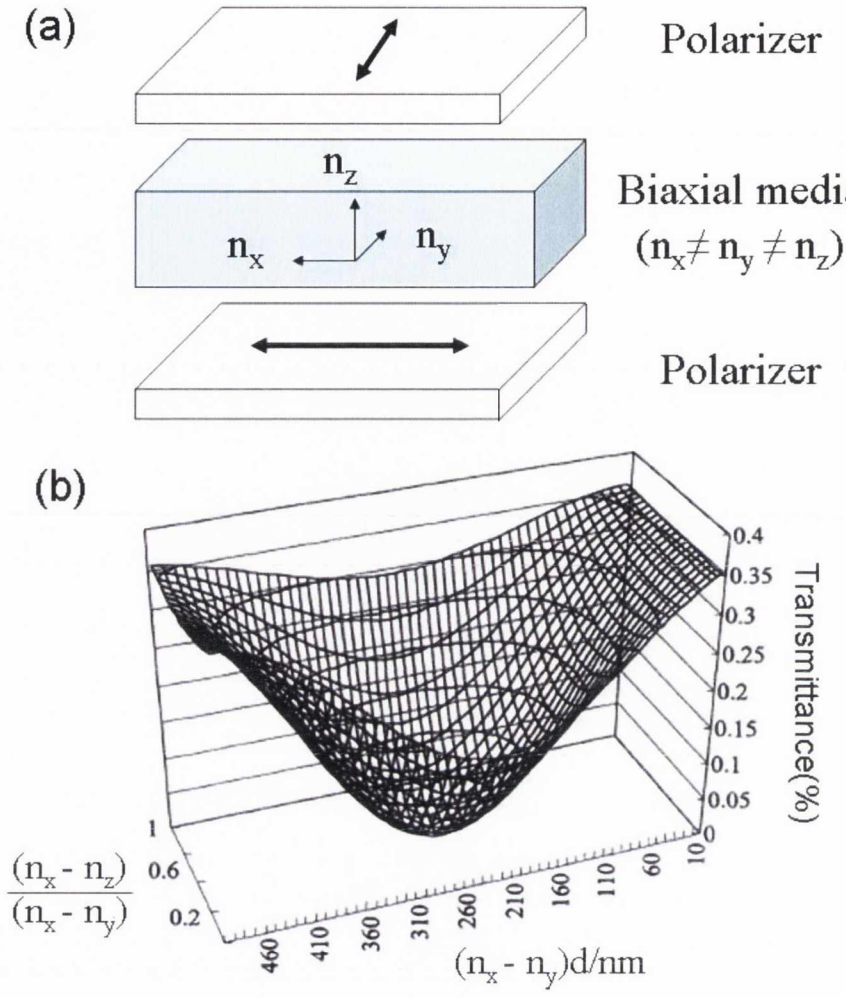

Figure 9.9: (a) an optical configuration composed of a pair of crossed polarizers and a biaxial film between the polarizers. (b) Transmittance of the system at an oblique angle (see Fig. 9.8 (b)) as a function of $\frac{n_x - n_z}{n_x - n_y}$ as well as $(n_x - n_y)d$. Redrawn from Ref. [89].

longer time for the directors of the cluster to return to the initial state due to small elastic constants.

Another limitation of the system is found in the magnitude of the biaxiality. In Chap. 8, we found that the retardation $(n_x - n_y)$ arising from the biaxility of the nematic phase is approximately 0.01. This implies that the cell gap necessary for the application to a LCD is about 30 μm. Practically, such a large cell gap value is a big obstacle for such a display to be commercialized. Therefore the material with larger biaxiality should be developed for practical use. Above all, this system opens a possibility for a new type of LC mode.

9.4 Conclusion

A liquid crystal display that uses a biaxial nematic phase is very attractive for both scientific and commercial reasons. The display using this mode will overcome the limitations of both speed and viewing angle imposed by using liquid crystal in the uniaxial nematic phase. In order to achieve faster switching, the reorientation of the major directors should be frozen. Such a system has been investigated with in-plane electrodes and homeotropically aligned configuration. Unfortunately, the response of the system is too slow to be satisfactorily applicable to displays. The main cause lies in the origin of the biaxiality of the nematic phase. According to the cluster model given in Chap. 4, instead of reorienting individual liquid crystalline molecules, the biaxial cluster reorients with applied field. Even though such a system has not been examined in detail. It would seem that the reorientation of the cluster in unfavorable for the fast response. Above all, this study is a worthy first step for a competitive type of LC mode using liquid crystals in its biaxial nematic phase.

Chapter 10

Conclusion and future works

10.1 Conclusion and the summary of the thesis

Liquid crystals provide an attractive field of study for various reasons. The variety of physical characteristics and phases, their great success in many applications, and their relevance to other fields such as biology and nano-science. Their interesting properties mostly originate from the special shapes of liquid crystalline molecules and moderate intermolecular interactions between the molecules, leading to numerous different types of LC phases between solids and liquid. The fundamental property which distinguishes liquid crystals from these two more common states of matter is the unique combination of order and mobility. This means that in these materials there is long range order, leading to anisotropic physical properties and fluidity which allows these materials to change their configuration under the influence of external stimuli, such as a mechanical force, electric or magnetic fields. This combination of properties is essential for technological applications.

The nematic phase is the simplest, least ordered and most fluid LC state in which the intermolecular interactions are not strong and the alignment of directors is easily distorted by the relatively weak external fields. Formation of the nematic phase requires a distinct anisotropy of the molecular shape. It can be formed by a variety of molecular and supramolecular entities, but the two fundamental major shapes are rod-like and disc-like. Such anisometric molecules have a high tendency to align parallel to each other in order to minimize the excluded volume and to maximize the attractive van de Waals interactions between them (see Fig. 1.1 (a) and (b)). However, in recent years there have been several exciting new developments in the field of nematic mesogens, for example by using new materials with new molecular shapes, such as bent-core mesogens. Apart from the banana phases [4, 5], the bent-core mesogens form clusters in the nematic phase leading to the cybotactic nematic phase. The understanding of the relationship between the molecular structure of the bent-core mesogen used in this thesis and the formation of the cybotactic cluster in the nematic phase was introduced in Chap. 3. The presence of the cluster in the nematic phase was investigated by X-ray technique. The formation of the cluster in the nematic phase is closely related to the length of the terminal chains in the molecules. This implies that the correlation between the molecules with long terminal chains is stronger than that with the short terminal terminal chains. Such a correlation is also observed in the dielectric response of the materials. In Chap. 5, we investigated the materials by dielectric spectroscopy. C4 with the short terminal chains is well explained by the M-M model based on the molecular field theory. The materials with longer chains (C7, C9) show different behavior from C4. This disagreement has been interpreted in terms of the Kirkwood correlation factor having value different from unity in the M-M equation (see Eqns. 5.1 and 5.2). We introduced a smectic like model (Eqns. 5.14 and 5.15) to analyse the polar correlation length. Interestingly, the results from X-ray experiments are comparable to those from the dielectric experiments (see Fig. 5.12). It should be noted that this comparison clears the controversy that exists in the literature [18, 47] in the interpretation of the splitting of small angle X-ray diffraction pattern. It is found from the results that the terminal chain of

the materials affects the intermolecular interaction leading to the formation of the cybotactic cluster, the origin of which is smectic C type. The key feature of smectic C type is the tilt of the molecules in the layer. This can be partly represented by the splitting of the small angel scattering in the X-ray diffraction pattern, for two representative materials C4 and C9 in the homologue series. The investigation using the IR spectrometer was carried out. The technique using IR spectrometer is useful for the investigation of conformational change in the molecular structure as well as for the molecular orientation with respect to the laboratory Z axis. For C4, the result from the IR experiments shows the averaged tilt angle of the molecules from normal to the substrates is zero in the nematic phase, whereas the molecules in the cluster are tilted with respect to the averaged layer normal parallel to the laboratory Z axis for C9. A comparison was made between the results from X-ray and IR experiments as shown in Fig. A.2. To my knowledge, the above two comparisons are the first substantial dielectric and optical approaches for the origin of the cybotactic nematic phase. Additionally, in Chap. 5 and 6, other complementary techniques were used. The third complementary technique is a comparison of the crossover frequency between the dielectric spectroscopy and the optical contrast spectroscopy. For the conventional DFNs (Dual frequency nematics), the crossover frequency is equal to the dielectric relaxation frequency arising from the end over end molecular rotation around the molecular short axis. However, for the bent-core mesogens, the crossover frequency as a function of temperature is not always consistent with the molecular rotation frequency over the entire range of temperatures and frequency in the nematic phase. The short range correlation from the cluster in the nematic phase alters the dielectric anisotropy as a function of temperature as well as frequency. This technique was used to investigate the conformation change in the molecular shape of a bent-core mesogen [67]. This motivated us to use another complementary technique for the investigation of the conformational change in the molecular shape of the materials under study. The measurement of birefringence provides a simple method to calculating the orientational order parameter as well as of finding conformational change in the liquid

crystalline phase. The investigation using the PEM, does not exhibit any substantial change in the molecular shape for all the materials leading to the unusual optical and dielectric behaviors as a function of temperature . Undoubtedly, the different dielectric behavior of the materials results from intermolecular interactions in the nematic phase and this is confirmed by means of the complementary approaches which are effective to avoid interpretation errors.

bent-core mesogens were reported to have macroscopic chirality in the mesophases via a self assembly of transient chiral conformers [4, 5, 73, 76]. Interestingly, in the materials, only C5 shows chirality in the entire nematic phase whose chain length is in between the nematic phase consistent with the M-M theory (C4) and the cybotactic nematic phase composed of the smectic C like cluster. Even though the materials (C6, C7 and C9) having SmC like clusters in the nematic phase do not show any chirality in the nematic phase. The probability that chirality of C5 is induced by a chiral impurity either during synthesis or during cell preparation was investigated. Comparisons of cells made from different materials, different surface conditions with various cell gaps allow us to rule out chiral contamination as the source of chirality. Secondly, induction of chirality from synthesis was considered. Two syntheses from different starting materials were carried out for C5. C5 samples from both syntheses show chirality in the nematic phase. This means that the chirality is a property of the material. Actually, immediately after the transition to the nematic phase, a couple of domains are observed and these domains merge into a most stable domain with a single handedness within a short time. Interestingly, one of the domains that appears initially has opposite handedness to the stable domain. This implies that the chirality is not induced by a chiral impurity. Instead, it can be interpreted as the degeneracy of two chiral domains which is broken by the confined anchoring condition. The measured pitch length of C5 is 9 μm which represents considerable twisting power and a large twist elastic constant. If there is a deviation between the two rubbing directions in the planar cell, the twist energy in terms of the twist angle is different from each other, leading to an energy gap between two helical states in the planar cell (see Eqn. 7.3). It should be noted that C5 seems to be different from the previously

reported chirality of achiral bent-core mesogens in terms of twisting power and the chiral origin [4, 5, 73, 76]. As mentioned above, C5 does not show substantial clusters in the nematic phase. This means that chiral induction via self assembly or supramolecular structure is not applicable to C5. In order to interpret the chiral origin of C5, the most simplest cluster structure consisting of a pair of bent-core molecules was proposed and discussed in Chap. 7. As a consequence, the chiral behavior of C5 is suggested in terms of a new type of chiral generation based on the interlocked system between two achiral bent-core molecules.

The biaxial nematic phase has been one of the most contemporary and interesting topics in the field of liquid crystals since the prediction made by Freiser. As reviewed in Chap. 9, the optical biaxiality of the phase is versatile in switching of the minor directors as well as in realizing the wide viewing angle of LC mode. For this reason the biaxial nematic phase has been expected as a strong candidate for replacing the conventional uniaxial nematic phase used in LCDs. We found optical biaxiality of PAL1 in the nematic phase prior to the transition to the smectic phase. The birefringence from ordering of the minor directors was quantitatively measured by the system using the PEM under various surface anchoring conditions. The results of the experiment gave useful new scientific information regarding the biaxiality in the nematic phase. As predicted in Chap. 4, the macroscopic biaxiality of the nematic phase arises from the alignment of the biaxial clusters in the nematic phase under external stimuli. The measured value of the optical biaxiality in the nematic phase is affected by the type of anchoring conditions which determine the initial configuration of the major as well as of the minor directors. For example, the moderate rubbing of the substrates in the homeotropic alignment sets the minor directors aligned along the rubbing direction, while the major director keeps the homeotropic alignment. In the homogeneous anchoring condition, the minor director is normal to the surface while the major director aligns along the rubbing direction. It is natural that the ordering of the minor director is dependent of the anchoring condition. The ordering of the minor director is expressed in terms of the birefringence. Such a control of the configuration of the minor director is very attractive for the application to the LCD. Above all, the response time of the

biaxial nematic phase is found to be too slow to be used in LCDs. This limitation of the biaxial nematic phase originates from the clusters. The intermolecular interaction reflected by the elastic constants and viscosity is stronger in the cluster than in the usual nematic state. This implies that the macroscopic biaxiality under electric field is due to the reorientation of the biaxial clusters rather than of the switching of the molecules in the cluster. Pending a full theoretical treatment, we intuitively expect that the reorientation of the cluster takes a larger time.

So far, we have found the relationship between the molecular structure of 4-cyanosubstituted bent-core mesogens and the molecular interaction in the nematic phase. Basically, the elongated terminal chain increases the correlation between the molecules leading to the formation of the cybotactic clusters. The size of the cluster and the number of molecules in the cluster can be determined by analyzing the dielectric spectra recorded from the planar and homeotropic cells. The extent of the correlation creates interesting physical phenomena in the nematic phase. For C5, the correlation between the molecules is such that a pairing of the two bent-core molecules leads to its chirality. For C7, the correlation with temperature gives rise to a change in the sign of dielectric anisotropy different from DFNs. For C9, the correlation is strong enough to have negative sign of the dielectric anisotropy over the entire range of temperatures in the nematic phase. For PAL1, the asymmetric terminal chains enhance the stability of the biaxiality in the nematic phase to the extent that the ordering and the switching of the minor directors is realized. In this way, the molecular interaction is the most important factor that determines the physical properties of liquid crystals, and in particular, the level of the correlations provides a direct and simple way to explain the various physical phenomena occurring in the nematic phase containing clusters. Different techniques used for the work described in this thesis allow us to understand the various phenomena in the nematic phase. Many of the new findings in this thesis are related to the analysis of the results of the experiments and an application of the proper models to the physical phenomena under discussion. The conventional LC modes used in LCDs for mass production had been reviewed in

Chap. 9. Basically, the switching is the act of converting the state of polarized light passing through the LC layer to achieve certain transmission to display a gray level. Therefore, the design of the LC mode that is better than an existing mode begins from the understanding of the polarization conversion. Each mode was analysed in terms of the *Stokes parameters* on the *Poincare sphere*. The principle of the compensation for the retardation at oblique angles was interpreted in terms of the *Stokes parameters* on the *Poincare sphere* for a better viewing angle of a display. The biaxial nematic phase is more versatile than the uniaxial nematic phase in achieving wider viewing angle. Its inherent biaxiality can be used not only for realizing a gray scale by switching the minor directors but also for minimizing transmittance arising from the optical system of LCD at oblique angles thus leading to wider viewing angle displays.

10.2 Future work

One of the goals in the LC research is to improve the LCD technology for better displays. For a practical application of the biaxial nematic phase, the phase stability should increase. Actually, the liquid crystalline material used in LCDs is a mixture composed of various single LC materials which contribute to the requirements of the LCD. The composition of the mixture is determined by the specification of the device such as the response time, the large transmittance, low viscosity, low driving voltage, *etc.* As a first step to a practical use of bent-core mesogens in LCDs, studies of mixtures of the bent-core mesogens are necessary. It is clear that a single bent-core mesogen cannot be used in the device for general user environments. For this reason, the study with an isomer of PAL1 seems to be quite interesting. PAL7 which has the same mesogenic group and terminal chains, only difference is the position of the cyanyl group in the central aromatic ring, shows different phase behavior with temperature. The various positions of the cyanyl group in PAL7 provide a different polar effect with the molecular interaction, leading to the creation of properties different from those observed in PAL1.

Moreover, the mixture composed of PAL1 and PAL7 is likely to have various effects due to correlations between the combinations of PAL1 and PAL7 molecules. It seems interesting to study the mixtures of C4, C5, C6, C7, C9 which show different correlations between the molecules. Useful physical parameters can be tuned to the requirement by altering the composition of the mixture.

Appendix.

Appendix A

A.1 Tilt angle of molecules in the cluster

For biaxial nematic phase, IR absorbance components along the laboratory system are given as follows [33, 71]:

$$A_{XX}/A_0 = 1 + (S - P)(\frac{3}{2}\sin^2\beta' - 1) + \frac{1}{2}(D - C)(\sin^2\beta'\cos 2\gamma') \quad \text{(A.1)}$$

$$A_{YY}/A_0 = 1 + (S + P)(\frac{3}{2}\sin^2\beta' - 1) + \frac{1}{2}(D + C)(\sin^2\beta'\cos 2\gamma') \quad \text{(A.2)}$$

$$A_{ZZ}/A_0 = 1 + S(2 - 3\sin^2\beta') - D\sin^2\beta'\cos 2\gamma' \quad \text{(A.3)}$$

In order to apply the above model to the system with clusters, the orientational order parameter of the clusters should be considered. According to the extended M-S theory (see Chap.4), the cybotactic cluster in the nematic phase can be considered as a single molecule in the M-S formulation. Conceptually, two kinds of primary order parameters, S' and S'' are introduced in a uniaxial cybotactic nematic phase. The latter is the degree of ordering of the clusters in the macroscopic sample, and the former is the degree of the molecular ordering within the cluster. The macroscopic order parameter is given by $S = S'S''$. C9 shows optically uniaxial nematic phase even though the cluster is of biaxial smectic C type. For simplicity, the biaxial cluster can be treated as a biaxial molecule for the purpose of calculating its contribution to the IR abosrbance. All order parameters of the molecules in the cluster are assumed to be equal to unity as used in Eqns. (5.14) and (5.15) [25]. Therefore, the order parameters in Eqns. (A.1) and (A.2) can

simply be replaced by the order parameters of the clusters with a tilt angle of θ' with respect to layer normal. It should be mentioned that $S(= S'S'')$ against temperature obtained through the measurement of Δn in the planar cell can be used for the calculation of the averaged angle of transition dipole moment with respect to the laboratory Z axis. For the cyanyl stretching band of C9 shown in Fig. 6.7, the biaxial order parameter due to the cluster and the tilt of molecular long axis within the cluster have not been considered. Although a polymer layer is used to obtain a homeotropic configuration, at a microscopic level, the molecules in the cluster are tilted to the layer normal and the layer normal has the orientational order defined as S'' which is confined by the homeotropic surface anchoring. For C9, A_{XX}/A_0 is equal to A_{YY}/A_0. Therefore the order parameters due to the biaxial phase is neglected. The assumptions used in the calculation are based on the the cluster model introduced in Chap. 4. After all, the aborbance of the transition dipole moment tilted to the layer normal can be given by a simple expression of Eqn. (6.8). Here we have only one situation to consider in the calculation of the tilt angle of molecules with respect to layer normal. So far all the molecules in the cluster are perfectly ordered($S = 1$). For this reason, it is needed to consider two types of tilt configurations of molecules in the cluster. Fig. A.1 shows a schematic of a bent core molecule (a) and two types of tilt in the cluster: (b) the molecular flat plane including the cyanyl stretching vibration is orthogonal to the tilt plane and (c) the molecular flat plane is parallel to the tilt plane. Normally, bent core LCs prefer (b) to (c) [4, 5]. According to the cluster model, the minor director of the cluster is equally probable around its major director unless an external stimulus is not present (see Fig. 4.2). Therefore D can be assumed to be zero in Eqn. (A.3). By a application of the Euler rotation matrix (see Fig. 1.4), Eqn. (A.3) can be expressed in terms of S, β' and θ' as below:

$$A_\perp/A_0 = 1 - \frac{1}{2}S(3\cos^2\beta'\cos^2\theta' - 1) \tag{A.4}$$

$$\cos\theta' = \frac{\cos\beta''}{\cos\beta'} \tag{A.5}$$

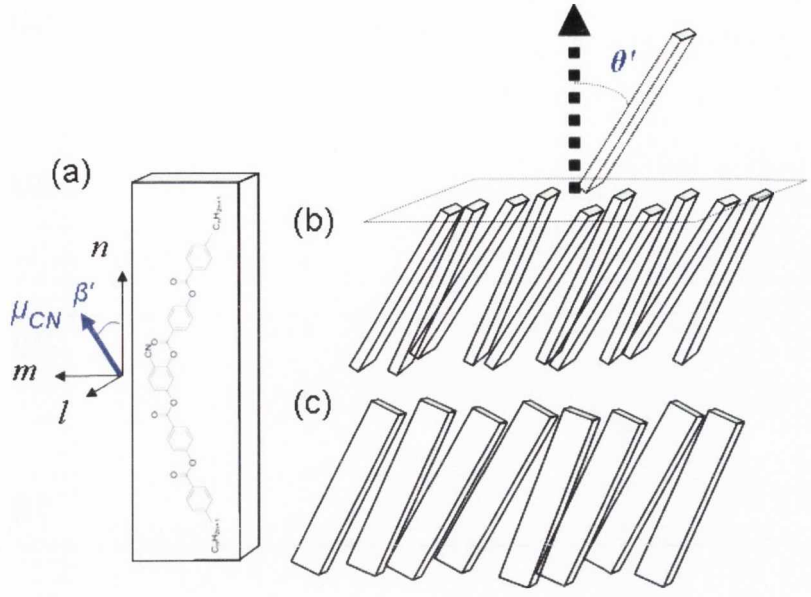

Figure A.1: Schematics for the orderings and tilt of molecular short axis. (a) shows the schematic of a biaxial molecule, the cyanyl stretching is in the plane containing the molecular short axis.

where β'', β' are the angles that the transition dipole moment makes with the cluster normal and molecular long axis respectively . θ' is the tilt angle of the molecule within the cluster. If the β' and its temperature dependence for the cyanyl stretching of C4 are consistent with that of C9, the temperature dependence of θ' for C9 can be obtained through Eqns. (A.4) and (A.5) β' in Fig. 6.7 is expressed in terms of the tilt angle (θ') of molecular long axis with respect to the layer normal of clusters. Fig. A.2 shows the tilt angle, θ' for C9 with respective to the layer normal of the cluster. $\Delta\chi$, the splitting angle between the maxima of small angle X-ray scattering is taken from Ref. [18]. The difference between two results increases with reduced temperature and the value turn over in the *CybC* phase. Here, it is needed to recall that for C9, the tilt angle of molecules in the cluster is not proportional to $\Delta\chi/2$, as mentioned in Chap. 3.3. According to the results and interpretations of X-ray experiment, $\Delta\chi$, splitting of the small angle scattering of C9 is affected by the form factor as well as the structural factor. Above all the results from IR absorbance for C9 provides information about the type of the clusters in the nematic phase. The results from X-ray and IR experiments are broadly in agreement with each other as shown in Fig. A.2.

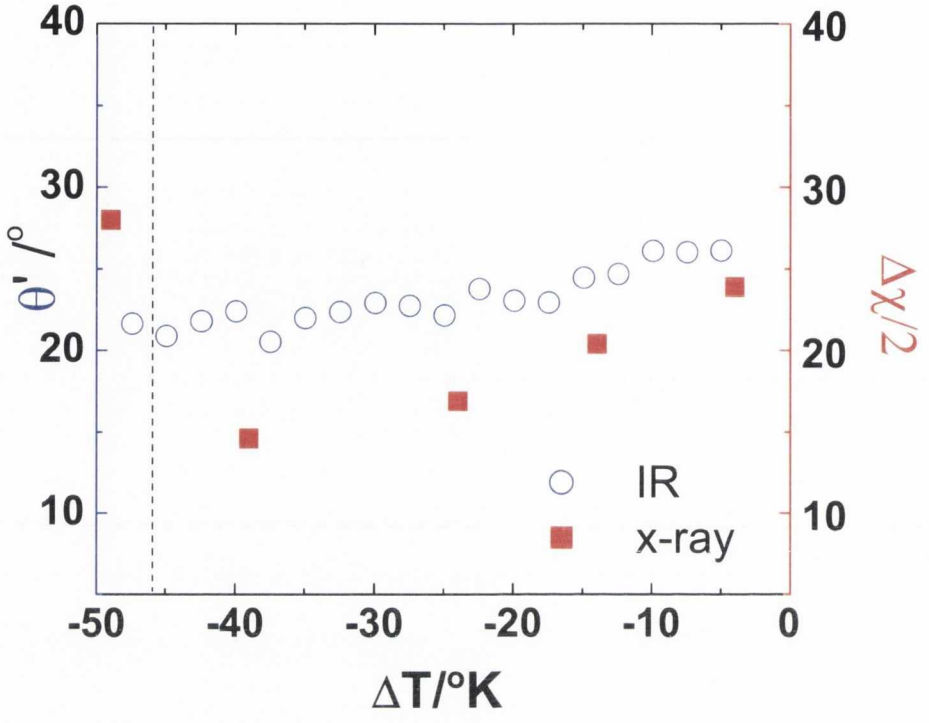

Figure A.2: A comparison of the tilt angle (θ') with respect to the layer normal of the cluster and the splitting of small angle scattering dependent on temperature. Blue circle denotes θ' for C9 obtained by Eqn. (A.4) and (A.5) in which β' is assumed to be the same as for C4. Red square mean half of the splitting angle ($\Delta\chi$) of the small angle X-ray scatter. Vertical dash line means transition to *CybC* phase.

A.2 Fitting parameters

The default value of ϵ_∞ does not affect the relaxation frequency and the dielectric strength.

Table A.1: Fitting parameters of f_{00} for C4.

Temp. [°C]	T*/T	σ [S/cm]	Exp.	τ_{Max}	$\delta\epsilon$	τ	$1/(2\pi\tau)$	ϵ_{Inf}	γ	λ	AC Volt
115	0.98712	1.618E-8	0.8872	5.25E-7	5.176	5.41E-7	294186	1	1	0.96	0.1
114	0.98967	1.531E-8	0.8935	5.572E-7	5.173	5.741E-7	277225	1	1	0.96	0.1
113	0.99223	1.452E-8	0.8987	5.895E-7	5.186	6.074E-7	262026	1	1	0.96	0.1
112	0.99481	1.379E-8	0.9016	6.227E-7	5.169	6.416E-7	248059	1	1	0.96	0.1
111	0.9974	1.315E-8	0.9035	6.646E-7	4.976	6.848E-7	232410	1	1	0.96	0.1
110	1	1.249E-8	0.905	8.702E-7	3.848	8.967E-7	177489	1	1	0.96	0.1
109	1.00262	1.147E-8	0.9093	1.359E-6	3.919	1.4E-6	113682	1	1	0.96	0.1
108	1.00525	1.079E-8	0.9128	1.571E-6	3.638	1.619E-6	98304	1	1	0.96	0.1
107	1.00789	1.014E-8	0.9167	1.77E-6	3.461	1.824E-6	87255	1	1	0.96	0.1
106	1.01055	9.538E-9	0.9202	2.015E-6	3.273	2.076E-6	76664	1	1	0.96	0.1
105	1.01322	8.981E-9	0.9234	2.275E-6	3.173	2.385E-6	66731	1	1	0.94	0.1
104	1.01591	8.424E-9	0.9268	2.532E-6	3.162	2.711E-6	58707	1	1	0.92	0.1
103	1.01861	7.937E-9	0.9296	2.831E-6	3.114	3.031E-6	52509	1	1	0.92	0.1
102	1.02132	7.463E-9	0.9323	3.159E-6	3.096	3.382E-6	47059	1	1	0.92	0.1
101	1.02405	7.005E-9	0.9351	3.537E-6	3.088	3.787E-6	42026	1	1	0.92	0.1
100	1.0268	6.592E-9	0.9376	3.909E-6	3.105	4.186E-6	38020	1	1	0.92	0.1
99	1.02956	6.19E-9	0.9398	4.336E-6	3.123	4.643E-6	34278	1	1	0.92	0.1
98	1.03233	5.821E-9	0.9417	4.796E-6	3.134	5.135E-6	30994	1	1	0.92	0.1
97	1.03512	5.469E-9	0.9436	5.296E-6	3.162	5.671E-6	28064	1	1	0.92	0.1
96	1.03792	5.127E-9	0.9456	5.854E-6	3.191	6.268E-6	25391	1	1	0.92	0.1
95	1.04074	4.811E-9	0.947	6.456E-6	3.226	6.913E-6	23022	1	1	0.92	0.1
94	1.04358	4.508E-9	0.9485	7.134E-6	3.26	7.639E-6	20834	1	1	0.92	0.1
93	1.04643	4.226E-9	0.9497	7.831E-6	3.307	8.387E-6	18976	1	1	0.92	0.1
92	1.04929	3.954E-9	0.9513	8.604E-6	3.357	9.223E-6	17256	1	0.99	0.92	0.1
91	1.05218	3.667E-9	0.955	9.496E-6	3.461	1.019E-5	15618	1	0.98	0.92	0.1
90	1.05507	3.422E-9	0.9572	1.041E-5	3.539	1.118E-5	14235	1	0.97	0.92	0.1
89	1.05799	3.175E-9	0.9597	1.154E-5	3.61	1.24E-5	12835	1	0.97	0.92	0.1
88	1.06092	2.953E-9	0.9616	1.276E-5	3.662	1.373E-5	11591	1	0.96	0.92	0.1
87	1.06386	2.733E-9	0.9647	1.417E-5	3.742	1.526E-5	10429	1	0.95	0.92	0.1
86	1.06682	2.535E-9	0.9669	1.572E-5	3.806	1.694E-5	9395	1	0.94	0.92	0.1
85	1.0698	2.353E-9	0.9683	1.749E-5	3.85	1.885E-5	8443	1	0.94	0.92	0.1
84	1.0728	2.189E-9	0.9693	1.937E-5	3.89	2.089E-5	7618	1	0.94	0.92	0.1
83	1.07581	2.026E-9	0.971	2.16E-5	3.938	2.33E-5	6830	1	0.93	0.92	0.1
82	1.07884	1.879E-9	0.9715	2.404E-5	3.978	2.594E-5	6135	1	0.93	0.92	0.1
81	1.08189	1.735E-9	0.9735	2.675E-5	4.031	2.888E-5	5510	1	0.93	0.92	0.1
80	1.08495	1.609E-9	0.9736	2.968E-5	4.068	3.205E-5	4965	1	0.93	0.92	0.1
79	1.08803	1.491E-9	0.9727	3.298E-5	4.102	3.562E-5	4468	1	0.92	0.92	0.1
78	1.09113	1.382E-9	0.9715	3.655E-5	4.138	3.948E-5	4031	1	0.92	0.92	0.1
77	1.09425	1.28E-9	0.9707	4.063E-5	4.173	4.391E-5	3624	1	0.92	0.92	0.1
76	1.09738	1.175E-9	0.9721	4.549E-5	4.244	4.92E-5	3234	1	0.91	0.92	0.1
75	1.10053	1.064E-9	0.9781	5.158E-5	4.365	5.588E-5	2848	1	0.9	0.92	0.1
74	1.1037	9.913E-10	0.9732	5.704E-5	4.364	6.179E-5	2575	1	0.9	0.92	0.1
73	1.10689	9.219E-10	0.9675	6.345E-5	4.357	6.874E-5	2315	1	0.9	0.92	0.1
72	1.1101	8.629E-10	0.9596	7.007E-5	4.338	7.591E-5	2096	1	0.9	0.92	0.1
71	1.11332	8.111E-10	0.9485	7.736E-5	4.294	8.381E-5	1898	1	0.9	0.92	0.1
70	1.11657	7.687E-10	0.9332	8.525E-5	4.229	9.235E-5	1723	1	0.9	0.92	0.1

Table A.2: Fitting parameters of f_{11} for C4.

Temp. [°C]	T*/T	σ [S/cm]	Exp.	τ_{Max}	$\delta\epsilon$	τ	$1/(2\pi\tau)$	ϵ_{Inf}	γ	λ	AC Volt
115	0.98712	9.588E-9	0.9239	7.105E-8	4.238	7.105E-8	2.24004E6	1	0.98	1	0.1
114	0.98967	9.043E-9	0.936	7.732E-8	4.135	7.732E-8	2.05839E6	1	0.98	1	0.1
113	0.99223	8.577E-9	0.9376	8.378E-8	4.102	8.378E-8	1.89968E6	1	0.99	1	0.1
112	0.99481	8.136E-9	0.9402	9.026E-8	4.129	9.026E-8	1.76329E6	1	0.99	1	0.1
111	0.9974	7.674E-9	0.9462	9.879E-8	4.07	9.879E-8	1.61104E6	1	0.99	1	0.1
110	1	7.234E-9	0.9492	1.043E-7	4.169	1.043E-7	1.52593E6	1	0.98	1	0.1
109	1.00262	6.871E-9	0.9516	1.068E-7	4.572	1.068E-7	1.49021E6	1	0.96	1	0.1
108	1.00525	6.516E-9	0.954	1.059E-7	4.972	1.059E-7	1.50288E6	1	0.95	1	0.1
107	1.00789	6.11E-9	0.9582	1.067E-7	5.134	1.067E-7	1.49161E6	1	0.95	1	0.1
106	1.01055	5.74E-9	0.9615	1.074E-7	5.247	1.074E-7	1.48189E6	1	0.945	1	0.1
105	1.01322	5.398E-9	0.964	1.124E-7	5.242	1.124E-7	1.41597E6	1	0.945	1	0.1
104	1.01591	5.091E-9	0.9653	1.155E-7	5.296	1.155E-7	1.37796E6	1	0.945	1	0.1
103	1.01861	4.785E-9	0.9678	1.195E-7	5.261	1.195E-7	1.33184E6	1	0.945	1	0.1
102	1.02132	4.5E-9	0.9699	1.214E-7	5.462	1.214E-7	1.311E6	1	0.935	1	0.1
101	1.02405	4.235E-9	0.9712	1.271E-7	5.431	1.271E-7	1.2522E6	1	0.935	1	0.1
100	1.0268	3.983E-9	0.9728	1.333E-7	5.379	1.333E-7	1.19396E6	1	0.93	1	0.1
99	1.02956	3.742E-9	0.9741	1.33E-7	5.408	1.33E-7	1.19665E6	1	0.93	1	0.1
98	1.03233	3.514E-9	0.9752	1.405E-7	5.289	1.405E-7	1.13278E6	1	0.93	1	0.1
97	1.03512	3.305E-9	0.9763	1.455E-7	5.263	1.455E-7	1.09385E6	1	0.92	1	0.1
96	1.03792	3.094E-9	0.9782	1.53E-7	5.102	1.53E-7	1.04023E6	1	0.92	1	0.1
95	1.04074	2.907E-9	0.9783	1.607E-7	5.031	1.607E-7	990385.45795	1	0.92	1	0.1
94	1.04358	2.728E-9	0.9786	1.692E-7	4.973	1.692E-7	940632.05137	1	0.92	1	0.1
93	1.04643	2.555E-9	0.9796	1.754E-7	4.919	1.754E-7	907382.79984	1	0.92	1	0.1
92	1.04929	2.392E-9	0.9805	1.902E-7	4.699	1.902E-7	836776.77756	1	0.91	1	0.1
91	1.05218	2.237E-9	0.9809	2.01E-7	4.649	2.01E-7	791815.63727	1	0.91	1	0.1
90	1.05507	2.096E-9	0.9811	2.139E-7	4.563	2.139E-7	744062.38005	1	0.91	1	0.1
89	1.05799	1.955E-9	0.9815	2.319E-7	4.436	2.319E-7	686308.50837	1	0.91	1	0.1
88	1.06092	1.812E-9	0.9847	2.457E-7	4.34	2.457E-7	647761.26615	1	0.90	1	0.1
87	1.06386	1.689E-9	0.985	2.65E-7	4.226	2.65E-7	600584.69091	1	0.90	1	0.1
86	1.06682	1.581E-9	0.983	2.885E-7	4.092	2.885E-7	551663.58091	1	0.9	1	0.1
85	1.0698	1.473E-9	0.9827	3.115E-7	4.037	3.115E-7	510930.79644	1	0.9	1	0.1
84	1.0728	1.371E-9	0.9827	3.368E-7	3.94	3.368E-7	472550.30609	1	0.9	1	0.1
83	1.07581	1.26E-9	0.9869	3.644E-7	3.852	3.644E-7	436758.89981	1	0.9	1	0.1
82	1.07884	1.172E-9	0.9862	3.895E-7	3.805	3.895E-7	408613.46108	1	0.9	1	0.1
81	1.08189	1.084E-9	0.9865	4.219E-7	3.774	4.219E-7	377233.80681	1	0.9	1	0.1
80	1.08495	1.005E-9	0.9862	4.515E-7	3.739	4.515E-7	352502.64251	1	0.9	1	0.1
79	1.08803	9.311E-10	0.9854	4.873E-7	3.702	4.873E-7	326605.67021	1	0.9	1	0.1
78	1.09113	8.604E-10	0.985	5.259E-7	3.681	5.259E-7	302633.47232	1	0.9	1	0.1
77	1.09425	7.95E-10	0.9839	5.667E-7	3.665	5.667E-7	280845.14398	1	0.9	1	0.1
76	1.09738	7.342E-10	0.9828	6.119E-7	3.633	6.119E-7	260099.59649	1	0.9	1	0.1
75	1.10053	6.763E-10	0.9821	6.663E-7	3.619	6.663E-7	238863.78972	1	0.9	1	0.1
74	1.1037	6.239E-10	0.98	7.194E-7	3.607	7.194E-7	221232.89282	1	0.9	1	0.1
73	1.10689	5.734E-10	0.9787	7.787E-7	3.603	7.787E-7	204385.44124	1	0.9	1	0.1
72	1.1101	5.269E-10	0.978	8.455E-7	3.597	8.455E-7	188237.66185	1	0.9	1	0.1
71	1.11332	4.853E-10	0.9733	9.172E-7	3.583	9.172E-7	173522.61567	1	0.9	1	0.1
70	1.11657	4.469E-10	0.968	1.011E-6	3.595	1.011E-6	157423.28694	1	0.9	1	0.1

Table A.3: Fitting parameters of f_{00} for C5.

Temp. [°C]	T*/T	σ [S/cm]	Exp.	τ_{Max}	$\delta\epsilon$	τ	$1/(2\pi\tau)$	ϵ_{Inf}	γ	λ	AC Volt
115	0.98197	3.431E-9	0.9343	3.918E-7	1.778	3.918E-7	406214	1	1	1	0.1
114	0.9845	3.287E-9	0.972	4.246E-7	1.788	4.342E-7	366547	1	1	0.97	0.1
113	0.98705	3.201E-9	0.9735	4.619E-7	1.797	4.723E-7	336978	1	1	0.97	0.1
112	0.98961	3.117E-9	0.9733	5.072E-7	1.795	5.186E-7	306893	1	1	0.97	0.1
111	0.99219	3.026E-9	0.9736	5.637E-7	1.795	5.764E-7	276118	1	1	0.97	0.1
110	0.99478	2.936E-9	0.9724	6.339E-7	1.795	6.482E-7	245533	1	1	0.97	0.1
109	0.99738	2.824E-9	0.9747	6.65E-7	1.779	6.65E-7	239330	1	0.98	1	0.1
108	1	2.738E-9	0.9716	7.658E-7	1.769	7.658E-7	207828	1	0.97	1	0.1
107	1.00263	2.652E-9	0.9655	1.092E-6	1.769	1.19E-6	133743	1	0.97	0.9	0.1
106	1.00527	2.504E-9	0.969	1.597E-6	2.744	1.735E-6	91731	1	1	0.9	0.1
105	1.00793	2.341E-9	0.9742	1.806E-6	3.22	1.966E-6	80953	1	0.98	0.9	0.1
104	1.01061	2.224E-9	0.9748	2.03E-6	3.343	2.21E-6	72015	1	0.98	0.9	0.1
103	1.01329	2.116E-9	0.9751	2.269E-6	3.425	2.47E-6	64435	1	0.98	0.9	0.1
102	1.01599	2.007E-9	0.9761	2.523E-6	3.514	2.748E-6	57916	1	0.98	0.9	0.1
101	1.01871	1.895E-9	0.9778	2.804E-6	3.61	3.056E-6	52079	1	0.98	0.9	0.1
100	1.02144	1.792E-9	0.9791	3.102E-6	3.699	3.382E-6	47059	1	0.97	0.9	0.1
99	1.02418	1.689E-9	0.9811	3.425E-6	3.791	3.738E-6	42577	1	0.97	0.9	0.1
98	1.02694	1.596E-9	0.9817	3.782E-6	3.872	4.128E-6	38554	1	0.96	0.9	0.1
97	1.02972	1.505E-9	0.9828	4.167E-6	3.96	4.553E-6	34956	1	0.96	0.9	0.1
96	1.03251	1.414E-9	0.9852	4.606E-6	4.036	5.034E-6	31615	1	0.95	0.9	0.1
95	1.03531	1.32E-9	0.9893	5.065E-6	4.145	5.545E-6	28702	1	0.94	0.9	0.1
94	1.03813	1.242E-9	0.9903	5.617E-6	4.206	6.149E-6	25883	1	0.94	0.9	0.1
93	1.04097	1.167E-9	0.991	6.206E-6	4.267	6.796E-6	23418	1	0.94	0.9	0.1
92	1.04382	1.094E-9	0.9929	6.864E-6	4.332	7.52E-6	21164	1	0.94	0.9	0.1
91	1.04668	1.019E-9	0.9963	7.606E-6	4.416	8.341E-6	19081	1	0.93	0.9	0.1
90	1.04957	9.58E-10	0.9965	8.387E-6	4.467	9.198E-6	17303	1	0.93	0.9	0.1
89	1.05246	8.931E-10	0.9988	9.315E-6	4.529	1.022E-5	15572	1	0.93	0.9	0.1
88	1.05538	8.341E-10	1	1.027E-5	4.616	1.127E-5	14122	1	0.9229	0.9	0.1
87	1.05831	7.796E-10	1	1.138E-5	4.662	1.249E-5	12742	1	0.9229	0.9	0.1
86	1.06126	7.285E-10	1	1.262E-5	4.712	1.386E-5	11483	1	0.9203	0.9	0.1
85	1.06422	6.775E-10	1	1.401E-5	4.755	1.539E-5	10341	1	0.9203	0.9	0.1
84	1.0672	6.333E-10	1	1.556E-5	4.793	1.71E-5	9307	1	0.9172	0.9	0.1
83	1.0702	5.89E-10	1	1.731E-5	4.836	1.903E-5	8363	1	0.9138	0.9	0.1
82	1.07321	5.461E-10	1	1.938E-5	4.862	2.131E-5	7468	1	0.9136	0.9	0.1
81	1.07624	5.082E-10	1	2.151E-5	4.916	2.367E-5	6723	1	0.9085	0.9	0.1
80	1.07929	4.709E-10	1	2.401E-5	4.962	2.643E-5	6021	1	0.9049	0.9	0.1
79	1.08235	4.357E-10	1	2.679E-5	5.016	2.951E-5	5393	1	0.9019	0.9	0.1
78	1.08543	4.021E-10	1	2.999E-5	5.04	3.304E-5	4817	1	0.9	0.9	0.1
77	1.08853	3.69E-10	1	3.386E-5	5.063	3.73E-5	4266	1	0.9	0.9	0.1
76	1.09165	3.422E-10	1	3.781E-5	5.092	4.165E-5	3821	1	0.9	0.9	0.1
75	1.09479	3.158E-10	1	4.229E-5	5.102	4.659E-5	3416	1	0.9	0.9	0.1
74	1.09794	2.906E-10	1	4.633E-5	5.124	5.104E-5	3118	1	0.9	0.9	0.1
73	1.10111	2.686E-10	1	5.234E-5	5.137	5.766E-5	2760	1	0.9	0.9	0.1
72	1.1043	2.466E-10	1	5.853E-5	5.161	6.448E-5	2468	1	0.9	0.9	0.1
71	1.10751	2.279E-10	1	6.55E-5	5.161	7.216E-5	2205	1	0.9	0.9	0.1
70	1.11074	2.11E-10	0.9888	7.339E-5	5.155	8.085E-5	1968	1	0.9	0.9	0.1

Table A.4: Fitting parameters of f_{11} for C5.

Temp. [°C]	T*/T	σ [S/cm]	Exp.	τ_{Max}	$\delta\epsilon$	τ	$1/(2\pi\tau)$	ϵ_{Inf}	γ	λ	AC Volt
115	0.98	1.79E-09	0.99	6.29E-08	2.17	6.90E-08	2.31E+06	1	0.92	0.9	0.1
114	0.98	1.77E-09	0.99	6.48E-08	2.28	7.13E-08	2.23E+06	1	0.91	0.9	0.1
113	0.99	1.73E-09	0.99	7.17E-08	2.20	7.89E-08	2.02E+06	1	0.91	0.9	0.1
112	0.99	1.69E-09	0.99	7.55E-08	2.26	8.31E-08	1.91E+06	1	0.9	0.9	0.1
111	0.99	1.64E-09	0.99	7.74E-08	2.31	8.52E-08	1.87E+06	1	0.9	0.9	0.1
110	0.99	1.59E-09	0.99	8.52E-08	2.30	9.39E-08	1.70E+06	1	0.9	0.9	0.1
109	1.00	1.54E-09	0.99	9.18E-08	2.30	1.01E-07	1.57E+06	1	0.9	0.9	0.1
108	1.00	1.48E-09	0.98	1.02E-07	2.33	1.12E-07	1.42E+06	1	0.9	0.9	0.1
107	1.00	1.41E-09	0.98	9.38E-08	2.53	1.03E-07	1.54E+06	1	0.9	0.9	0.1
106	1.01	1.34E-09	0.98	9.31E-08	2.61	1.03E-07	1.55E+06	1	0.9	0.9	0.1
105	1.01	1.28E-09	0.98	9.47E-08	2.65	1.04E-07	1.53E+06	1	0.9	0.9	0.1
104	1.01	1.22E-09	0.99	9.69E-08	2.71	1.07E-07	1.49E+06	1	0.9	0.9	0.1
103	1.01	1.16E-09	0.99	9.77E-08	2.74	1.08E-07	1.48E+06	1	0.9	0.9	0.1
102	1.02	1.10E-09	0.99	9.87E-08	2.77	1.09E-07	1.46E+06	1	0.9	0.9	0.1
101	1.02	1.05E-09	0.99	1.01E-07	2.77	1.11E-07	1.43E+06	1	0.9	0.9	0.1
100	1.02	9.96E-10	0.99	1.05E-07	2.79	1.16E-07	1.37E+06	1	0.9	0.9	0.1
99	1.02	9.46E-10	0.99	1.10E-07	2.81	1.21E-07	1.31E+06	1	0.9	0.9	0.1
98	1.03	8.97E-10	0.99	1.15E-07	2.83	1.27E-07	1.26E+06	1	0.9	0.9	0.1
97	1.03	8.49E-10	0.99	1.21E-07	2.84	1.33E-07	1.20E+06	1	0.9	0.9	0.1
96	1.03	8.04E-10	0.99	1.26E-07	2.85	1.39E-07	1.14E+06	1	0.9	0.9	0.1
95	1.04	7.59E-10	0.98	1.32E-07	2.87	1.46E-07	1.09E+06	1	0.9	0.9	0.1
94	1.04	7.15E-10	0.99	1.40E-07	2.88	1.54E-07	1.04E+06	1	0.9	0.9	0.1
93	1.04	6.74E-10	0.99	1.47E-07	2.90	1.62E-07	9.84E+05	1	0.9	0.9	0.1
92	1.04	6.34E-10	0.99	1.55E-07	2.91	1.70E-07	9.35E+05	1	0.9	0.9	0.1
91	1.05	5.98E-10	0.98	1.63E-07	2.92	1.80E-07	8.87E+05	1	0.9	0.9	0.1
90	1.05	5.64E-10	0.98	1.72E-07	2.93	1.90E-07	8.38E+05	1	0.9	0.9	0.1
89	1.05	5.30E-10	0.98	1.82E-07	2.94	2.01E-07	7.93E+05	1	0.9	0.9	0.1
88	1.06	4.97E-10	0.98	1.94E-07	2.95	2.13E-07	7.46E+05	1	0.9	0.9	0.1
87	1.06	4.66E-10	0.98	2.05E-07	2.96	2.26E-07	7.05E+05	1	0.9	0.9	0.1
86	1.06	4.36E-10	0.98	2.18E-07	2.97	2.40E-07	6.62E+05	1	0.9	0.9	0.1
85	1.06	4.08E-10	0.98	2.32E-07	2.98	2.56E-07	6.22E+05	1	0.9	0.9	0.1
84	1.07	3.81E-10	0.98	2.47E-07	2.99	2.73E-07	5.84E+05	1	0.9	0.9	0.1
83	1.07	3.55E-10	0.98	2.64E-07	3.00	2.90E-07	5.48E+05	1	0.9	0.9	0.1
82	1.07	3.31E-10	0.98	2.82E-07	3.01	3.10E-07	5.13E+05	1	0.9	0.9	0.1
81	1.08	3.07E-10	0.98	3.01E-07	3.02	3.32E-07	4.80E+05	1	0.9	0.9	0.1
80	1.08	2.85E-10	0.98	3.23E-07	3.04	3.55E-07	4.48E+05	1	0.9	0.9	0.1
79	1.08	2.64E-10	0.98	3.46E-07	3.05	3.81E-07	4.17E+05	1	0.9	0.9	0.1
78	1.09	2.44E-10	0.97	3.72E-07	3.06	4.10E-07	3.89E+05	1	0.9	0.9	0.1
77	1.09	2.26E-10	0.97	4.00E-07	3.08	4.41E-07	3.61E+05	1	0.9	0.9	0.1
76	1.09	2.06E-10	0.98	4.25E-07	3.08	4.68E-07	3.40E+05	1	0.9	0.9	0.1
75	1.09	1.90E-10	0.98	4.60E-07	3.10	5.06E-07	3.14E+05	1	0.9	0.9	0.1
74	1.10	1.75E-10	0.98	4.97E-07	3.12	5.48E-07	2.90E+05	1	0.9	0.9	0.1
73	1.10	1.60E-10	0.97	5.40E-07	3.14	5.95E-07	2.68E+05	1	0.9	0.9	0.1
72	1.10	1.48E-10	0.97	5.81E-07	3.15	6.40E-07	2.49E+05	1	0.9	0.9	0.1
71	1.11	1.35E-10	0.96	6.28E-07	3.17	6.92E-07	2.30E+05	1	0.9	0.9	0.1
70	1.11	1.23E-10	0.96	6.82E-07	3.19	7.51E-07	2.12E+05	1	0.9	0.9	0.1

Table A.5: Fitting parameters of f_{00} for C7.

Temp. [°C]	T*/T	σ [S/cm]	Exp.	τ_{Max}	$\delta\epsilon$	τ	$1/(2\pi\tau)$	ϵ_{Inf}	γ	λ	AC Volt
115	0.99	6.62E-10	0.97	3.01E-07	0.54	3.29E-07	4.83E+05	1	0.95	0.9	0.1
114	0.99	6.38E-10	0.97	3.33E-07	0.53	3.64E-07	4.37E+05	1	0.95	0.9	0.1
113	0.99	6.16E-10	0.97	3.84E-07	0.52	4.21E-07	3.78E+05	1	0.95	0.9	0.1
112	0.99	5.93E-10	0.98	4.45E-07	0.49	4.87E-07	3.27E+05	1	0.94	0.9	0.1
111	1.00	5.71E-10	0.98	5.57E-07	0.44	5.57E-07	2.86E+05	1	0.93	1	0.1
110	1.00	5.51E-10	0.98	8.36E-07	0.65	8.36E-07	1.90E+05	1	0.93	1	0.1
109	1.00	5.31E-10	0.98	9.95E-07	0.82	9.95E-07	1.60E+05	1	0.93	1	0.1
108	1.01	5.11E-10	0.98	1.13E-06	0.94	1.13E-06	1.40E+05	1	0.93	1	0.1
107	1.01	4.92E-10	0.98	1.29E-06	1.00	1.29E-06	1.23E+05	1	0.94	1	0.1
106	1.01	4.71E-10	0.98	1.45E-06	1.03	1.45E-06	1.10E+05	1	0.94	1	0.1
105	1.01	4.49E-10	0.98	1.62E-06	1.05	1.62E-06	9.83E+04	1	0.94	1	0.1
104	1.02	4.28E-10	0.98	1.80E-06	1.06	1.80E-06	8.83E+04	1	0.94	1	0.1
103	1.02	4.08E-10	0.98	1.99E-06	1.08	1.99E-06	8.00E+04	1	0.94	1	0.1
102	1.02	3.88E-10	0.98	2.20E-06	1.09	2.20E-06	7.24E+04	1	0.94	1	0.1
101	1.02	3.69E-10	0.98	2.41E-06	1.11	2.41E-06	6.60E+04	1	0.94	1	0.1
100	1.03	3.50E-10	0.98	2.63E-06	1.13	2.63E-06	6.04E+04	1	0.93	1	0.1
99	1.03	3.32E-10	0.98	2.87E-06	1.15	2.87E-06	5.55E+04	1	0.93	1	0.1
98	1.03	3.14E-10	0.98	3.14E-06	1.17	3.14E-06	5.08E+04	1	0.92	1	0.1
97	1.04	2.98E-10	0.99	3.40E-06	1.19	3.40E-06	4.69E+04	1	0.92	1	0.1
96	1.04	2.81E-10	0.99	3.72E-06	1.21	3.72E-06	4.28E+04	1	0.91	1	0.1
95	1.04	2.66E-10	0.99	4.07E-06	1.22	4.07E-06	3.91E+04	1	0.91	1	0.1
94	1.04	2.51E-10	0.99	4.41E-06	1.25	4.41E-06	3.61E+04	1	0.9	1	0.1
93	1.05	2.37E-10	0.99	4.84E-06	1.25	4.84E-06	3.29E+04	1	0.9	1	0.1
92	1.05	2.23E-10	0.99	5.31E-06	1.26	5.31E-06	3.00E+04	1	0.9	1	0.1
91	1.05	2.10E-10	0.99	5.83E-06	1.27	5.83E-06	2.73E+04	1	0.9	1	0.1
90	1.06	1.98E-10	0.99	6.37E-06	1.28	6.37E-06	2.50E+04	1	0.9	1	0.1
89	1.06	1.86E-10	1.00	7.11E-06	1.28	7.11E-06	2.24E+04	1	0.88	1	0.1
88	1.06	1.74E-10	1.00	7.82E-06	1.29	7.82E-06	2.04E+04	1	0.88	1	0.1
87	1.06	1.63E-10	1.00	8.57E-06	1.31	8.57E-06	1.86E+04	1	0.88	1	0.1
86	1.07	1.53E-10	1.00	9.41E-06	1.32	9.41E-06	1.69E+04	1	0.87	1	0.1
85	1.07	1.43E-10	1.00	1.03E-05	1.32	1.03E-05	1.54E+04	1	0.87	1	0.1
84	1.07	1.34E-10	1.00	1.14E-05	1.33	1.14E-05	1.40E+04	1	0.87	1	0.1
83	1.08	1.25E-10	1.00	1.25E-05	1.34	1.25E-05	1.27E+04	1	0.87	1	0.1
82	1.08	1.16E-10	1.00	1.37E-05	1.35	1.39E-05	1.14E+04	1	0.87	0.99	0.1
81	1.08	1.07E-10	1.00	1.52E-05	1.39	1.54E-05	1.03E+04	1	0.85	0.99	0.1
80	1.08	9.96E-11	1.00	1.67E-05	1.40	1.69E-05	9.41E+03	1	0.84	0.99	0.1
79	1.09	9.26E-11	1.00	1.84E-05	1.42	1.87E-05	8.53E+03	1	0.84	0.99	0.1
78	1.09	8.59E-11	1.00	2.01E-05	1.42	2.04E-05	7.79E+03	1	0.84	0.99	0.1
77	1.09	7.95E-11	1.00	2.24E-05	1.42	2.27E-05	7.00E+03	1	0.83	0.96	0.1
76	1.10	7.34E-11	1.00	2.48E-05	1.44	2.52E-05	6.31E+03	1	0.82	0.99	0.1
75	1.10	6.82E-11	1.00	2.82E-05	1.50	3.44E-05	4.63E+03	1	0.85	0.82	0.1
74	1.10	6.29E-11	1.00	3.16E-05	1.51	3.86E-05	4.13E+03	1	0.85	0.82	0.1
73	1.11	5.78E-11	1.00	3.51E-05	1.51	4.28E-05	3.72E+03	1	0.85	0.82	0.1
72	1.11	5.32E-11	1.00	3.87E-05	1.51	4.72E-05	3.37E+03	1	0.85	0.82	0.1
71	1.11	4.88E-11	1.00	4.30E-05	1.51	5.26E-05	3.03E+03	1	0.85	0.82	0.1
70	1.12	4.46E-11	1.00	4.80E-05	1.53	5.87E-05	2.71E+03	1	0.85	0.82	0.1

Table A.6: Fitting parameters of f_{11} for C7.

Temp. [°C]	T*/T	σ [S/cm]	Exp.	τ_{Max}	$\delta\epsilon$	τ	$1/(2\pi\tau)$	ϵ_{Inf}	γ	λ	AC Volt
115	0.983	2.56E-9	0.946	8.63E-8	1.53	8.71E-8	1.83E6	1.00	1.00	0.988	0.1
114	0.986	2.46E-9	0.948	9.06E-8	1.60	9.15E-8	1.74E6	1.00	1.00	0.988	0.1
113	0.988	2.36E-9	0.949	9.55E-8	1.65	9.64E-8	1.65E6	1.00	1.00	0.988	0.1
112	0.991	2.24E-9	0.951	1.00E-7	1.72	1.01E-7	1.57E6	1.00	1.00	0.988	0.1
111	0.993	2.10E-9	0.954	1.05E-7	1.83	1.06E-7	1.50E6	1.00	0.990	0.988	0.1
110	0.996	1.96E-9	0.957	1.04E-7	1.97	1.05E-7	1.52E6	1.00	0.989	0.988	0.1
109	0.999	1.85E-9	0.960	1.04E-7	2.01	1.05E-7	1.51E6	1.00	0.988	0.988	0.1
108	1.00	1.76E-9	0.962	1.05E-7	2.05	1.06E-7	1.50E6	1.00	0.986	0.988	0.1
107	1.00	1.68E-9	0.963	1.07E-7	2.08	1.08E-7	1.47E6	1.00	0.982	0.988	0.1
106	1.01	1.60E-9	0.965	1.07E-7	2.17	1.08E-7	1.47E6	1.00	0.971	0.988	0.1
105	1.01	1.52E-9	0.968	1.06E-7	1.99	1.06E-7	1.51E6	1.00	0.995	1.00	0.1
104	1.01	1.46E-9	0.969	1.08E-7	2.20	1.12E-7	1.42E6	1.00	0.976	0.957	0.1
103	1.01	1.39E-9	0.970	1.11E-7	2.02	1.11E-7	1.44E6	1.00	0.996	1.00	0.1
102	1.02	1.32E-9	0.971	1.14E-7	2.03	1.14E-7	1.40E6	1.00	0.997	1.00	0.1
101	1.02	1.26E-9	0.972	1.16E-7	2.11	1.16E-7	1.37E6	1.00	0.985	1.00	0.1
100	1.02	1.20E-9	0.973	1.19E-7	2.15	1.19E-7	1.33E6	1.00	0.982	0.993	0.1
99	1.03	1.15E-9	0.973	1.22E-7	2.16	1.22E-7	1.30E6	1.00	0.980	1.00	0.1
98	1.03	1.09E-9	0.974	1.25E-7	2.17	1.25E-7	1.27E6	1.00	0.979	1.00	0.1
97	1.03	1.04E-9	0.975	1.28E-7	2.24	1.28E-7	1.24E6	1.00	0.965	1.00	0.1
96	1.03	9.85E-10	0.976	1.30E-7	2.33	1.35E-7	1.18E6	1.00	0.959	0.955	0.1
95	1.04	9.36E-10	0.977	1.35E-7	2.28	1.35E-7	1.18E6	1.00	0.958	1.00	0.1
94	1.04	8.89E-10	0.978	1.39E-7	2.29	1.39E-7	1.14E6	1.00	0.957	1.00	0.1
93	1.04	8.44E-10	0.979	1.43E-7	2.29	1.43E-7	1.11E6	1.00	0.955	1.00	0.1
92	1.05	8.02E-10	0.979	1.40E-7	2.38	1.40E-7	1.13E6	1.00	0.936	1.00	0.1
91	1.05	7.60E-10	0.978	1.51E-7	2.32	1.51E-7	1.05E6	1.00	0.949	0.998	0.1
90	1.05	7.36E-10	0.967	1.60E-7	2.08	1.73E-7	9.21E5	1.00	0.900	0.918	0.1
89	1.05	6.88E-10	0.970	1.57E-7	1.68	1.73E-7	9.20E5	1.00	0.900	0.900	0.1
88	1.06	6.54E-10	0.964	1.71E-7	2.52	1.71E-7	9.32E5	1.00	0.900	1.00	0.1
87	1.06	6.18E-10	0.965	1.82E-7	2.51	1.95E-7	8.18E5	1.00	0.900	0.928	0.1
86	1.06	5.80E-10	0.975	2.06E-7	2.05	2.27E-7	7.01E5	1.00	0.900	0.900	0.1
85	1.07	5.48E-10	0.974	2.12E-7	2.08	2.29E-7	6.94E5	1.00	0.900	0.918	0.1
84	1.07	5.15E-10	0.977	2.25E-7	2.04	2.34E-7	6.80E5	1.00	0.900	0.957	0.1
83	1.07	4.84E-10	0.978	2.40E-7	2.02	2.60E-7	6.13E5	1.00	0.900	0.918	0.1
82	1.07	4.56E-10	0.979	2.72E-7	1.92	2.72E-7	5.86E5	1.00	0.900	1.00	0.1
81	1.08	4.28E-10	0.980	2.80E-7	2.04	2.97E-7	5.36E5	1.00	0.900	0.938	0.1
80	1.08	4.03E-10	0.980	3.14E-7	1.90	3.14E-7	5.07E5	1.00	0.900	1.00	0.1
79	1.08	3.78E-10	0.981	3.13E-7	2.09	3.45E-7	4.61E5	1.00	0.900	0.900	0.1
78	1.09	3.54E-10	0.981	3.42E-7	2.10	3.75E-7	4.25E5	1.00	0.900	0.906	0.1
77	1.09	3.32E-10	0.981	3.73E-7	2.13	4.11E-7	3.88E5	1.00	0.900	0.900	0.1
76	1.09	3.11E-10	0.981	4.05E-7	2.13	4.46E-7	3.57E5	1.00	0.900	0.900	0.1
75	1.10	2.95E-10	0.951	4.62E-7	2.00	5.09E-7	3.13E5	1.00	0.900	0.900	0.1
74	1.10	2.75E-10	0.950	4.94E-7	2.06	5.45E-7	2.92E5	1.00	0.900	0.900	0.1
73	1.10	2.57E-10	0.948	5.34E-7	2.09	5.89E-7	2.70E5	1.00	0.900	0.900	0.1
72	1.11	2.40E-10	0.947	5.80E-7	2.10	6.39E-7	2.49E5	1.00	0.900	0.900	0.1
71	1.11	2.23E-10	0.947	6.31E-7	2.12	6.95E-7	2.29E5	1.00	0.900	0.900	0.1
70	1.11	2.08E-10	0.945	6.90E-7	2.13	7.60E-7	2.09E5	1.00	0.900	0.900	0.1

Table A.7: Fitting parameters of f_{00} for C9.

Temp. [°C]	T*/T	σ [S/cm]	Exp.	τ_{Max}	$\delta\epsilon$	τ	$1/(2\pi\tau)$	ϵ_{Inf}	γ	λ	AC Volt
115	0.974	3.06E-9	0.988	1.28E-7	2.21	1.41E-7	1.13E6	1.00	0.930	0.900	0.1
114	0.977	3.00E-9	0.985	1.28E-7	2.21	1.41E-7	1.13E6	1.00	0.911	0.900	0.1
113	0.979	2.90E-9	0.986	1.52E-7	2.23	1.67E-7	9.56E5	1.00	0.924	0.900	0.1
112	0.982	2.81E-9	0.986	1.63E-7	2.23	1.79E-7	8.91E5	1.00	0.924	0.900	0.1
111	0.984	2.73E-9	0.986	1.78E-7	1.99	1.80E-7	8.84E5	1.00	0.916	0.987	0.1
110	0.987	2.64E-9	0.990	2.11E-7	1.97	2.19E-7	7.28E5	1.00	0.916	0.963	0.1
109	0.990	2.57E-9	0.987	2.25E-7	1.97	2.33E-7	6.83E5	1.00	0.900	0.963	0.1
108	0.992	2.50E-9	0.986	4.06E-7	1.06	4.42E-7	3.60E5	1.00	0.982	0.900	0.1
107	0.995	2.42E-9	0.986	4.70E-7	1.01	5.11E-7	3.12E5	1.00	0.987	0.900	0.1
106	0.997	2.35E-9	0.985	5.53E-7	0.965	6.02E-7	2.64E5	1.00	0.988	0.900	0.1
105	1.00	2.29E-9	0.985	6.41E-7	0.983	6.98E-7	2.28E5	1.00	0.975	0.900	0.1
104	1.00	2.21E-9	0.984	1.11E-6	1.79	1.21E-6	1.32E5	1.00	0.974	0.900	0.1
103	1.01	2.09E-9	0.988	1.39E-6	2.25	1.52E-6	1.05E5	1.00	0.977	0.900	0.1
102	1.01	1.98E-9	0.988	1.62E-6	2.31	1.76E-6	9.02E4	1.00	0.981	0.900	0.1
101	1.01	1.88E-9	0.989	1.84E-6	2.38	2.00E-6	7.95E4	1.00	0.982	0.900	0.1
100	1.01	1.79E-9	0.989	2.08E-6	2.42	2.26E-6	7.04E4	1.00	0.982	0.900	0.1
99	1.02	1.69E-9	0.989	2.34E-6	2.44	2.55E-6	6.24E4	1.00	0.982	0.900	0.1
98	1.02	1.60E-9	0.989	2.63E-6	2.46	2.86E-6	5.56E4	1.00	0.982	0.900	0.1
97	1.02	1.51E-9	0.989	2.93E-6	2.48	3.20E-6	4.98E4	1.00	0.982	0.900	0.1
96	1.02	1.42E-9	0.989	3.28E-6	2.50	3.57E-6	4.46E4	1.00	0.980	0.900	0.1
95	1.03	1.34E-9	0.990	3.65E-6	2.52	3.98E-6	4.00E4	1.00	0.980	0.900	0.1
94	1.03	1.26E-9	0.990	4.06E-6	2.54	4.43E-6	3.60E4	1.00	0.977	0.900	0.1
93	1.03	1.18E-9	0.992	4.51E-6	2.56	4.91E-6	3.24E4	1.00	0.973	0.900	0.1
92	1.04	1.10E-9	0.993	5.01E-6	2.58	5.47E-6	2.91E4	1.00	0.967	0.900	0.1
91	1.04	1.03E-9	0.995	5.56E-6	2.59	6.07E-6	2.62E4	1.00	0.967	0.900	0.1
90	1.04	9.64E-10	0.994	6.16E-6	2.59	6.72E-6	2.37E4	1.00	0.967	0.900	0.1
89	1.04	9.00E-10	0.994	6.85E-6	2.60	7.47E-6	2.13E4	1.00	0.967	0.900	0.1
88	1.05	8.41E-10	0.994	7.59E-6	2.60	8.28E-6	1.92E4	1.00	0.967	0.900	0.1
87	1.05	7.83E-10	0.993	8.42E-6	2.60	9.19E-6	1.73E4	1.00	0.967	0.900	0.1
86	1.05	7.28E-10	0.993	9.35E-6	2.60	1.02E-5	1.56E4	1.00	0.967	0.900	0.1
85	1.06	6.76E-10	0.992	1.04E-5	2.60	1.13E-5	1.41E4	1.00	0.967	0.900	0.1
84	1.06	6.28E-10	0.991	1.15E-5	2.60	1.25E-5	1.27E4	1.00	0.966	0.900	0.1
83	1.06	5.80E-10	0.992	1.28E-5	2.61	1.39E-5	1.14E4	1.00	0.964	0.900	0.1
82	1.06	5.38E-10	0.990	1.41E-5	2.60	1.54E-5	1.03E4	1.00	0.960	0.900	0.1
81	1.07	4.88E-10	1.00	1.58E-5	2.65	1.73E-5	9.19E3	1.00	0.945	0.900	0.1
80	1.07	4.50E-10	1.00	1.76E-5	2.65	1.93E-5	8.25E3	1.00	0.945	0.900	0.1
79	1.07	4.15E-10	1.00	1.96E-5	2.64	2.15E-5	7.41E3	1.00	0.945	0.900	0.1
78	1.08	3.83E-10	0.998	2.17E-5	2.64	2.37E-5	6.72E3	1.00	0.945	0.900	0.1
77	1.08	3.52E-10	0.997	2.42E-5	2.62	2.65E-5	6.01E3	1.00	0.945	0.900	0.1
76	1.08	3.24E-10	0.996	2.69E-5	2.62	2.95E-5	5.40E3	1.00	0.943	0.900	0.1
75	1.09	2.97E-10	0.998	3.01E-5	2.62	3.29E-5	4.83E3	1.00	0.939	0.900	0.1
74	1.09	2.71E-10	0.998	3.36E-5	2.61	3.68E-5	4.32E3	1.00	0.936	0.900	0.1
73	1.09	2.48E-10	0.998	3.75E-5	2.61	4.11E-5	3.87E3	1.00	0.934	0.900	0.1
72	1.10	2.27E-10	0.999	4.18E-5	2.61	4.59E-5	3.47E3	1.00	0.929	0.900	0.1
71	1.10	2.07E-10	1.00	4.68E-5	2.62	5.13E-5	3.10E3	1.00	0.924	0.900	0.1
70	1.10	1.82E-10	1.00	5.38E-5	2.69	5.93E-5	2.68E3	1.00	0.900	0.900	0.1

Table A.8: Fitting parameters of f_{11} for C9.

Temp. [°C]	T*/T	σ [S/cm]	Exp.	τ_{Max}	$\delta\epsilon$	τ	$1/(2\pi\tau)$	ϵ_{Inf}	γ	λ	AC Volt
115	0.97	3.17E-09	0.98	1.56E-07	2.8	1.70E-07	9.37E+05	1	0.97	0.9	0.1
114	0.98	3.04E-09	0.98	1.66E-07	2.39	1.81E-07	8.79E+05	1	0.96	0.9	0.1
113	0.98	2.99E-09	0.98	6.74E-08	3.05	6.74E-08	2.36E+06	1	0.99	1	0.1
112	0.98	2.94E-09	0.98	7.17E-08	3.1	7.17E-08	2.22E+06	1	0.99	1	0.1
111	0.98	2.90E-09	0.98	7.56E-08	3.21	7.57E-08	2.10E+06	1	0.98	1	0.1
110	0.99	2.85E-09	0.98	7.85E-08	3.38	7.86E-08	2.03E+06	1	0.97	1	0.1
109	0.99	2.80E-09	0.98	8.18E-08	3.45	8.18E-08	1.95E+06	1	0.97	1	0.1
108	0.99	2.76E-09	0.98	8.57E-08	3.54	8.57E-08	1.86E+06	1	0.96	1	0.1
107	1	2.71E-09	0.98	8.89E-08	3.69	8.89E-08	1.79E+06	1	0.94	1	0.1
106	1	2.67E-09	0.98	9.55E-08	3.69	9.55E-08	1.67E+06	1	0.94	1	0.1
105	1	2.63E-09	0.98	1.05E-07	3.65	1.05E-07	1.51E+06	1	0.94	1	0.1
104	1	2.63E-09	0.98	1.07E-07	3.95	1.07E-07	1.49E+06	1	0.94	1	0.1
103	1.01	2.67E-09	0.98	1.01E-07	4.63	1.01E-07	1.58E+06	1	0.93	1	0.1
102	1.01	2.64E-09	0.98	1.04E-07	4.77	1.04E-07	1.53E+06	1	0.93	1	0.1
101	1.01	2.59E-09	0.98	1.08E-07	4.85	1.08E-07	1.47E+06	1	0.93	1	0.1
100	1.01	2.54E-09	0.98	1.14E-07	4.88	1.14E-07	1.40E+06	1	0.93	1	0.1
99	1.02	2.49E-09	0.98	1.19E-07	4.91	1.19E-07	1.34E+06	1	0.93	1	0.1
98	1.02	2.44E-09	0.98	1.25E-07	4.93	1.25E-07	1.27E+06	1	0.93	1	0.1
97	1.02	2.38E-09	0.98	1.32E-07	4.96	1.32E-07	1.21E+06	1	0.93	1	0.1
96	1.02	2.33E-09	0.98	1.39E-07	4.95	1.40E-07	1.14E+06	1	0.94	1	0.1
95	1.03	2.27E-09	0.98	1.52E-07	4.84	1.52E-07	1.05E+06	1	0.94	1	0.1
94	1.03	2.21E-09	0.98	1.62E-07	4.87	1.62E-07	9.82E+05	1	0.95	1	0.1
93	1.03	2.15E-09	0.98	1.72E-07	4.93	1.72E-07	9.23E+05	1	0.95	1	0.1
92	1.04	2.09E-09	0.98	1.84E-07	4.96	1.84E-07	8.63E+05	1	0.95	1	0.1
91	1.04	2.04E-09	0.98	1.98E-07	4.99	1.98E-07	8.04E+05	1	0.95	1	0.1
90	1.04	1.98E-09	0.98	2.12E-07	5.02	2.13E-07	7.49E+05	1	0.95	1	0.1
89	1.04	1.91E-09	0.98	2.29E-07	5.08	2.29E-07	6.96E+05	1	0.95	1	0.1
88	1.05	1.85E-09	0.98	2.47E-07	5.14	2.47E-07	6.45E+05	1	0.95	1	0.1
87	1.05	1.80E-09	0.98	2.67E-07	5.23	2.67E-07	5.97E+05	1	0.95	1	0.1
86	1.05	1.73E-09	0.98	2.89E-07	5.31	2.90E-07	5.50E+05	1	0.95	1	0.1
85	1.06	1.67E-09	0.98	3.15E-07	5.36	3.16E-07	5.04E+05	1	0.95	1	0.1
84	1.06	1.61E-09	0.98	3.43E-07	5.44	3.43E-07	4.65E+05	1	0.95	1	0.1
83	1.06	1.55E-09	0.98	3.76E-07	5.52	3.76E-07	4.23E+05	1	0.95	1	0.1
82	1.06	1.49E-09	0.98	4.11E-07	5.62	4.11E-07	3.87E+05	1	0.95	1	0.1
81	1.07	1.43E-09	0.98	4.51E-07	5.74	4.51E-07	3.53E+05	1	0.95	1	0.1
80	1.07	1.37E-09	0.98	4.96E-07	5.81	4.96E-07	3.21E+05	1	0.95	1	0.1
79	1.07	1.31E-09	0.98	5.38E-07	5.96	5.39E-07	2.96E+05	1	0.95	1	0.1
78	1.08	1.25E-09	0.98	5.95E-07	6.09	5.96E-07	2.67E+05	1	0.95	1	0.1
77	1.08	1.19E-09	0.98	6.59E-07	6.24	6.59E-07	2.42E+05	1	0.95	1	0.1
76	1.08	1.13E-09	0.98	7.31E-07	6.4	7.31E-07	2.18E+05	1	0.95	1	0.1
75	1.09	1.08E-09	0.98	8.07E-07	6.58	8.07E-07	1.97E+05	1	0.95	1	0.1
74	1.09	1.02E-09	0.98	9.01E-07	6.76	9.01E-07	1.77E+05	1	0.95	1	0.1
73	1.09	9.70E-10	0.98	9.92E-07	6.99	9.93E-07	1.60E+05	1	0.94	1	0.1
72	1.1	9.18E-10	0.98	1.10E-06	7.2	1.10E-06	1.45E+05	1	0.94	1	0.1
71	1.1	8.66E-10	0.98	1.23E-06	7.43	1.23E-06	1.29E+05	1	0.94	1	0.1
70	1.1	8.08E-10	0.99	1.37E-06	7.67	1.38E-06	1.16E+05	1	0.94	1	0.1

Bibliography

[1] De Vries. *Mol. Cryst. Liq. Cryst.*, 10:219, 1970.

[2] De Vries. *Mol. Cryst. Liq. Cryst.*, 20:119, 1973.

[3] E. T. Samulski. *Liq. Cryst.*, 37:669, 2010.

[4] H. Takezoe and Y. Takanishi. *Jpn. J. Appl. Phys.*, 45:597, 2006.

[5] R. A. Reddy and C. Tschierske. *J. Mater. Chem.*, 16:907, 2006.

[6] P. G. de Gennes and J. Prost. *The physics of Liquid Crystals (2nd edition).* Oxford University Press, New York, USA, 1993.

[7] Edited by D. Demus, J. W. Goodby, G. W. Gray, H. W. Spiess, and V. Vill. *Handbook of Liq. Crys., Vol. 1.* Wiley-VCH, 1998.

[8] A. G. Vanakaras and D. J. Photinos. *J. Chem. Phys*, 128:154512, 2008.

[9] S. D. Peroukidis, P. K. Karahaliou, A. G. Vanakaras, and D. J. Photinos. *Liq. Cryst.*, 36:727, 2009.

[10] S. Droulias, A.G. Vanakaras, and D.J. Photinos. *Liq. Crys.*, 37:969, 2010.

[11] D. A. Dunmur, G. R. Luckhurst, M. R. de la Fuente, S. Diez, and M. A. P. Jubindo. *J. Chem. Phys*, 115:8681, 2001.

[12] M. Stocchero, A. Ferrarini, G. J. Moro, D. A. Dunmur, and G. R. Luckhurst. *J. Chem. Phys*, 121:8079, 2004.

[13] V. P. Panov, M. Nagaraj, J. K. Vij, Yu. P. Panarin, A. Kohlmeier, M. G. Tamba, R. A. Lewis, and G. H. Mehl. *Phys. Rev. Lett.*, 105:167801, 2010.

[14] Martin A. Bates and Geoffrey R. Luckhurst. *Phys. Rev. E*, 72:051702, 2005.

[15] G.R. Luckhurst. *Thin Solid Films*, 393:40, 2001.

[16] D. Wiant, K. Neupane, S. Sharma, J. T. Gleeson, S. Sprunt, A. Jákli, N. Pradhan, and G. Iannacchione. *Phys. Rev. E*, 77:061701, 2008.

[17] L. G. Fel. *Phys. Rev. E*, 52:702, 1995.

[18] C. Keith, A. Lehmann, U. Baumeister, M. Prehm, and C. Tschierske. *Soft Matter*, 6:1704, 2010.

[19] W. H. de Jeu, W. J. A. Goossens, and P. Bordewijk. *J. Chem. Phys*, 61:1985, 1974.

[20] S. Stojadinovic, A. Adorjan, S. Sprunt, H. Sawade, and A. Jakli. *Phys. Rev. E*, 66:060701(R), 2002.

[21] S. H. Hong, R. Verduzco, J. C. Williams, R. J. Twieg, E. DiMasi, R. Pindak, A. Jakli, J. T. Gleeson, and S. Sprunt. *Soft Matter*, 6:4819, 2010.

[22] Verena Gortz, Christopher Southern, Nicholas W. Roberts, Helen F. Gleeson, and John W. Goodby. *Soft Matter*, 5:463, 2009.

[23] Oriano Francescangeli and Edward T. Samulski. *Soft Matter*, 6:2413, 2010.

[24] M. Salamonczyk A. Kovarova J. Svoboda M. Osipov D. Pociecha N. Vaupotíc, J. Szydlowska and E. Gorecka. *Phys. Rev. E*, 80:030701(R), 2009.

[25] C. Tschierske and D. J. Photinos. *J. Mater. Chem.*, 20:4263, 2010.

[26] R. Stannarius, A. Eremin, M.-G. Tamba, G. Pelzl, and W. Weissflog. *Phys. Rev. E*, 76:061704, 2007.

[27] A. Saupe. *Mol. Cryst. Liq. Cryst.*, 1:527, 1966.

[28] D. A. Dunmur, D. A. Hitchen, and X.-Y. Hong. *Mol. Cryst. Liq. Cryst.*, 140: 303, 1986.

[29] J. F. Nye. *Physical properties of Crystals*. Oxford University Press, Oxford, UK, 1957.

[30] N. W. Ashcroft and N. D. Mermin. *Solid State Physics*. WB Saunders and Co, 1976.

[31] Y. Jang, V. P. Panov, C. Keith, C. Tschierske, and J. K. Vij. *Appl. Phy. Lett.*, 97:152903, 2010.

[32] K. Merkel, A. Kocot, J. K. Vij, G. H. Mehl, and T. Meyer. *J. Chem. Phys*, 121:5012, 2004.

[33] K. Merkel, A. Kocot, J. K. Vij, R. Korlacki, G. H. Mehl, and T. Meyer. *Phys. Rev. Lett.*, 93:237801, 2004.

[34] Y. Ouchi, T. Shingu, H. Takezoe, A. Fukuda, E. Kuze, M. Koga, and N. Goto. *Jpn. J. Appl. Phys.*, 23:660, 1984.

[35] K. Hori. *Mol. Cryst. Liq. Cryst.*, 100:75, 1983.

[36] A. D. L. Chandani, N. M. Shtykov, V. P. Panov, A. V. Emelyanenko, A. Fukuda, and J. K. Vij. *Phys. Rev. E*, 72:041705, 2005.

[37] N. M. Shtykov, A. D. L. Chandani, A. V. Emelyanenko, A. Fukuda, , and J. K. Vij. *Phys. Rev. E*, 71:021711, 2005.

[38] F. Gouda, K. Skarp, and S. T. Lagerwall. *Ferroelectrics*, 113:165, 1991.

[39] A. Levstik, T. Carlsson, C. Filipic, I. Levstik, and B. Zeks. *Phys. Rev. Lett.*, 35:3527, 1987.

[40] J. C. Kemp. *J, Opt. Soc. Am.*, 59:950, 1969.

[41] P. Yeh. *Optical Waves in Layered Media.* John Wiley & Sons, Inc., New York, 1988.

[42] R. C. Jones. *J, Opt. Soc. Am.*, 31:488, 1941.

[43] P. Yeh. *J. Opt. Soc. Am.*, 72:507, 1982.

[44] Y.Liu, G. A. Jones, Y. Peng, and T. H. Shen. *J. Appl. Phy.*, 100:063537, 2006.

[45] O. Francescangeli, V. Stanic, S. Torgova, A. Strigazzi, N. Scaramuzza, C. Ferrero, I. P. Dolbnya, T. M. Weiss, R. Berardi, L. Muccioli, S. Orlandi, and C. Zannoni. *Adv. Func. Mater.*, 19:2592, 2009.

[46] O. Francescangeli, F. Vita, C. Ferrero, T. Dingemans, and E. T. Samulski. *Soft Matter*, 7:895, 2011.

[47] V. Prasad B. R. Acharya, S-W. Kang and S. Kumar. *J. Phys. Chem. B*, 113: 3845, 2009.

[48] W. Weissflog, H. Ndasi, U. Dunemann, G. Pelzl, S. Diele, A. Eremin, and H. Kresse. *J. Mater. Chem*, 11:2748, 2001.

[49] V. Prasad, S.-W. Kang, K. A. Suresh, L. Joshi, Q. Wang, and S. Kumar. *J. Am. Chem. Soc.*, 127:17224, 2005.

[50] A. Primak B. R. Acharya and S. Kumar. *Phys. Rev. Lett.*, 92:145506, 2004.

[51] A. Immirzi and B. Perini. *Acta Cryst.Sect. A.*, 33:216, 1977.

[52] W. Maier and A. Saupe. *Z. Naturforsch. A*, 13a:564, 1958.

[53] W. Maier and A. Saupe. *Z. Naturforsch. A*, 14a:882, 1959.

[54] W. Maier and A. Saupe. *Z. Naturforsch. A*, 15a:287, 1960.

[55] L. A. Madsen, T. J. Dingemans, M. Nakata, and E. T. Samulski. *Phys. Rev. Lett.*, 92, 2004.

[56] W. Maier and G. Meier. *Z. Naturforsch. A*, 16A:262, 1961.

[57] Jan Jadzyn, Grzegorz Czechowski, Redouane Douali, and Christian Legrand. *Liq. Crys.*, 26:1591, 1999.

[58] D. A. Dunmur. *Liq. Crys.*, 32:1379, 2005.

[59] Y. P. Kalmykov. *Liq. Cryst.*, 10:519, 1991.

[60] D. Dunmur and K. Toriyama. *In Physical Properties of Liquid Crystal: Demus, D., Ed.;*, volume Demus, D., Ed. 1999.

[61] Pier L. Nordio, G. Rigatti, and U. Segre. *Molecular Physics*, 25:129, 1973.

[62] H. Xianyu, S.-T. Wu, and C.-L Lin. *Liq. Cryst.*, 36:717, 2009.

[63] Y. Yin, S. V. Shiyanovskii, and O. D. Lavrentovich. *Phys. Rev. Lett.*, 98: 097801, 2007.

[64] S. Havriliak and S. Negami. *Polymer*, 8:161, 1967.

[65] M. Nagaraj, Y. P. Panarin, U. Manna, J. K. Vij, C. Keith, and C. Tschierske. *Appl. Phy.Lett.*, 96(1):011106, 2010.

[66] P. S. Salter, C. Tschierske, S. J. Elston, and E. P. Raynes. *Phys. Rev. E*, 84: 031708, 2011.

[67] H-G. Yoon, S-W. Kang, R. Y. Dong, A. Marini, K. A. Suresh, M. Srinivasarao, and S. Kumar. *Phys. Rev. E*, 81:051706, 2010.

[68] Zolina V. *Trans. Faraday Soc.*, 29:919, 1933.

[69] Zwetkoff V. *Acta Physikochim. URSS*, 3:879, 1935.

[70] M. F. Vuks. *Opt. Spec.*, 20:644, 1966.

[71] A. Kocot and J.K. Vij. *Liq. Cryst.*, 37:653, 2010.

[72] G. Pelzl, A Eremin, S. Diele, H. Kresse, and W. Weissflog. *J. Mater. Chem.*, 12:2591, 2002.

[73] P. S. Salter, P. W. Benzie, R. A. Reddy, C. Tschierske, S. J. Elston, and E. P. Raynes. *Phys. Rev. E*, 80:031701, 2009.

[74] I. Noyori, R. Tomino and M. Nishizawa. *Journal of the American Chemical Society*, 101:5843, 1979.

[75] David J. Earl, Mikhail A. Osipov, Hideo Takezoe, Yoichi Takanishi, and Mark R. Wilson. *Phys. Rev. E*, 71:021706, 2005.

[76] V. Gortz and J. W. Goodby. *Chem. Commun.*, page 3262, 2005.

[77] Fangyong Yan, Christopher Adam Hixson, and David J. Earl. *Phys. Rev. Lett.*, 101:157801, 2008.

[78] S. H. Hong, J. C. Williams, R. J. Twieg, A. Jákli, J. Gleeson, S. Sprunt, and Brett Ellman. *Phys. Rev. E*, 82:041710, 2010.

[79] S. D. Peroukidis, A. G. Vanakaras, and D. J. Photinos. *Phys. Rev. E*, 84: 010702, 2011.

[80] T. C. Lubensky and Leo Radzihovsky. *Phys. Rev. E*, 66:031704, 2002.

[81] L. Longa, G. Pajak, and T. Wydro. *Phys. Rev. E*, 79:040701, 2009.

[82] E. P. Raynes. *Liq. Crys.*, 33:1215, 2006.

[83] E-H. Kim, O. N. Kadkin, S-Y. Kim, and M-G. Choi. *European Journal of Inorganic Chemistry*, 2011:2933, 2011.

[84] H. Brand and H. Pleiner. *The European Physical Journal E: Soft Matter and Biological Physics*, 31:37, 2010.

[85] M. J. Freiser. *Phys. Rev. Lett.*, 24:1041, 1970.

[86] R. Berardi, L. Muccioli, and C. Zannoni. *The Journal of Chemical Physics*, 128:024905, 2008.

[87] H. Mori and P. J. Bos. *SID Symposium Digest of Technical Papers*, 29(1): 830, 1998.

[88] J. Chen, K.-H. Kim, J.-J. Jyu, J. H. Souk, J. R. Kelly, and P. J. Bos. *SID Symposium Digest of Technical Papers*, 29(1):315–318, 1998.

[89] Y. Saitoh, S. Kimura, K. Kusafuka, and H. Shimizu. *Jpn. J. Appl. Phys.*, 37: 4822, 1998.

[90] J.-H. Lee, T-K. Lim, W-T. Kim, and J-I. Jin. *J. Appl. Phy.*, 101:034105, 2007.

[91] R. Stannarius. *J. Appl. Phy.*, 104:036104, 2008.

[92] M. Chambers J. Harden Q. Li H. Takezoe K. V. Le, M. Mathews and A. Jakli. *Phys. Rev. E*, 79:030701, 2009.

[93] C. W. Oseen. *Trans. Faraday Soc.*, 29:883, 1933.

[94] F. C. Frank. *Disc. Faraday Soc.*, 25:19, 1958.

[95] P. Yeh and C. Gu. *Optics of liquid cyrstal displays.* 1999.